VOLUME 1, ISSUE 1 2018

CATALYSIS IN GREEN CHEMISTRY AND ENGINEERING

AN OFFICIAL JOURNAL OF THE CATALYSIS SOCIETY OF INDIA

begell
New York • Connecticut

AIMS AND SCOPE

Catalysis in Green Chemistry and Engineering (CGCE) aims to publish original research articles, review articles, mini-reviews, book reviews, short communications, and reviews on recent patents in catalysis. CGCE will consider topics related to the use of catalyst in green process and sustainable engineering, especially related catalyst synthesis, characterization and its applications. The ultimate aim is to reduce waste associated with use of materials and energy in a given process in consonance with principles of Green Chemistry and Engineering. The authors must give justification for their manuscripts and its relevance to the scope of the journal. CGCE is a continuation of the Bulletin of the Catalysis Society of India which has been published since 1992.

Any topics mentioned below will be considered for possible publication in CGCE.

All aspects of homogeneous, heterogeneous and biocatalysis
Air pollution technologies
Algal based technologies
Biomass conversion
Bioprocess engineering
Catalyst deactivation
Catalyst preparation and characterization
Catalytic membrane reactors
Catalytic microreactors
Catalytic Reaction engineering and scale up
Chiral Chemistry
CO2 conversion into chemicals, fuels and energy
Computational aspects in catalysis
Dyestuff technology
Electro catalysis
Energy
Environmental catalysis
Enzyme
Fermentation processes
Fertilizer production
Fine chemicals
Fine chemicals
Fischer Tropsch synthesis
Flow Chemistry
Food and Flavor industry
Friedel-Crafts reactions
Fuel cells
Hydrogen generation
Hydrogenation
Nanomaterials
New catalytic routes and processes
Oleochemicals
Organic process development using catalysis
Organo-catalysis
Oxidation
Pharmaceutical industry
Photocatalysis
Pigments
Polymers
Process intensification
Redox materials
Refinery processes
Solid acids
Solid bases
Surfactants
Wastes water treatment
Waste to wealth
Water

Catalysis in Green Chemistry and Engineering (ISSN 2572-9896) is published quarterly and owned by Begell House, Inc., 50 North Street, Danbury, CT 06810, telephone (203) 456-6161. USA subscription rate for 2018 is $1500.00. Add $10.00 per issue for foreign airmail shipping and handling fees to all orders shipped outside the United States or Canada. Subscriptions are payable in advance. Subscriptions are entered on an annual basis, i.e., January to December. For immediate service and charge card sales, call (203) 456-6161 Monday through Friday 9 AM–5 PM EST. Fax orders to (203) 456-6167. Send written orders to Subscriptions Department, Begell House, Inc., 50 North Street, Danbury, CT 06810. You can also visit our website at http://www.begellhouse.com/ or http://www.dl.begellhouse.com/.

CATALYSIS IN GREEN CHEMISTRY AND ENGINEERING

AN OFFICIAL JOURNAL OF THE CATALYSIS SOCIETY OF INDIA

EDITOR-IN-CHIEF

ASSOCIATE EDITORS

EDITORIAL BOARD

INMACULADA ORTIZ
Dpto. Chemical and Biomolecular Engineering
E.T.S.I. Industriales y Telecomunicación (UC)
Avda/ Los Castros s/n, 39005
Santander (Cantabria), SPAIN
E- mail: ortizi@unican.es

KULAMANI PARIDA
Professor in Chemistry, Director, Centre for Nano Science and Nano Technology, Institute of Technical Education and Research, Siksha 'O' Anusandhan University
Bhubaneswar-751030, Odisha, India
Email: kulamaniparida@soauniversity.ac.in, paridakulamani@yahoo.com

L. A. PETROV
Chemical and Materials Engineering Department
Faculty of Engineering, King Abdulaziz University
PO Box 80204, Jeddah 21589, Kingdom of Saudi Arabia
E-mails: lachezarptrv@yahoo.com; lpetrov@kau.edu.sa; petrov@ic.bas.bg

VIRENDRA K. RATHOD
Professor of Chemical Engineering, Institute of Chemical Technology, Matunga, Mumbai- 400019
Email: vk.rathod@ictmumbai.edu.iin

SADHANA RAYALU
Head, Environmental Materials Division
CSIR-National Environmental Engineering Research Institute (NEERI), Nagpur
Email: s_rayalu@neeri.res.in

B.M. REDDY
Scientist G, Inorganic and Physical Chemistry Division
CSIR- Indian Institute of Chemical Technology, Hyderabad
Email: bmreddy@iict.res.in

C.V. RODE
CEPD Division, CSIR- National Chemical Laboratory
Dr Homi Bhabha Road, Pune-411008
Email: cv.rode@ncl.res.in

TAKEHIKO SASAKI
Department of Complexcity and Engineering
The University of Tokyo, Kasiwa Campus, Tokyo
Email: takehiko@k.u-tokyo.ac.jp

P. SELVAM
National Centre for Catalysis Research
Department of Chemistry, IIT-Madras
Chennai 600 036, India
Email: selvam@iitb.ac.in

ROGER SHELDON
CLEA Technologies B.V. The Netherlands
School of Chemistry, University of the Witwatersrand
Johannesburg, Republic of South Africa
E-mail: r.sheldon@clea.nl

RAJENDER S. VARMA
Sustainable Technology Division
National Risk Management Research Laboratory
U.S. Environmental Protection Agency
26 West M.L.K. Dr., MS 443
Cincinnati, Ohio 45268, USA
Email: Varma.Rajender@epa.gov, rajvarma@hotmail.com

BALASUBRAMANIAN VISWANATHAN
Emeritus Professor
IIT Madras, India
Email: bvnathan@iitm.ac.in

KAREN WILSON
Professor of Catalysis and Research Director
Aton University, UK
Email: k.wilson@aston.ac.uk

LEE D. WILSON
Department of Chemistry, University of Saskatchewan
Saskatoon, SK. S7N 5C9 Canada
Email: lee.wilson@usask.ca

VIKRAMADITYA G. YADAV
Department of Chemical and Biological Engineering
University of British Columbia
Vancouver, Canada
Email: vikramaditya.yadav@ubc.ca

FENGYU ZHAO
Laboratory of Green Chemistry and Process
Changchun Institute of Applied Chemistry
Chinese Academy of Sciences
Changchun 130022, China
Email: zhaofy@ciac.ac.cn

CATALYSIS IN GREEN CHEMISTRY AND ENGINEERING

VOLUME 1, ISSUE 1 **2018**

CONTENTS

GUEST EDITORS

GANAPATI D. YADAV & M. LAKSHMI KANTAM

BEGINNING OF A NEW ERA: INAUGURAL ISSUE OF CATALYSIS IN GREEN CHEMISTRY AND ENGINEERING

We are launching a new journal for the benefit of those involved in research, education, practice and administration in the production of chemicals, materials and energy by using processes and practices that cover all those principles envisaged in Green Chemistry as well as Green Engineering which will also include all waste management and process intensification efforts from gram to kilogram to ton depending on the type of industry and need.

We are most delighted to present to our readers with the first issue of "*Catalysis in Green Chemistry and Engineering*" (CGCE), the Avatar of erstwhile Bulletin of the Catalysis Society of India. Catalysis Society of India (CSI) represents more than 1000 members from academia, industry, and government organizations. CSI was formally founded in March 1973 at Banaras with Prof. S.K. Bhattacharyya as the President and Prof. J.C. Kuriacose as the Secretary. The main mandates of CSI are to encourage catalysis research in India, to organize professional meetings between researchers, to enhance mutual interactions, and to encourage cooperation between industry and academia. During the last three decades, the catalysis community in India has made significant strides both in applied and fundamental research.

Several issues of the first volume will include the selected papers that were presented at the "7th Asia Pacific Congress on Catalysis (APCAT7)". APCAT is an International Conference which gathers fellow scientists, academicians, students, and delegates from industries all over the world with the aim to provide a high-profile and internationally renowned forum for researchers in catalysis science and technology. This event is organized every three years and for the first time, it was organized in India under Chairmanship of Professor G.D. Yadav, Vice Chancellor, Institute of Chemical Technology (ICT), Mumbai (also President of Catalysis Society of India) and Supported by Catalysis Society of India (CSI). The event was held from January 17 to January 21, 2017, at The Lalit, Mumbai, India. The theme of the event was *"Catalysis for Sustainable Development, Peace and Prosperity"*. More than 500 delegates from 30 countries participated in this event. At this conference, 175 oral and 115 posters were presented along with 30 invited lectures that included plenary, keynote, and invited talks.

We have invited 45 selected papers presented in the conference and after a rigorous peer review 18 papers were accepted for publication. Most of these papers covered the work on catalysts synthesis and its characterization and their applications for various reactions.

We would like take this opportunity to thank all who kindly contributed their papers for these special issue of "*Catalysis in Green Chemistry and Engineering*" and reviewers for their kind help and co-operation. We are also obligated to Begell House Publishers, particularly, Dr. Yelena Shafeyeva, President, Begell House Inc. and the publishing and production teams for their assistance in preparation and publication of the journal.

Editors for the Special Issue:

Ganapati D. Yadav
M. Lakshmi Kantam

2572–9896/18/$35.00

PEG SUPPORTED PROLINE AS A LIQUID-LIQUID BIPHASIC CATALYST IN KNOEVENAGEL CONDENSATION REACTIONS

Nisha D. Kadam & Radha V. Jayaram*

Department of Chemistry, Institute of Chemical Technology, Matunga, Mumbai-400 019, India

*Address all correspondence to: Radha V. Jayaram, Department of Chemistry, Institute of Chemical Technology, Matunga, Mumbai-400 019, India; Tel.: +91-22 3361 2601; Fax: +91-22 3361 1020, E-mail: rv.jayaram@ictmumbai.edu.in

Original Manuscript Submitted: 6/28/2017; Final Draft Received: 10/28/2017

Proline, generally used as a base catalyst for organic reactions, was modified by supporting on PEG (polyethylene glycol) and used as an acid catalyst. The supported material was applied as a nonaqueous biphasic catalytic system in the Knoevenagel condensation for the synthesis of α, β-unsaturated compounds under mild reaction conditions and the proposed mechanism was supported by kinetic studies. After completion of the reaction, the catalyst could be separated and reused by selective product extraction. The catalyst was characterized by techniques such as FT-IR, NMR, CHN, and TGA-DSC analysis.

KEY WORDS: *acid catalyst, kinetic study, Knoevenagel condensation, proline*

1. INTRODUCTION

Two strategies are described in the literature for solving the problem of separating and reusing homogeneous catalysts. One is to immobilize the catalyst on solid supports, and the other is to immobilize the same on a "mobile phase," generally described as a liquid/liquid biphasic system (Liu et al., 2015).

Biphasic catalytic systems are of two types—aqueous and nonaqueous. Nonaqueous biphasic systems have to be used in the case of water sensitive reactions. In these systems, the catalyst can exhibit phase selective solubility and hence be separated by a simple extraction described as "selective product extraction" (Bergbreiter and Sung, 2006). Biphasic catalytic processes offer the benefits of both homogeneous and heterogeneous catalysis (Sun et al., 2012; Cecchini et al., 2014; Majumdar et al., 2012; Herrmann and Kohlpaintner, 1993).

Though proline is used as a base catalyst (List, 2002), it can be modified by supporting on PEG to make an acid catalyst. In the present work, catalytic activity of PEG supported proline was used as an acid catalyst for Knoevenagel condensation. The Knoevenagel reaction is a condensation between activated methylene and carbonyl compounds, for the formation of a carbon−carbon double bond (Knoevenagel, 1898; Tietze, 1996; Ogiwara et al., 2015; Wang et al., 2001). The substituted alkenes can further be used for a variety of molecular transformations such as Michael additions and Diels−Alder reactions, (An-guo et al., 2009; Siddiqui and Khan, 2013). Knoevenagel condensation is widely used for the production of fine chemicals and pharmaceutical products.

This condensation reaction is catalyzed by both acids and bases (Wang et al., 2001; Memarian and Soleymani, 2011; Hu et al., 2005). There is still a lot of scope in maximizing the advantages such as reducing the time of the reaction and simplifying operational conditions (Delgado et al., 1995; Jenner, 2001; McNulty et al., 1998; Bigi et al., 2000).

2. MATERIALS AND METHODS

All chemicals were procured from S D Fine-Chem, India, and used without further purification or pretreatment. ^{1}H NMR and ^{13}C NMR spectra were recorded with a Bruker Avance (400 MHz) instrument. IR spectra were recorded

as KBr pellets with a PerkinElmer FT-IR spectrometer. All products were characterized by GC–MS analysis (Shimadzu QP2010). Percentage conversions were determined by GC analysis (PerkinElmer Clarus 580) using an internal standard. Thermogravimetric analysis (TGA) was performed on a Mettler Toledo (TGA/SDTA851) thermal analyzer. Differential scanning calorimetry (DSC) studies were carried out using a Mettler Toledo DSC823 instrument.

2.1 Catalyst Preparation (Scheme 1)

2.1.1 Synthesis of Compound 1

To a solution of pyridine (1.58 mL, 2 mmol) in 50 mL of toluene, polyethylene glycol 1500 (PEG-1500; 15 g, 1 mmol) was added. To this solution, thionylchloride (1.58 mL, 2 mmol) was added slowly with stirring, over a period of 30 min. The mixture was then refluxed for about 10 h. After cooling and filtering the precipitate of pyridine hydrochloride, the solvent was removed under vacuum. The residue was dissolved in dichloromethane, filtered, and evaporated to dryness to give Cl−PEG1500-Cl (14 g, 89% yield) (Patil et al., 2008; Zhi et al., 2009).

2.1.2 Synthesis of Compound 2

Proline (3.4 g, 5 mmol) and sodium hydroxide (2.7 g, 6.2 mmol) were dissolved in methanol (50 mL) and stirred at 70°C for 8 h. After removing methanol by rotary evaporation under reduced pressure, the residue was washed with diethyl ether and dried under vacuum to give compound **2** (89% yield).

2.1.3 Synthesis of Compound 3

Compound **1** (15.6 g, 1 mmol) and compound **2** (2 g, 2.25 mmol) were dissolved together in ethanol (50 mL) and stirred at reflux for 10 h. The solvent was removed using a rotary evaporator under reduced pressure. The residue obtained was dissolved in chloroform and washed with water. The chloroform layer was concentrated under reduced pressure and dried to get compound **3** as a colorless viscous liquid (85% yield).

^{1}H NMR (300 MHz, $CDCl_3$) δ 3.88 (t, 4H), 3.74 – 3.56 (m, 92H), 3.41 (t, 4H), 3.22 (s, 2H), 1.27 (ddd, $J = 23.2$, 20.7, 12.9 Hz, 12H).

^{13}C NMR (75 MHz, $CDCl_3$) δ 171.39, 72.52, 70.24, 69.89, 66.33, 61.24, 42.49, 29.39, 14.76.

CHN analysis: anal. Calc for $C_{60}H_{116}O_{50}N_2$: C, 43.26%; H, 6.97%; N, 1.68%; O, 48.07%. Found: C, 44.544%; H, 6.747%; N, 1.621%; O, 42.912%.

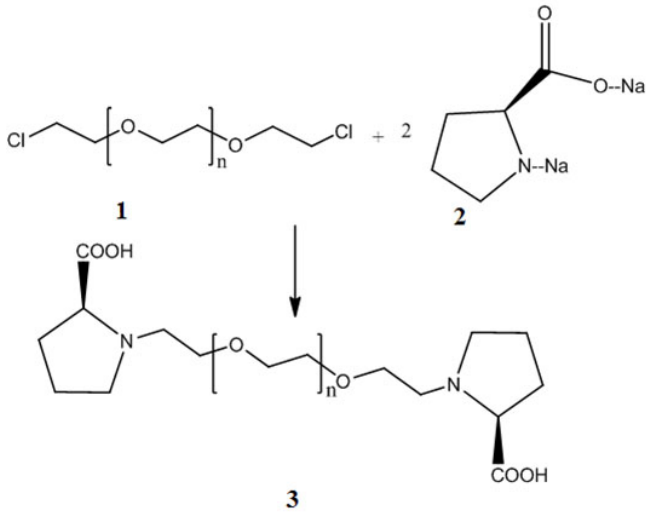

SCHEME 1: Synthesis of PEG supported proline

2.2 Typical Procedure of Knoevenagel Condensation

A mixture of aromatic aldehyde (1 mmol) and malononitrile (1.2 mmol) with 2 mL toluene was stirred at room temperature with compound **3** as catalyst (0.3 mmol). After completion of the reaction, hexane was added, decanted, and concentrated. The lower layer containing the catalyst was used for subsequent reactions.

3. RESULTS AND DISCUSSION

3.1 Characterization of the Catalyst

Polyethylene glycol (PEG) supported proline was characterized by FT-IR, ^{1}H-NMR, ^{13}C-NMR, TGA-DSC techniques, and CHN analysis.

3.1.1 Thermal Stability

In Fig. 1, from DSC studies the melting point (T_m) of PEG supported proline was found to be around 49°C. TGA and DSC studies indicate that PEG supported proline is thermally stable up to 250°C.

3.1.2 Acidity of PEG Supported Proline

In Fig. 2, PEG supported proline has two carboxylic groups shown with dissociation constants 1.35×10^{-3} and 2.24×10^{-5}, respectively (25°C). The pH values of 0.01 M aqueous solutions of proline, PEG, and PEG supported proline are 5.82, 3.27, and 3.74, respectively.

3.1.3 Solubility of PEG Supported Proline

The solubility of PEG supported proline was checked in different solvents. It was found to be soluble in almost all polar solvents and insoluble in mostly nonpolar solvents (Table 1). The solubilities of PEG supported proline in water, toluene, and hexane were 41.81%, 38.64%, and < 0.01%, respectively, at 25°C.

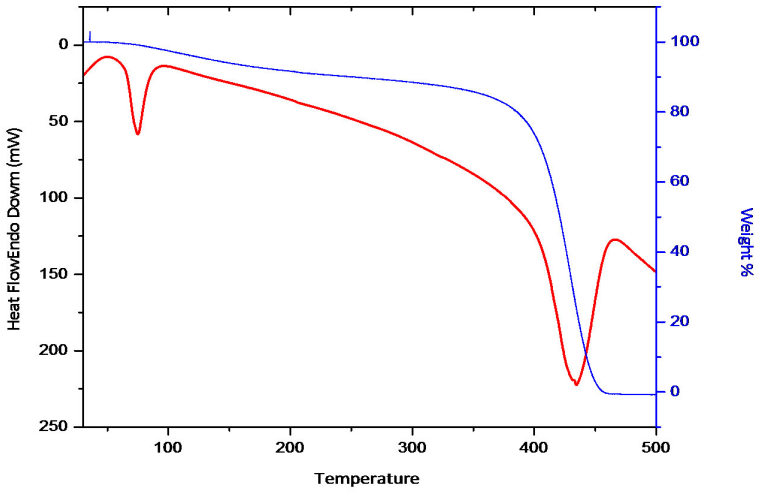

FIG. 1: TGA and DSC of PEG supported proline

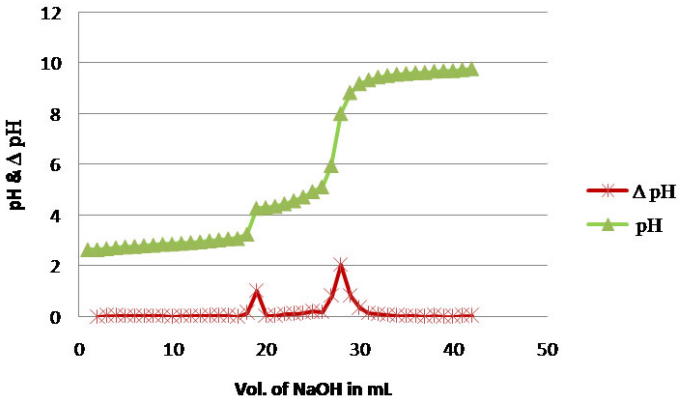

FIG. 2: pH and ΔpH vs. volume of NaOH in mL

TABLE 1: Solubility of PEG supported proline

Solvent	Solubility of PEG Supported Proline
Water	++
Ethanol	++
Methanol	++
Chloroform	++
Dichloromethane	++
Toluene	++
Ethyl acetate	++
DMF	++
ACN	++
IPA	++
Xylene	++
Ethyl lactone	++
Hexane	−−
Pet ether	−−
Heptane	−−
Diethyl ether	−−

++ : soluble; −− : insoluble at 25°C

3.2 Catalytic Activity of PEG Supported Proline

Catalytic activity of PEG supported proline was studied for the Knoevenagel condensation of substituted benzaldehydes with malononitrile at 25°C with toluene as solvent (Scheme 2).

3.2.1 Effect of Catalyst Concentration

Figure 3 shows the effect of catalyst concentration on the percentage conversion of benzaldehyde in the condensation product, benzylidene malononitrile, when 1 mmol of benzaldehyde and 1.2 mmol of malononitrile were reacted at 25°C in the presence of PEG supported proline as catalyst.

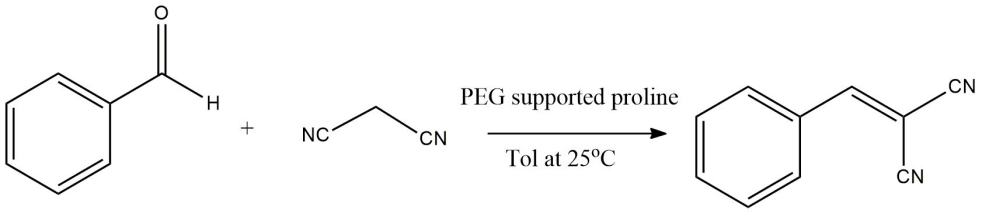

SCHEME 2: Knoevenagel condensation reaction using PEG supported proline as a catalyst

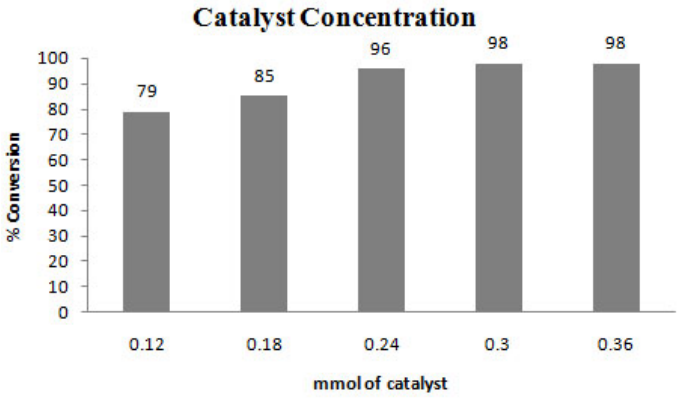

FIG. 3: Effect of catalyst concentration in the percent conversion of benzaldehyde

3.2.2 Effect of Supporting Proline on PEG

From the percent conversion vs. time plots (Fig. 4) the initial rates for conversion of benzaldehyde and the formation of benzylidenemalononitrile were determined (Table 2).

PEG supported proline gave a better yield as compared to only proline and a physical mixture of PEG and proline (0.3 mmol each) (Liu et al., 2008).

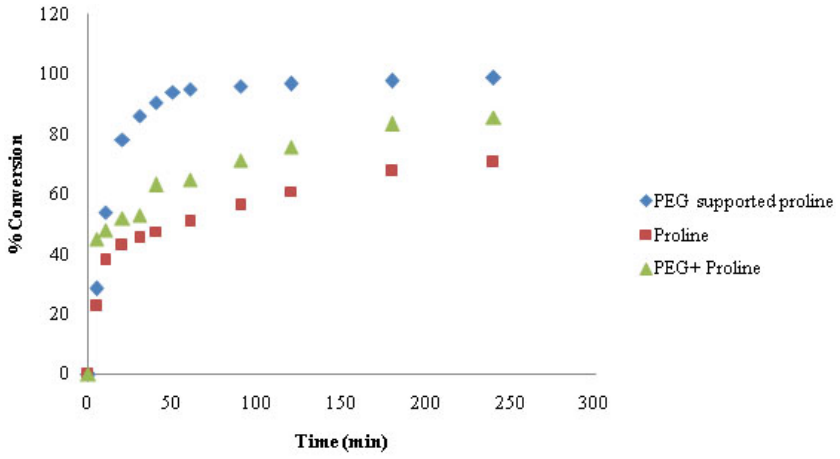

FIG. 4: Percent conversion vs. time plots for percent conversion of benzaldehyde in the presence of different catalysts

TABLE 2: Initial rates for the formation of benzylidene malononitrile

Sr. No.	Catalyst	Initial Rate/mmol min^{-1}
1	PEG supported proline	8.118×10^{-2}
2	PEG + proline	3.054×10^{-2}
3	Proline	1.215×10^{-2}

3.2.3 Separation of the Catalyst in a Nonaqueous Biphasic Catalytic System

In nonaqueous catalysis systems, the reaction medium consists of an organic phase (in this case, toluene) that contains the catalyst. After completion of the reaction, a selective extraction procedure using a suitable solvent (in this case, hexane) would enable the recovery of the products. The catalyst left behind would be used as such for further reactions (Fig. 5).

Different solvents were used in the reaction (Fig. 6). This reaction is known to proceed better in polar solvents (Senapati et al., 2014), but in the present study, we found higher conversion in a nonpolar solvent such as toluene than a polar solvent such as water. Toluene gave a better yield compared to other solvents. All further studies were carried out with only toluene, as it gave maximum conversion under similar reaction conditions.

3.2.4 Catalyst Reusability

The catalyst could be reused for at least up to five cycles without loss in activity (Fig. 7). Separation and reusability of this catalyst are simple.

3.2.5 Effect of Substituents on Benzaldehyde and Active Methylene Groups in the Condensation Reaction

Under the same reaction conditions (Scheme 3), the effects of substituents in benzaldehyde were studied using PEG supported proline as a catalyst (Table 3). Knoevenagel condensation reaction of aldehydes, with the substitution electron donating groups in the aromatic ring, would give lower yields of the condensation product than that with electron withdrawing groups like p-NO_2 > m-Cl > H > p-OCH_3 > p-OH > p-$N(CH_3)_2$ for the same reaction time (2 h). Hence the activity towards the condensation reaction in terms of average rate is as follows: malononitrile > ethyl cyanoacetate > ethyl acetoacetate > acetylacetone.

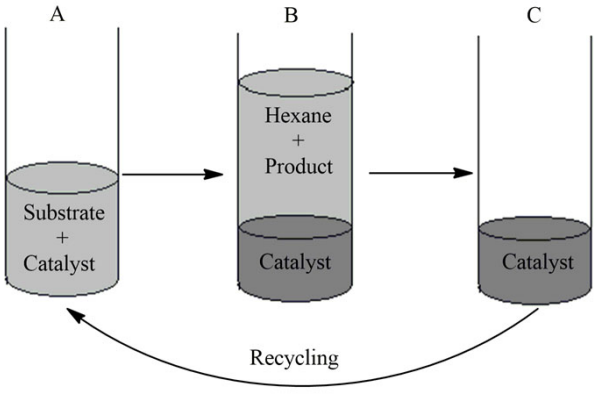

FIG. 5: (A) Reaction mixture with catalyst after reaction; (B) selective extraction of product by addition of hexane; (C) Decanted hexane layer and catalyst left behind

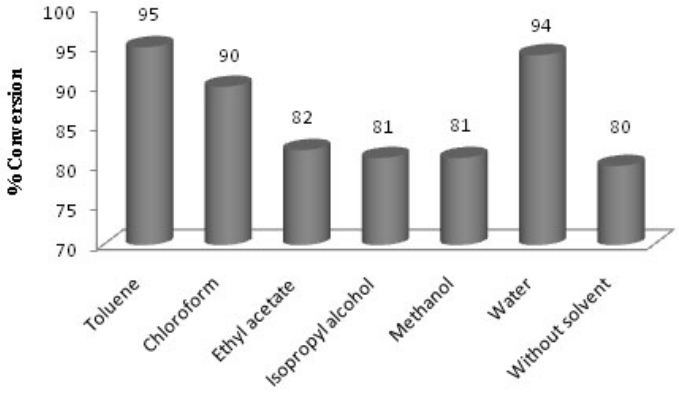

FIG. 6: Different solvents used for the condensation reaction

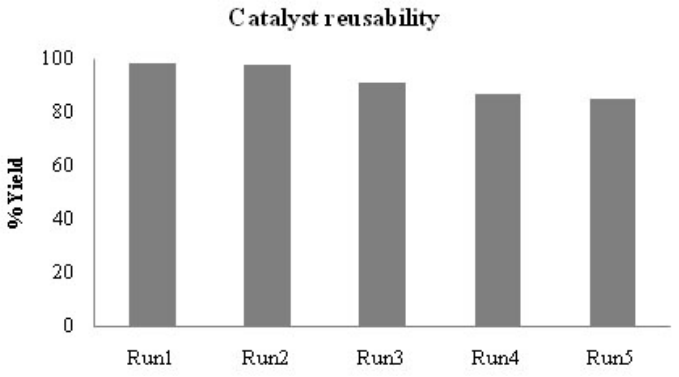

FIG. 7: Catalyst reusability up to five runs

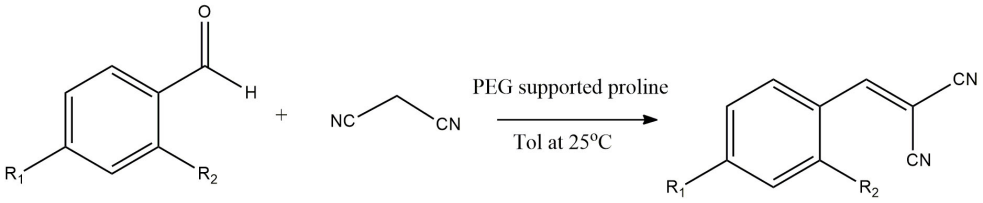

SCHEME 3: Knoevenagel condensation of substituents on benzaldehyde with malononitrile in presence of PEG supported proline as catalyst

3.2.6 Mechanism

In this study, PEG supported proline was used as a catalyst for the Knoevenagel condensation reaction. In this catalyst, the amine group was locked by PEG and it became a tertiary amine (basicity $2° > 3°$) and the carboxylic group became active. Because of that, PEG supported proline acts as an acid catalyst. In condensation, the active methylene group attacked a carbocation of aldehyde formed because of the catalyst, mediating the proton transfer necessary to get to a simple aldol-like intermediate, which under goes dehydration to afford the final product. This was proved further by kinetic study also (Medien, 2002).

TABLE 3: Effect of substituents in benzaldehyde and active methylene groups in Knoevenagel condensation reaction using PEG supported proline as a catalyst

Sr. No.	$-R_1$	$-R_2$	Active Methylene Group	% Yield*	MP (°C)
4	-H	-H	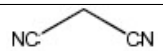	95	80
5	$-OCH_3$	-H		48	111
6	-H	-Cl	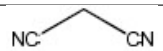	93	115
7	$-N(CH_3)_2$	-H	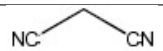	45	171
8	$-NO_2$	-H	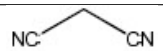	98	161
9	-OH	-H	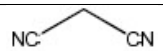	47	188
10	-H	-H	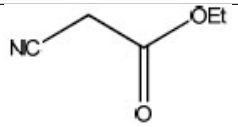	59	52
11	-H	-H	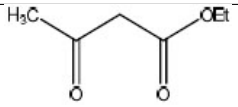	51	61
12	-H	-H	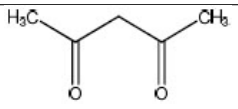	45	105

Reaction condition: 25°C with toluene as solvent system and reaction time: 2 h

3.2.7 Kinetic Studies

A kinetic study was carried out to get the rate expression for the condensation reaction. In all the experiments, the reaction mixtures were analyzed at fixed intervals of time using gas chromatography.

3.2.7.1 Formulation of the Kinetic Rate Law

The reaction steps in the reaction of an active methylene group with aromatic aldehydes in the presence of a PEG supported proline catalyst can be written as follows.

$$[\mathrm{Ald}] + [\mathrm{Cat}] \overset{K_1}{\rightleftharpoons} \left[\mathrm{Ald\ H^+}\right] + \left[\mathrm{Cat^-}\right] \qquad \text{(i)}$$

$$[\mathrm{MN}] + \left[\mathrm{Cat^-}\right] \overset{K_2}{\rightleftharpoons} \left[\mathrm{MN^-}\right] + [\mathrm{Cat}] \qquad \text{(ii)}$$

$$\left[\mathrm{Ald\ H^+}\right] + \left[\mathrm{MN^-}\right] \xrightarrow{k_3} \mathrm{Product} \qquad \text{(iii)}$$

The first two steps are fast equilibrium steps and hence the concentrations of the deprotonated and protonated forms of the catalyst, [Cat] and [Cat^-], can be obtained from the equilibrium constants K_1 and K_2 of the equilibria represented in (i) and (ii).

The rate of the reaction is thus

$$d[\mathrm{P}]/dt = k_3 \left[\mathrm{Ald\ H^+}\right] \left[\mathrm{MN^-}\right] \qquad \text{(iv)}$$

$$d[\mathrm{P}]/dt = k_3 K_1 K_2 [\mathrm{Ald}] [\mathrm{MN}] \qquad \text{(v)}$$

From the data compiled in Table 4, it was shown that for all aldehydes studied the kinetics is second order overall and it can be seen that the proposed mechanism is in accordance with the experimental rate law (Medien, 2002; Boronat et al., 2010).

Initial rates were determined from the slopes of concentration vs. time plots (Fig. 8). From the plots of log initial rates vs. log [reactant], the first order of the reaction with respect to both the reactants was found out.

3.2.7.2 Estimation of Activation Energy (EA)

The kinetics of the Knoevenagel condensation between benzaldehyde and malononitrile catalyzed by PEG supported proline was studied at different temperatures to obtain the experimental activation energy (Fig. 9). The rates of the reaction of benzaldehyde were determined at 278, 288, 298, and 313 K. The activation energy was determined from the slope of the Arrhenius plot as 30.0 kJ·mol^{-1}.

4. CONCLUSIONS

In conclusion, we have demonstrated that the Knoevenagel condensation between aromatic aldehydes and active methylene compounds can be effectively carried out at room temperature with PEG supported L-proline as catalyst. Normally, proline is used as a base catalyst for reactions, but it can be modified by supporting on PEG to become an acid catalyst. The reactions do not require inert conditions and could be carried out at room temperature. The proposed mechanism was supported by kinetic studies. The catalyst could be separated by selective product extraction and reused. These aspects make the biphasic catalytic system environmentally viable and operationally simple.

TABLE 4: Rate constants of the reaction of benzaldehyde with malononitrile at 298 K

[Benzaldehyde] mM•dm^{-3}	[Malononitrile] mM•dm^{-3}	Initial Rate (υ_0) mM•dm^{-3}•min^{-1}
0.5	5	0.0893
1	5	0.1778
1.5	5	0.2556
5	0.5	0.1027
5	1	0.2025
5	1.5	0.3148

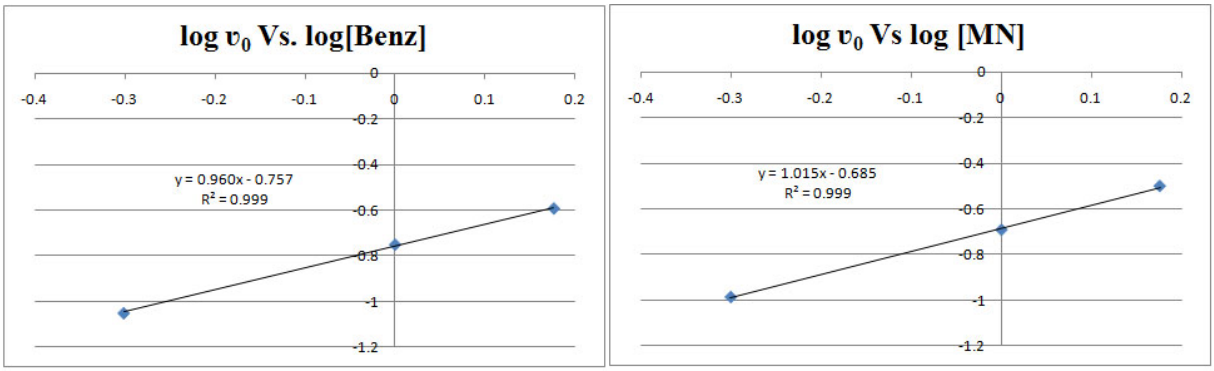

FIG. 8: Plots of log initial rate (υ_0) vs. log [reactant] for the Knoevenagel condensation of benzaldehyde and malononitrile catalyzed by PEG supported proline

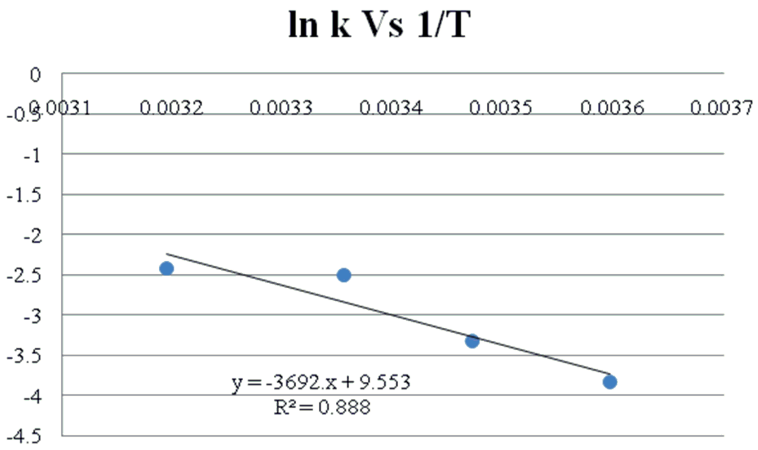

FIG. 9: Plots of ln k vs. 1/T for the Knoevenagel condensation catalyzed by PEG supported proline

ACKNOWLEDGMENT

This work was supported by the University Grants Commission, India, under the UGC–SAP, BSR programmes. Some of the instrumental facilities were procured through TEQIP.

REFERENCES

An-guo, Y., Luo, L.I.U., Guo-feng, W.U., Xin-zhi, C., and Wei-dong, Y.E., Knoevenagel Condensation Catalyzed by DBU Brönsted Ionic Liquid without Solvent, *Chem. Res. Chin. Univ.*, vol. **25**, no. 6, pp. 876–881, 2009.

Bergbreiter, D.E. and Sung, S.D., Liquid/Liquid Biphasic Recovery/Reuse of Soluble Polymer-Supported Catalysts, *Adv. Synth. Catal.*, vol. **348**, nos. 12-13, pp. 1352–1366, 2006.

Bigi, F., Conforti, M.L., Maggi, R., and Piccinno, A., Clean Synthesis in Water: Uncatalysed Preparation of Ylidenemalononitriles, *Green Chem*., vol. **2**, pp. 101–103, 2000. DOI:10.1039/b001246g

Boronat, M., Climent, M.J., Corma, A., Iborra, S., Montn, R., and Sabater, M.J., Bifunctional Acid–Base Ionic Liquid Organocatalysts with a Controlled Distance between Acid and Base Sites, *Chem. Eur. J*., vol. **16**, pp. 1221–1231, 2010. DOI:10.1002/chem.200901519

Cecchini, M.M., Charnay, C., De Angelis, F., Lamaty, F., Martinez, J., and Colacino, E., Poly(Ethylene Glycol)-Based Ionic Liquids: Properties and Uses as Alternative Solvents in Organic Synthesis and Catalysis, *ChemSusChem*, vol. **7**, no. 1, pp. 45–65, 2014.

Delgado, F., Tamariz, J., Zepeda, G., Landa, M., Miranda, R., and García, J., Knoevenagel Condensation Catalyzed by a Mexican Bentonite using Infrared Irradiation, *Synth. Commun.*, vol. **25**, no. 5, pp. 753–759, 1995.

Jenner, G., Steric Effects in High Pressure Knoevenagel Reactions, *Tetrahedron Lett.*, vol. **42**, pp. 243–245, 2001.

Herrmann, W.A. and Kohlpaintner, C.W., Water-Soluble Ligands, Metal Complexes, and Catalysts: Synergism of Homogeneous and Heterogeneous Catalysis, *Angew. Chem., Int. Ed. Engl.*, vol. **32**, no. 11, pp. 1524–1544, 1993.

Hu, Y., Chen, J., Le, Z.G., Zheng, Q.G., and Chen, J., Organic Reactions in Ionic Liquids: Ionic Liquids Ethylammonium Nitrate Promoted Knoevenagel Condensation of Aromatic Aldehydes with Active Methylene Compounds, *Synth. Commun.*, vol. **35**, pp. 739–744, 2005.

Knoevenagel, E., Condensation of Malonic Acid with Aromatic Aldehydes via Ammonia and Amines, *Ber. Dtsch. Chem. Ges.*, vol. **31**, no. 3, pp. 2596–2619, 1898. DOI:10.1002/cber.18980310308

List, B., Proline-Catalyzed Asymmetric Reactions, *Tetrahedron*, vol. **58**, no. 28, pp. 5573–5590, 2002.

Liu, C., Li, X., and Jin, Z., Progress in Thermoregulated Liquid/Liquid Biphasic Catalysis, *Catal. Today*, vol. **247**, pp. 82–89, 2015.

Liu, Y., Liang, J., Liu, X.H., Fan, J.C., and Shang, Z.C., Polyethylene Glycol (PEG) as a Benign Solvent for Knoevenagel Condensation, *Chin. Chem. Lett*., vol. **19**, pp. 1043–1046, 2008.

Majumdar, K.C., Taher, A., and Nandi, R.K., Synthesis of Heterocycles by Domino-Knoevenagel-Hetero-Diels-Alder Reactions, *Tetrahedron*, vol. **68**, no. 29, pp. 5693–5718, 2012.

McNulty, J., Steere, I.J.A., and Wolf, S., The Ultrasound Promoted Knoevenagel Condensation of Aromatic Aldehydes 2R = OH, *Tetrahedron Lett.*, vol. **39**, pp. 8013–8016, 1998.

Medien, H.A.A., Kinetic Studies of Condensation of Aromatic Aldehydes with Meldrum's Acid, vol. **57b**, pp. 1320–1326, 2002.

Memarian, H.R. and Soleymani, M., Ultrasound Assisted Dehydrogenation of 2-Oxo-1,2,3,4-Tetrahydropyrimidine-5-Carboxamides, *Ultrason. Sonochem.*, vol. **18**, no. 3, pp. 745–752, 2011.

Ogiwara, Y., Takahashi, K., Kitazawa, T., and Sakai, N., Indium (III)-Catalyzed Knoevenagel Condensation of Aldehydes and Activated Methylenes using Acetic Anhydride as a Promoter, *J. Org. Chem*., vol. **80**, pp. 3101–3110, 2015.

Patil, Y.P., Tambade, P.J., Jagtap, S.R., and Bhanage, B.M., Synthesis of 2-Oxazolidinones/2-Imidazolidinones from CO_2, Different Epoxides and Amino Alcohols/Alkylene Diamines using Br-Ph3+P-PEG600-P+Ph3Br- as Homogenous Recyclable Catalyst, *J. Mol. Catal. A: Chem.*, vol. **289**, nos. 1-2, pp. 14–21, 2008.

Jenner, G., Steric Effects in High Pressure Knoevenagel Reactions, *Tetrahedron Lett.*, vol. **42**, pp. 243–245, 2001.

Senapati, K.K., Borgohain, C., and Phukan, P., Synthesis of Highly Stable $CoFe_2O_4$ Nanoparticles and their Use as Magnetically Separable Catalyst for Knoevenagel Reaction in Aqueous Medium, *J. Mol. Catal. A: Chem.*, vol. **339**, nos. 1-2, pp. 24–31, 2011.

Siddiqui, Z.N. and Khan, T., Sulfuric Acid-Modified PEG-6000 (PEG-OSO3H): A Biodegradable, Reusable Solid Acid Catalyst for Highly Efficient and Eco-Friendly Synthesis of Novel Bis-Knoevenagel Products under Solvent-Free Conditions, *Tetrahedron Lett.*, vol. **54**, no. 29, pp. 3759–3764, 2013.

Sun, Z., Wang, Y., Niu, M., Yi, H., Jiang, J., and Jin, Z., Poly(Ethylene Glycol)-Stabilized Rh Nanoparticles as Efficient and Recyclable Catalysts for Hydroformylation of Olefins, *Catal. Commun.*, vol. **27**, pp. 78–82, 2012.

Tietze, L.F., Domino Reactions in Organic Synthesis, *Chem. Rev.*, vol. **96**, pp. 115–136, 1996.

Wang, S., Ren, Z., Cao, W., and Tong, W., The Knoevenagel Condensation of Aromatic Aldehydes with Malononitrile or Ethyl Cyanoacetate in the Presence of CTMAB in Water, *Synth. Commun.*, vol. **31**, no. 5, pp. 673–677, 2001.

Zhi, H., Lu, C., Zhang, Q., and Luo, J., A New PEG-1000-Based Dicationic Ionic Liquid Exhibiting Temperature-Dependent Phase Behavior with Toluene and its Application in One-Pot Synthesis of Benzopyrans, *Chem. Commun.*, vol. **20**, pp. 2878–2880, 2009. DOI:10.1039/b822481a

HYDROGENOLYSIS OF GLYCEROL: COMPARISON OF CONTINUOUS AND BATCH MODE REACTIONS OVER Ni-ZnO CATALYSTS

Miryala Balaraju, Voggu Rekha, Narsinga Raju, & Nakka Lingaiah*

Catalysis Laboratory, I&PC Division, CSIR-Indian Institute of Chemical Technology, Hyderabad-500 007, Telangana, India

*Address all correspondence to: Nakka Lingaiah, Catalysis Laboratory, I&PC Division, CSIR-Indian Institute of Chemical Technology, Hyderabad-500 007, Telangana, India; Tel.: +91 40 27191722, E-mail: nakkalingaiah@iict.res.in

Original Manuscript Submitted: 6/7/2017; Final Draft Received: 10/28/2017

Ni-Zn mixed oxide catalysts with varying mole ratios were prepared by the coprecipitation method. These catalysts were characterized by Brunauer-Emmett-Teller (BET) surface area, X-ray diffraction, temperature programmed reduction, H_2 chemisorption, transmission electron microscopy, and X-ray photoelectron spectroscopy. Selective hydrogenolysis of glycerol to 1,2-propanediol was carried out with these catalysts both in continuous (fixed bed) and batch (liquid phase) conditions. Higher glycerol conversion was achieved in a fixed bed than in liquid phase glycerol hydrogenolysis. The selectivity to 1,2-propanediol was more in batch mode hydrogenolysis, whereas acetol is the main product in the continuous mode. The activity of catalysts depended on the Ni to Zn mole ratio, which in turn influenced the metal surface area of Ni on ZnO. The catalyst with a Ni to Zn mole ratio of 2 exhibited the highest activity. The observed activity was corroborated with the derived physicochemical properties of the catalysts. Different reaction parameters were studied and optimum reaction conditions were established.

KEY WORDS: *glycerol, hydrogenolysis, 1,2-propanediol, nickel, zinc*

1. INTRODUCTION

Glycerol, the by-product of the biodiesel industry, is a potential biorefinery feedstock (Hu et al., 2013). Glycerol has a great number of common applications and has been used in pharmaceuticals, cosmetics, soaps, toothpastes, candies, cakes, and as a wetting agent in tobacco (Pachauri and He, 2006; Pagliaro et al., 2007). Even though it has lot of applications, it is creating a glut in the global market due to the biodiesel industry (Hosgun et al., 2012). The usage of low-grade glycerol obtained from biodiesel production is a big challenge, as this glycerol cannot be used for food and cosmetic applications (Balaraju et al., 2010). An effective usage or conversion of crude glycerol to specific products will cut down the biodiesel production costs (Len and Luque, 2014).

Glycerol is a highly functionalized molecule and a variety of value added chemicals can be produced by catalytic conversion through different reactions (Len and Luque, 2014). Catalytic conversion of crude glycerol to value added chemicals by a green catalytic process is a challenging area of research. It is required to develop a highly active heterogeneous catalyst to produce desired chemicals using crude glycerol. 1,2-Propanediol or propylene glycol (1,2-PDO) is an important commodity chemical. It can be produced through selective hydrogenolysis of glycerol (Balaraju et al., 2009). 1,2-PDO and its derivatives are used in the synthesis of polyester resins, liquid detergents, pharmaceuticals, cosmetics, tobacco humectants, flavors and fragrances, personal care, paints, animal feed, antifreeze, etc. (Sharma et al., 2014; Balaraju et al., 2008). It is an alternative to toxic ethylene glycol as a deicing or antifreeze agent. Traditionally, propylene glycol was produced from propylene oxide and propylene which are derived from petrochemical sources (Zhengxi et al., 2009). The demand for 1,2-PDO is increasing day by day with a 4% annual growth in the

global market (Zhou et al., 2008). Glycerol can be converted to 1,2-PDO using heterogeneous, homogeneous, or biocatalysts (Len and Luque, 2014). Catalytic conversion of glycerol to propylene glycol with a heterogeneous catalyst is an attractive process from an economic and environmental perspective.

Generally, selective hydrogenolysis of glycerol to 1,2-PDO has been carried out in liquid phase batch with with H_2 pressure between 100 and 250 bars at 150°C–320°C with heterogeneous catalysts (Casale and Gomez, 1994, 1993). Two types of catalysts are reported for the glycerol hydrogenolysis reaction. Supported noble metal (Ru, Rh, Pd, Pt) catalysts and catalysts containing transition metal oxides (Cu-ZnO/Al_2O_3, Cu/SiO_2, Cu chromite, Raney Ni) are used for synthesis of 1,2-PDO (Pavan Kumar et al., 2015; Montes et al., 2014; Li et al., 2014; Yuanqing et al., 2014; Xiao et al., 2013; Huang et al., 2008). Supported ruthenium metal catalysts are identified as better catalysts for obtaining high glycerol conversions. The drawback of Ru catalysts was related to their low selectivity as they break the C-C bond over the C-O bond of glycerol during the hydrogenolysis reaction, which leads to degradative products like lower alcohols. Moreover, Ru catalysts require acid cocatalysts for high glycerol conversion (Balaraju et al., 2009). Cu-based catalysts are better compared to Ru catalysts for obtaining high 1,2-PDO selectivity under mild reaction conditions.

Cu-based catalysts showed greater performance in the selective formation of 1,2-PDO. Cu-ZnO, Cu-SiO_2, and Cu-Al_2O_3 catalysts are reported as selective catalysts under mild reaction conditions (Yuanqing et al., 2014; Guo et al., 2009; Bienholz et al., 2010). However, overall conversion of glycerol is limited compared to Ru-based catalysts. Ni-based mixed oxide catalysts are also active for selective hydrogenolysis of glycerol. Dasari et al. (2005) studied hydrogenolysis of glycerol over commercial Raney Ni, Ni/C, and Ni/silica-alumina catalysts and achieved about 69% of selectivity towards 1,2-PDO. Meher et al. (2009) used a Ni/Mg/Al catalyst to convert glycerol into propylene glycol. However, the glycerol conversion and selectivity were poor. Yu et al. reported Ni/AC and Ni-Ce/AC catalysts for hydrogenolysis of glycerol and achieved good conversion with considerable selectivity (Yu et al., 2010; Lin et al., 2014). Even though Ni-based catalysts are used for glycerol hydrogenolysis, detailed studies about the role of its structural and surface characteristics in glycerol hydrogenolysis have not been explored. Supported Ni catalysts are well studied. There is no consensus about the support and its role. ZnO is an important support in Cu-based catalysts for glycerol hydrogenolysis (Bienholz et al., 2010; Wang et al., 2010). It will be interesting to deduce the role of ZnO in Ni-Zn catalysts. ZnO possesses an amount of appropriate acidity to catalyze the dehydration of glycerol to form acetol where this step is the initial one in glycerol hydrogenolysis. ZnO has a considerable amount of acidity and it stabilizes metal species on surface. Many researchers reported low selectivity towards 1,2-PDO over supported Ni catalysts for glycerol hydrogenolysis (Dasari et al., 2005; Meher et al., 2009; Yu et al., 2010; Lin et al., 2014). It is anticipated that dispersing Ni on ZnO will enhance the conversion and selectivity in glycerol hydrogenolysis.

In the present study, a series of Ni-ZnO catalysts were prepared with varying Ni to Zn ratio and studied for selective hydrogenolysis of glycerol both in continuous and batch mode operations. The aim of the study is to understand the influence of structural and surface characteristics of the catalysts on glycerol hydrogenolysis activity. A detailed study undertook to optimize the reaction parameters to achieve optimum results.

2. EXPERIMENTAL

2.1 Catalyst Preparation

Ni-Zn oxide catalysts with varying Ni/Zn mole ratios were prepared by the coprecipitation method. Calculated amounts of aqueous solutions containing $Ni(NO_3)_2{\cdot}6H_2O$ and $Zn(NO_3)_2{\cdot}6H_2O$ were taken and precipitated by dropwise addition of a 0.5M solution of potassium carbonate under vigorous stirring. The concentrations of Ni^{2+} and Zn^{2+} in the solutions were varied to change the Ni/Zn mole ratio. After completion of precipitation, the obtained suspension was stirred for 12 h. The solution was filtered and washed thoroughly with distilled water. The solid mass was dried in an oven overnight at 120°C and finally calcinated in air at 500°C for 3 h. The catalysts were designated as NiZn-12, NiZn-11, NiZn-21, and NiZn-31 where the numerical numbers indicate the number of moles of Ni and Zn, respectively.

2.2 Catalysts' Characterization

The surface area, pore volume, and average pore diameter of the samples were measured by N_2-physisorption at –196°C using Micromeritics ASAP 2000 instrument. Approximately 0.2 g of sample was used for each analysis. The moisture and other adsorbed gases present in the sample were removed before analysis by degassing the sample at 200°C for 2 h.

X-ray powder diffraction (XRD) patterns of the catalysts were recorded on a Rigaku Miniflex (Rigaku Corporation, Japan) X-ray diffractometer using Ni-filtered Cu $K\alpha$ radiation ($\lambda = 1.5406$ Å) with a scan speed of 2° min^{-1} and a scan range of 10°–80°at 30 kV and 15 mA.

Temperature programmed reduction (TPR) of the catalysts was carried out in a flow of a 5% H_2/Ar mixture gas at a flow rate of 60 mL/min with a temperature ramp of 10°C/min. Before the TPR run the catalysts were pretreated in Ar at 300°C for 2 h. The hydrogen consumption was monitored using a thermal conductivity detector.

Temperature programmed desorption of ammonia (TPDA) was carried out on a laboratory-built apparatus equipped with a gas chromatograph using a TCD detector. In a typical experiment about 0.05 g of the oven-dried sample was taken in a quartz tube. Prior to TPDA studies, the catalyst sample was treated at 300°C for 1 h by passing pure helium (99.9%, 50 mL/min). After pretreatment, the sample was saturated with anhydrous ammonia (10% NH_3) at 100°C at a flow rate of 50 mL/min for 1 h and subsequently flushed with He gas at the same temperature to remove physisorbed ammonia. The process was continued until a stabilized base line was obtained in the gas chromatograph. Then the TPD analysis was carried out from ambient temperature to 700°C at a heating rate of 10°C/min. The amount of NH_3 evolved was calculated from the peak area of the already calibrated TCD signal.

Hydrogen chemisorption measurements were carried out on an AutoChem 2910 instrument. Prior to adsorption measurements, about 0.1 g of the sample was reduced in a flow of hydrogen (30 mL/min) at 450°C for 2 h and flushed out subsequently in Ar gas flow for 1 h at the same temperature. The sample was subsequently cooled to ambient temperature in the same Ar gas stream. Hydrogen uptake was determined by injecting pulses of 5% H_2 balanced Ar from a calibrated online sampling valve into the Ar stream passing over reduced samples. The nickel surface area was calculated assuming a stoichiometry of one hydrogen molecule per two surface nickel atoms and by taking an atomic cross-sectional area of 6.49×10^{-20} m^2/Ni atom. Adsorption was deemed to be complete after at least three successive peaks showed similar areas.

XPS measurements were conducted on a Kratos AXIS 165 with a dual anode (Mg and Al) apparatus using the Mg $K\alpha$ anode. The nonmonochromatized Al $K\alpha$ X-ray source ($h\nu = 1486.6$ eV) was operated at 12.5 kV and 16 mA. Before acquisition of the data the sample was outgassed for about 3 h at 100°C under a vacuum of 1.0×10^{-7} Torr to minimize surface contamination. The XPS instrument was calibrated using Au as the standard. For energy calibration, the carbon $1S$ photoelectron line was used. The carbon $1S$ binding energy was taken as 285 eV. Charge neutralization of 2 eV was used to balance the charge-up of the sample. The spectra were deconvoluted using the Sun Solaris based Vision-2 curve resolver. The location and the full width at half maximum (FWHM) value for the species were first determined using the spectrum of the pure sample. Symmetric Gaussian shapes were used in all cases. Binding energies for identical samples were, in general, reproducible within $\pm$ 0.1 eV.

The morphology features of the catalysts were characterized by transmission electron microscopy (TEM). TEM investigations were carried out using a Philips CM20 (100 kV) transmission electron microscope equipped with a NARON energy-dispersive spectrometer with a germanium detector. The specimens were prepared by dispersing the samples in methanol using an ultrasonic bath and evaporating a drop of resultant suspension onto the Lacey carbon support grid. The sizes of the catalyst particles were measured by digital micrograph software (version 3.6.5, Gatan Inc.).

2.3 Activity Measurements

2.3.1 Batch Mode Hydrogenolysis of Glycerol

Hydrogenolysis of glycerol was carried out in a 100-mL Hastelloy PARR 4843 autoclave. An aqueous glycerol solution (50 wt%) was used as the feed. Prior to the reaction, the catalyst was reduced at 500°C for 3 h with H_2 flow (30 mL/min). In a typical run, 50 g of the aqueous glycerol solution and 1 g of the catalyst were loaded into

the reactor. The autoclave was purged with H_2 flow to drive off the air present in it. After the purge, the reaction temperature and hydrogen pressure were raised to required levels. During the reaction it was observed that a decrease in hydrogen pressure and the pressure compensated by passing H_2 gas.

2.3.2 Fixed Bed Hydrogenolysis of Glycerol

Hydrogenolysis of the glycerol reaction was carried out in a fixed bed reactor under atmospheric pressure. In a typical experiment, about 1 g of catalyst was suspended between two quartz wool plugs of a tubular reactor and was reduced in a flow of hydrogen (30 mL/min) at 500°C for 3 h prior to the reaction. After bringing the temperature of the catalyst bed to 250°C, H_2 (240 mL/min) and 50 wt% aqueous glycerol solution were introduced into the reactor through a heated evaporator by means of a microprocessor-based feed pump (Braun Corporation, Germany). The liquid products were collected in a condenser in order to be analysed by gas chromatography.

2.4 Product Analysis

In the case of glycerol hydrogenolysis in batch mode, the autoclave was allowed to cool down to room temperature and the gas products were collected in a gas bag and the liquid products were separated from the catalyst by filtration. These products were analyzed using a gas chromatograph (Shimadzu, 2010) equipped with a flame ionization detector (FID) by separating products on an INNOWax capillary column (30 m $\times$ 0.32 mm $\times$ 0.5 mm). The products were also identified by using GC-MS (Shimadzu, GCMS-QP2010S). The gas phase products were analyzed by a gas chromatograph equipped with Porapak Q column and thermal conductivity detector. The products identified during glycerol hydrogenolysis are 1,2-PDO, 1-hydroxypropan-2-one commonly known as acetol, 1-propanol (1-PO), and 2-propanol (2-PO) as hydrogenolysis products and ethylene glycol (EG), ethanol, methanol, ethane and methane are as degradation products. The details of the calculation for glycerol conversion and selectivity were reported elsewhere (Balaraju et al., 2010).

3. RESULTS AND DISCUSSION

3.1 Catalyst Characterization

The physicochemical properties of the catalysts are reported in Table 1. As the Ni/Zn mole ratio increased from 0.5 to 1, the specific surface area of the catalysts increased from 14 to 20 m^2/g. Thereafter surface area, pore volume, and pore diameter were marginally decreased due to the pore blockage by the crystallites of NiO.

Powder X-ray diffraction patterns of calcined Ni-Zn mixed oxide catalysts with varying Ni to Zn mole ratios are presented in Fig. 1. XRD patterns of the pure NiO and ZnO were included in the figure for the sake of comparison. The patterns related to the crystallite phases of ZnO and NiO were noticed. NiO peaks appeared at 2θ value of 37.3°,

TABLE 1: Physicochemical properties of Ni-based catalysts

Catalyst	Molar Ratio (Ni/Zn)	BET Surface Area (m^2/g)	Total Pore Volume (cm^3/g)	Pore Diameter (nm)	Ni Metal Surface Area* (m^2/g)	#Acidity $\times 10^{-4}$ moles	Particle size (nm)	
							NiO	ZnO
NiZn-12	0.5	14	0.059	16.4	14.2	5.4	19.2	39.7
NiZn-11	1	20	0.084	16.6	21.3	4.1	22.4	30.9
NiZn-21	2	17	0.057	13.7	24.2	3.9	22.4	27.9
NiZn-31	3	13	0.032	10.4	20.3	2.9	26.7	25.2

*Ni metal surface area determined from H_2 chemisorption; #acidity of catalyst measured by NH_3 desorption studies.

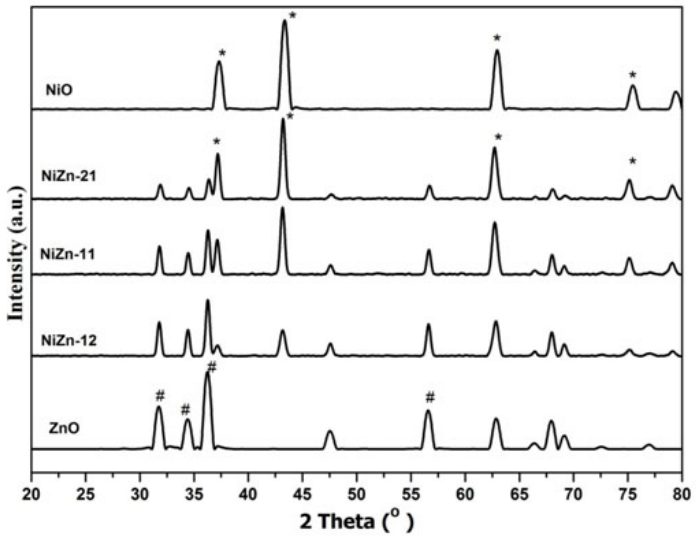

FIG. 1: X-ray diffraction patterns of calcined Ni-ZnO catalysts. (*) NiO, (@) Ni, (#) ZnO phases

43.3°, 62.9°, and 75.4°, which represent the indices of (111), (200), (220), and (311) planes of NiO, respectively. This shows the presence of face-centered structure of NiO in Ni-Zn catalysts. The patterns related to ZnO are observed at 2θ values of 31.8, 34.4, 36.3, and 56.6. There were no patterns related to the mixed Ni-Zn phase, nor for any Ni^{3+} species. Crystallite sizes of NiO and ZnO were calculated using the Debye-Scherrer equation and are shown in Table 1. As expected the crystallite size of NiO increased with increase of Ni loading in the catalysts. Similar behavior was also observed for ZnO. The catalyst with a Ni/Zn mole ratio of 2 had relatively small crystallite sizes compared to other catalysts.

TPR profiles of the samples are presented in Fig. 2. Ni-Zn samples have shown broad reduction peaks between 400°C and 550°C, which are attributed to single-step reduction of Ni^{2+} to Ni^0. This broad peak was a result of the reduction of NiO particles which were present in the surface and bulk of the support (Chin et al., 2009). It is known

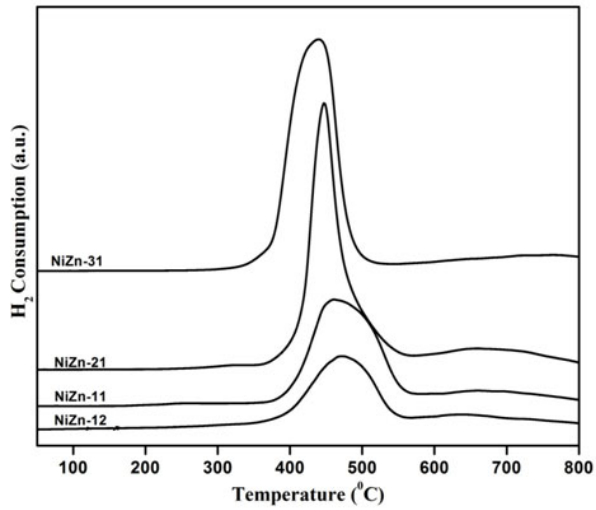

FIG. 2: Temperature programmed reduction profiles of Ni-ZnO catalysts

that the low-temperature peaks can be assigned to the reduction of the relatively noninteracted NiO species, while the high-temperature peaks can be attributed to the reduction of complex NiO species, which were strongly interacted with the support (Koo et al., 2009). As the Ni content increases, the reduction peak shifted toward low temperature which suggests the reduction of noninteracted NiO on the support. The high-temperature reduction was observed for the catalysts with low Ni content. The results envisage that the NiO particles are well dispersed on ZnO in the catalysts with low Ni/Zn ratio. TPR patterns suggested that the intensity of the reduction peak increased with nickel loading. This increase is related to the presence of easily reducible NiO on the support as is expected with the presence of a large amount of Ni. The presence of intense XRD peaks corresponding NiO suggests the easy reduction of NiO for the sample with more Ni content.

The ammonia adsorption-desorption technique usually enables the determination of the strength of acid sites present on a catalyst surface together with total acidity. The total acidity values of the catalysts were estimated from TPD analysis and are shown in Table 1. All the Ni-Zn catalysts showed a broad desorption peak related to the acidity of ZnO. This reveals that the surface acid strength is widely distributed. The acid strength of the NiZn-12 catalyst was found to be 5.4×10^{-4} moles/g. As the Ni/Zn mole ratio of the catalysts varied from 0.5 to 3, the acidity of the catalysts decreased from 5.4×10^{-4} to 2.9×10^{-4} moles/g. The results suggests that the acidity of the catalysts was influenced by ZnO content.

The metal surface area of Ni was measured by hydrogen chemisorption; the results are summarized in Table 1. It is generally known that Ni is an active metal for hydrogenation reactions including glycerol hydrogenolysis and alcohol steam reforming reactions (Yu et al., 2010; Chin et al., 2009; Yang et al., 2006). The Ni metal surface area increased with increase in the Ni to Zn ratio and the NiZn-21 catalyst exhibited about 24.2 m^2/g Ni metal area. Further enhancement in Ni content did not lead to an increase in Ni metal area as the dispersion of Ni attained a maximum. This is due to the presence of large crystallites of Ni as revealed by XRD and TPR analysis.

TEM analysis was carried out to know the morphology of the Ni-Zn catalysts. The micrograph of the NiZn-21 catalyst is shown in Fig. 3. NiO particles in the as-prepared catalyst were well spread over ZnO support. In order to investigate the dispersion, the particle size distribution was measured for a representative NiZn-21 catalyst from the TEM micrograph. The NiZn-21 catalyst has a broad particle size distribution. The average size of metal oxide particles was in between $\sim$ 30–40 nm. The TEM results demonstrated the high and uniform dispersion of NiO on ZnO support.

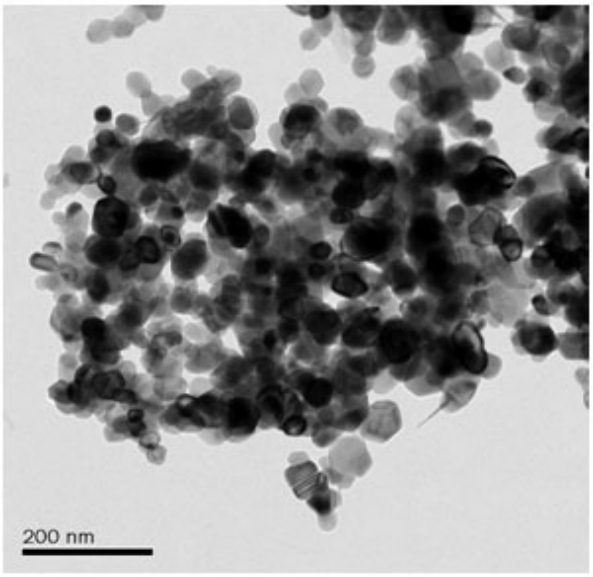

FIG. 3: TEM micrograph of NiZn-21 catalyst

3.2 Glycerol Hydrogenolysis Activity Measurements

3.2.1 Glycerol Hydrogenolysis Activity of Ni-Zn Catalysts in Batch and Continuous Mode Operation

In order to know the variation in the activity when the selective hydrogenolysis of glycerol is carried out in both batch and fixed bed conditions, the reaction was carried out using the NiZn-11 catalyst. The results obtained during batch and fixed bed hydrogenolysis are shown in Table 2. Glycerol conversion was higher in the fixed bed operation compared to liquid phase hydrogenolysis. However, the selectivity to 1,2-PDO was poor in continuous mode of operation. It is known that glycerol undergoes dehydration to acetol in the first step and subsequently acetol will be hydrogenated to 1,2-PDO on metallic sites (Montes et al., 2014; Wang and Liu, 2007). Acetol is the main product during continuous fixed bed operation. High acetol formation in fixed bed reaction confirms that the reaction mechanism of hydrogenolysis of glycerol to 1,2-PDO proceeds through dehydration-hydrogenation steps. From the observed results, it was concluded that the hydrogenolysis reaction proceeds via a two-step mechanism in the presence of the Ni-Zn catalyst.

Akiyama et al. (2009) effectively discussed fixed bed hydrogenation of glycerol to 1,2-PDO using equilibrium constants which were obtained from the data of hydrogenation of acetol. Optimum reaction temperatures are different for the dehydration and the hydrogenation steps involved glycerol hydrogenolysis. Hence, the high yield of about 96% of 1,2-PDO at gradient temperatures of 200°C for dehydration and 120°C for hydrogenation was achieved over Cu/Al_2O_3 in high hydrogen concentration. The present reactions were carried out at a constant temperature of 250°C. Low residence time of the reactants with relatively less hydrogen concentration and high constant reaction temperature under fixed bed conditions could be the main reasons for low activity towards 1,2-PDO. Interestingly, the selectivity towards EG is relatively more than 1,2-PDO in the fixed bed mode of operation.

3.2.2 Effect of Ni/Zn Mole Ratio on Glycerol Hydrogenolysis Activity

The effect of the Ni/Zn mole ratio on the hydrogenolysis activity in batch and continuous mode operation was studied; the results are shown in Table 3. The results suggested that with increasing the Ni/Zn mole ratio, the glycerol conversion increased up to a Ni/Zn ratio of 2. The activity of the catalyst was marginally decreased with further increase in the Ni/Zn mole ratio for both batch and continuous mode conditions. In the batch mode reaction, about 21% conversion for the catalyst with Ni/Zn ratio of 0.5 was observed, which increased up to 45.2% for the catalyst with a Ni/Zn ratio of 2. The selectivity to 1,2-PDO was always high (up to 93%) for all Ni-Zn catalysts. About 57% of glycerol conversion was achieved with the NiZn-21 catalyst in continuous mode operation. The Ni/Zn mole ratio of the catalysts has limited influence on glycerol conversion. A marginal increase in conversion was noticed and the product distribution is persistently the same. From these results it can be concluded that the Ni/Zn ratio has significant influence on glycerol conversion under batch mode conditions. A similar effect is marginal under continuous mode operation.

The conversion and selectivity depends on how efficiently the catalyst dehydrates glycerol and its subsequent hydrogenation. Hydrogenolysis of glycerol into 1,2-PDO over bifunctional catalysts has been explained to take place via dehydration followed by hydrogenation. There are contradictory reports available in the literature describing the

TABLE 2: Glycerol hydrogenolysis activity with Ni-Zn catalyst in batch and continuous mode

Mode of Reaction	Conversion (%)	Selectivity (%)			
		1,2-PDO	EG	Acetol	Others
Batch	30.2	93.8	2.5	1.9	1.8
Continuous	55.9	9.1	20.7	63.9	6.3

Batch mode conditions: 50 wt% glycerol conc.: 50 g; H_2 pressure: 40 bars; reaction time: 8 h; reaction temperature: 200°C; catalyst wt: 1 g. *Continuous mode conditions*: 50 wt% glycerol conc.: 5 mL/h; H_2 flow: 240 mL/min; reaction temperature: 250°C; catalyst wt: 1 g.

TABLE 3: Influence of Ni/Zn mole ratio of Ni-Zn catalysts on glycerol hydrogenolysis activity in batch and continuous mode

Catalyst	Ni/Zn Mole Ratio	Conversion (%)	Selectivity (%)			
			1,2-PDO	EG	Acetol	Others
NiZn-12	0.5	21.2 (51.5)	92.9 (5.8)	2.1 (13.1)	2.5 (68.7)	2.5 (12.4)
NiZn-11	1	30.2 (55.9)	93.8 (9.1)	2.5 (20.7)	1.9 (63.9)	1.8 (6.3)
NiZn-21	2	45.2 (57.2)	94.3 (12.5)	3.1 (20.2)	1.1 (60.8)	1.5 (6.5)
NiZn-31	3	35.8 (45.2)	92.5 (8.5)	2.9 (18.8)	0.9 (60.5)	3.7 (12.2)

Reaction condition (batch mode operation): 50 wt% glycerol conc.: 50 g; H_2 pressure: 40 bars; reaction time: 8 h; reaction temperature: 200°C, catalyst wt: 1 g. *(Continuous mode operation)*: 50 wt% glycerol conc.: 5 mL/h; H_2 flow: 240 mL/min; reaction temperature: 250°C; catalyst wt: 1 g.
Values in parentheses correspond to continuous mode operation.

nature of active sites responsible for acetol formation. The well-known reaction mechanism is the dehydration of glycerol to acetol on acidic sites of the catalysts. Kim et al. (2011) reported that acrolein is formed with the catalysts having Bronsted acid sites whereas acetol is formed on the concentration of Lewis acid sites. Kinage et al. (2010) described the acetol formation over sodium-doped metal oxide catalysts, by a dehydrogenation process followed by dehydration and enolization. On the other hand, some other researchers reported that the metal sites also might be involved in the dehydration of glycerol to acetol. As describd by Suprun et al. (2011), the redox properties of metal oxide catalysts could also influence the dehydration of glycerol. The reduced copper catalysts were effective for the dehydration of glycerol to hydroxyacetone via Cu-alkoxide species formed by the release of an OH radical from the primary OH groups, as reported by Sato et al. (2008). According to Bienholz et al. (2011), there was a linear relationship between the copper surface area and the reaction rate of both dehydration and hydrogenation reactions. The catalysts with large metal surface areas are desirable in order to obtain high yields of 1,2-PDO in the hydrogenolysis of glycerol.

The above works suggest that apart from acidic sites, metallic sites of the catalyst may also be involved in the formation of acetol which is a key step in glycerol conversion. This could be the reason for the higher activity of the NiZn-21 catalyst even though it has a ow amount of ZnO content. The present results of the NiZn-21 catalyst support the hypothesis about the participation of metal sites in both glycerol dehydration to acetol and subsequent hydrogenation to 1,2-PDO. The activity of the present catalyst depends on the specific Ni surface area on the support. The Ni particles may be involved in the dehydration of glycerol to acetol and subsequently hydrogenate to 1,2-PDO. A linear relationship between hydrogenolysis activity and the Ni metal area was observed. The catalyst with a high Ni metal surface showed the maximum conversion of glycerol. A considerable amount of ZnO is also needed to stabilize and disperse the Ni particles over the support. The NiZn-21 catalyst has a high metallic surface area among all catalysts with a reasonable amount of ZnO crystallites (Table 1) showing higher activity. The decrease in conversion with a high Ni content catalyst might be due to the insufficient number of active sites as this catalyst showed a decrease in Ni metal area and acidity.

3.2.3 Effect of Reaction Temperature

Reaction temperature has a significant effect on the conversion and selectivity during glycerol hydrogenolysis (Behr et al., 2008; Dasari et al., 2005). The effect of reaction temperature was studied in the NiZn-21 catalyst; the results are presented in Table 4. As the temperature increased a gradual increase in glycerol conversion from 3.6% to 75%

TABLE 4: Effect of reaction temperature during glycerol hydrogenolysis over NiZn-21 catalyst

Reaction Temperature (°C)	Conversion (%)	Selectivity (%)		
		1,2-PDO	EG	Others
160	3.6	90.5	5.1	4.4
180	15.6	93.3	2.7	4.0
200	45.2	94.3	3.1	2.6
220	65.5	60.8	5.2	34.0
240	75.7	45.1	1.9	53.0

Reaction conditions: 50 wt% glycerol conc.: 50 g; H_2 pressure: 40 bars; reaction time: 8 h; catalyst wt: 1 g.

was observed with the increase in reaction temperature from 160°C to 240°C. The selectivity to desired 1,2-PDO is constant up to 200°C and further increase in temperature led to a decrease in selectivity of 1,2-PDO. High temperature favors the breaking of C-C and C-O bonds which leads to degradative products. The low selectivity to 1,2-PDO at high temperatures is because of the formation of secondary products like lower alcohols (methanol, ethanol) and gaseous products like methane, ethane, and propane. High 1,2-PDO selectivity with reasonable glycerol conversions was obtained at a reaction temperature of 200°C.

3.2.4 Effect of Reaction Time

The influence of reaction time on the conversion of glycerol and propylene glycol selectivity at different reaction times was evaluated for the NiZn-21 catalyst; the results are shown in Fig. 4. About 25% of glycerol conversion with 93% selectivity towards 1,2-PDO was achieved within 4 h of reaction time. A linear relationship was noticed between glycerol conversion and reaction time. Glycerol conversion was increased up to 62% when the reaction was carried out for 12 h and thereafter the increase in conversion was marginal. In earlier studies, the glycerol hydrogenolysis reaction was carried at long reaction times (> 24 h) to obtain reasonable conversion (Chaminand et al., 2004). The present catalyst exhibited about 45.2% conversion within 8 h even with 50% glycerol solution. Cu-based catalysts

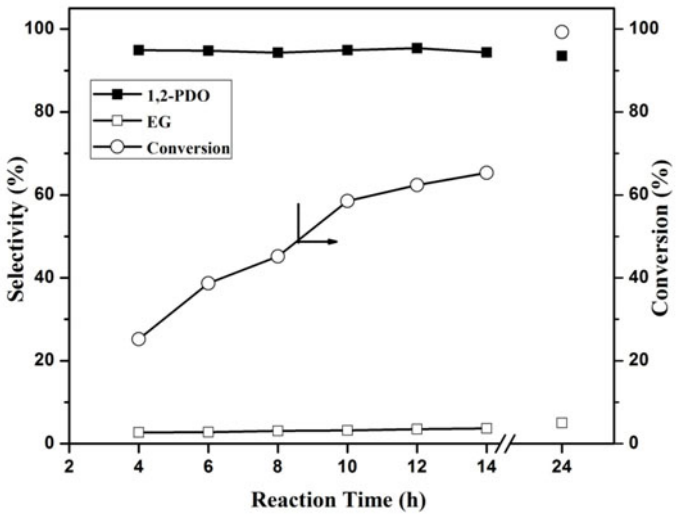

FIG. 4: Influence of reaction time during the glycerol hydrogenolysis with NiZn-21 catalyst

took longer reaction time to obtain reasonable conversion even with 20% glycerol solution (Balaraju et al., 2008; Chaminand et al., 2004). The present catalyst is selective in forming 1,2-PDO with more than 90% during the period of reaction time, which is up to 16 h. The reaction was carried out further, up to 24 h, to achieve 100% conversion. At this reaction time also the catalysts showed similar selectivity as obtained at lower reaction times. These results indicate that the products are not decomposed during the long reaction time with the present catalyst.

3.2.5 Effect of Catalyst Weight

The effect of catalyst weight on the conversion of glycerol to propylene glycol with the NiZn-21 catalyst was studied; the results are shown in Fig. 5. The glycerol conversion and the yield of 1,2-PDO increased with catalyst concentration. The increase in catalyst amount from 0.4 to 1.2 g results in an increase in glycerol conversion from 25% to 55%. The increase in conversion is due to the availability of a greater number of Ni and ZnO sites for the hydrogenolysis reaction to take place. It is interesting to see that there was no change in selectivity with increase in catalyst concentration. Dasari et al. (2005) suggested to use optimum catalyst weight to get better conversion with high selectivity to 1,2-PDO. They observed that an excess catalyst amount promotes 1,2-PDO into lower alcohol and gases. In the present case, the Ni-Zn catalysts are highly selective during glycerol hydrogenolysis even at high catalyst and glycerol concentrations.

3.2.6 Influence of Glycerol Concentration

The influence of glycerol concentration on the hydrogenolysis of glycerol was studied; the results are shown in Fig. 6. The glycerol conversion was increased up to a glycerol concentration of 50% and thereafter a decrease in conversion was noticed. The decrease in conversion at high glycerol concentration is due to the smaller number of available active sites of the catalyst as its concentration is constant in all reactions. The catalyst showed considerable conversion even at high glycerol concentration without any variation in selectivity. It is known that a decrease in the selectivity to 1,2-PDO at high glycerol concentrations is expected because of polymerization of the reaction products (Dasari et al., 2005). The present catalyst selectivity is as high as 93% even at high glycerol concentrations. This is one of the important points in scale-up studies where high glycerol concentrations are generally used.

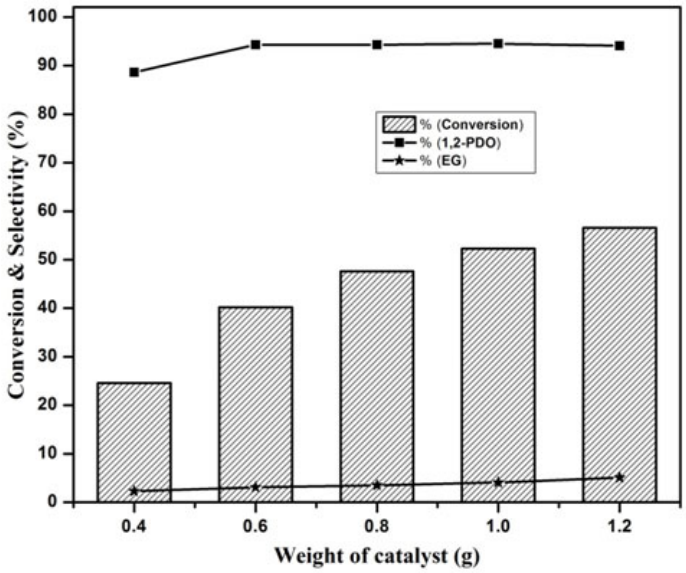

FIG. 5: Effect of catalyst weight in the hydrogenolysis of glycerol with NiZn-21 catalyst

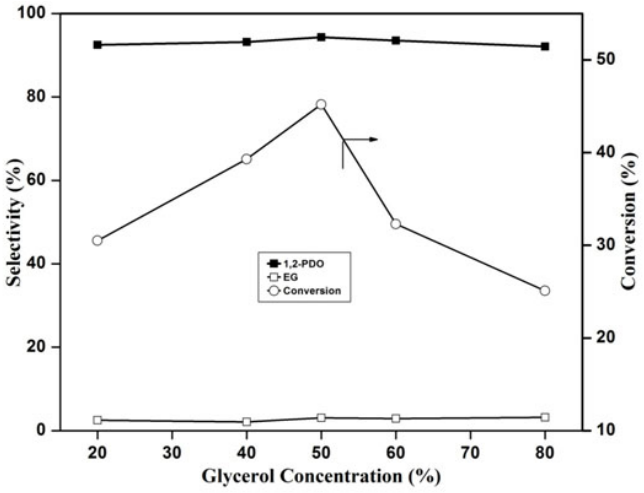

FIG. 6: Effect of glycerol concentration in the hydrogenolysis of glycerol with NiZn-21 catalyst

3.2.7 Reusability of the Catalyst

Reusability of the catalysts for glycerol hydrogenolysis is important for the practical applicability of the catalyst. After the reaction, the catalyst was separated from the liquid product by centrifugation. The catalyst was washed with methanol and followed by distilled water twice. This semi-dried catalyst was used for the reaction again under the same conditions. These experiments are repeated twice. The results suggest that the catalyst showed consistent activity with negligible variation in overall conversion of glycerol and selectivity to 1,2-PDO.

The glycerol hydrogenolysis activity is generally lowered during the reusability of Cu-based catalysts (Bienholz et al., 2010). There is a possibility of structural changes in the catalyst during the reaction and poisoning of active metal sites. The activity could not be completely recovered by simple water washing in the case of Cu-based catalysts. The present Ni-Zn catalyst showed consistent activity upon reuse without any pretreatment. Figure 7 shows

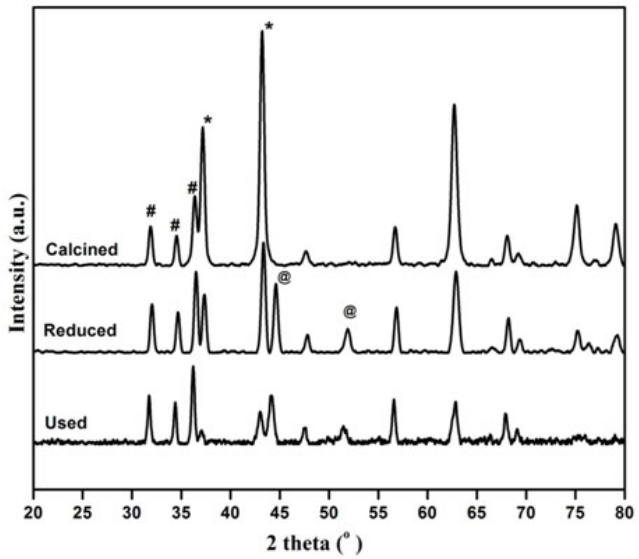

FIG. 7: X-ray diffraction patterns of used NiZn-21 catalyst. (*) NiO, (@) Ni, (#) ZnO phases

the XRD patterns of calcined, pre-reduced, and used NiZn-21 catalysts. XRD patterns indicate that there were no structural changes during the reaction. Moreover, a small amount of unreduced NiO present in the reduced catalyst was completely reduced to Ni during the reaction. This is a positive effect for glycerol hydrogenolysis.

4. CONCLUSIONS

Selective hydrogenolysis of glycerol was studied for Ni-Zn mixed oxide catalysts under continuous and batch mode conditions. Ni-Zn catalysts are identified as active catalysts for both operational conditions. The selectivity to 1,2-PDO is poor in continuous mode of reaction due to less residence time between catalyst and reactants. High selectivity to 1,2-PDO is achieved in batch phase hydrogenolysis. The activity of the catalyst depends on the Ni to Zn mole ratio and also on the Ni metal area. High glycerol conversion is achieved for the catalyst with a Ni to Zn mole ratio of 2. It was found that a relation exists between the Ni metal area and the activity of the catalyst. Highly dispersed and small crystallites of Ni and ZnO are required to obtain high activity. The glycerol conversion is also dependent on glycerol concentration, catalyst amount, reaction time, and also on reaction temperature. The Ni-ZnO catalysts are stable and reusable with consistent activity.

ACKNOWLEDGMENT

The author M.B. thanks CSIR, New Delhi, India for the award of Senior Research Fellowship.

REFERENCES

Akiyama, M., Sato, S., Takahashi, R., Inui, K., and Yokota, M., Dehydration-Hydrogenation of Glycerol into 1,2-Propanediol at Ambient Hydrogen Pressure, *Appl. Catal. A*, vol. **371**, pp. 60–66, 2009.

Balaraju, M., Rekha, V., Sai Prasad, P.S., Prasad, R.B.N., and Lingaiah, N., Selective Hydrogenolysis of Glycerol to 1, 2 Propanediol over Cu-ZnO Catalysts, *Catal. Lett.*, vol. **126**, pp. 119–124, 2008.

Balaraju, M., Rekha, V., Prabhavathi Devi, B.L.A., Prasad, R.B.N., Sai Prasad, P.S., and Lingaiah, N., Surface and Structural Properties of Titania-Supported Ru Catalysts for Hydrogenolysis of Glycerol, *Appl. Catal. A*, vol. **384**, pp. 107–114, 2010.

Balaraju, M., Rekha, V., Sai Prasad, P.S., Prabhavathi Devi, B.L.A., Prasad, R.B.N., and Lingaiah, N., Influence of Solid Acids as Co-Catalysts on Glycerol Hydrogenolysis to Propylene Glycol over Ru/C Catalysts, *Appl. Catal. A*, vol. **354**, pp. 82–87, 2009.

Behr, A., Eilting, J., Irawadi, K., Leschinski, J., and Lindner, F., Improved Utilization of Renewable Resources: New Important Derivatives of Glycerol, *Green Chem.*, vol. **10**, pp. 13–30, 2008.

Bienholz, A., Schwab, F., and Claus, P., Hydrogenolysis of Glycerol over a Highly Active CuO/ZnO Catalyst Prepared by an Oxalate Gel Method: Influence of Solvent and Reaction Temperature on Catalyst Deactivation, *Green Chem.*, vol. **12**, pp. 290–295, 2010.

Bienholz, A., Hofmann, H., and Claus, P., Selective Hydrogenolysis of Glycerol over Copper Catalysts both in Liquid and Vapour Phase: Correlation between the Copper Surface Area and the Catalyst's Activity, *Appl. Catal. A*, vol. **391**, pp. 153–157, 2011.

Casale, B. and Gomez, A.M., Method of Hydrogenating Glycerol., US Patent 5,214,219, filed July 9, 1992, and issued May 25, 1993.

Casale, B. and Gomez, A.M., Catalytic Method of Hydrogenating Glycerol, US Patent, 5,276,181, filed July 10, 1991, and issued Jan 4, 1994.

Chaminand, J., Djakovitch, L., Gallezot, P., Marion, P., Pinel, C., and Rosier, C., Glycerol Hydrogenolysis on Heterogeneous Catalysts, *Green Chem.*, vol. **6**, pp. 359–361, 2004.

Chin, S.Y., Lin, F.J., and Ko, A.N., Vapour Phase Hydrogenation of Cinnamaldehyde over Ni/Gamma-Al_2O_3 Catalysts: Interesting Reaction Network, *Catal. Lett.*, vol. **132**, pp. 389–394, 2009.

Dasari, M.A., Kiatsimkul, P., Sutterlin, W.R., and Suppes, G.J., Low-Pressure Hydrogenolysis of Glycerol to Propylene Glycol, *Appl. Catal. A*, vol. **281**, pp. 225–231, 2005.

Guo, L., Zhou, J., Mao, J., Guo, X., and Zhang, S., Supported Cu Catalysts for the Selective Hydrogenolysis of Glycerol to Propanediols, *Appl. Catal. A*, vol. **367**, pp. 93–98, 2009.

Hosgun, H.L., Yıldız, M., and Gercel, H.F., Hydrogenolysis of Aqueous Glycerol over Raney Nickel Catalyst: Comparison of Pure and Biodiesel By-Product, *Ind. Eng. Chem. Res*., vol. **51**, pp. 3863–3869, 2012.

Hu, J., Fan, Y., Pei, Y., Qiao, M., Fan, K., Zhang, X., and Zong, B., Shape Effect of ZnO Crystals as Cocatalyst in Combined Reforming-Hydrogenolysis of Glycerol, *ACS Catal.*, vol. **3**, pp. 2280–2287, 2013.

Huang, Z., Cui, F., Kang, H., Chen, J., Zhang, X., and Xia, C., Highly Dispersed Silica-Supported Copper Nanoparticles Prepared by Precipitation-Gel Method: A Simple but Efficient and Stable Catalyst for Glycerol Hydrogenolysis, *Chem. Mater.*, vol. **20**, pp. 5090–5099, 2008.

Kim, Y.T., Jung, K.D., and Park, E.D., Gas-Phase Dehydration of Glycerol over Silica-Alumina Catalysts, *Appl. Catal., B*, vol. **107**, pp. 177–187, 2011.

Kinage, A.K., Upare, P.P., Kasinathan, P., Hwang, Y.K., and Chang, J.S., Selective Conversion of Glycerol to Acetol over Sodium-Doped Metal Oxide Catalysts, *Catal. Commun.*, vol. **11**, pp. 620–623, 2010.

Koo, K.Y., Roh, H.S., Jung, U.H., and Yoon, W.L., CeO_2 Promoted Ni/Al_2O_3 Catalyst in Combined Steam and Carbon Dioxide Reforming of Methane for Gas to Liquid (GTL) Process, *Catal. Lett*., vol. **130**, pp. 217–221, 2009.

Len, C. and Luque, R., Continuous Flow Transformations of Glycerol to Valuable Products: An Overview, *Sustainable Chem. Processes*, vol. **2**, pp. 1–10, 2014.

Li, Y., Maa, L., Liu, H., and He, D., Influence of HZSM5 on the Activity of Ru Catalysts and Product Selectivity during the Hydrogenolysis of Glycerol, *Appl. Catal. A*, vol. **469**, pp. 45–51, 2014.

Lin, X., Lv, Y., Xi, Y., Qu, Y., Lee Phillips D., and Liu, C., Hydrogenolysis of Glycerol by the Combined Use of Zeolite and Ni/Al_2O_3 as Catalysts: A Route for Achieving High Selectivity to 1-Propanol, *Energy Fuels*, vol. **28**, pp. 3345–3351, 2014.

Meher, L.C., Gopinath, R., Naik, S.N., and Dalai, A.K., Catalytic Hydrogenolysis of Glycerol to Propylene Glycol over Mixed Oxides Derived from a Hydrotalcite-Type Precursor, *Ind. Eng. Chem. Res.*, vol. **48**, pp. 1840–1846, 2009.

Montes, V., Checa, M., Marinas, A., Boutonnet, M., Marinas, J.M., Urbano, F.J., Järas, S., and Pinel, C., Synthesis of Different ZnO-Supported Metal Systems through Micro Emulsion Technique and Application to Catalytic Transformation of Glycerol to Acetol and 1,2-Propanediol, *Catal. Today*, vol. **223**, pp. 129–137, 2014.

Pachauri, N. and He, B., Value-Added Utilization of Crude Glycerol from Biodiesel Production: A Survey of Current Research Activities, *Proc. of ASABE Annual International Meeting*, Portland, OR, July 9–12, 2006.

Pagliaro, M., Ciriminna, R., Kimura, H., Rossi, M., and Pina, C.D., From Glycerol to Value-Added Products, *Angew. Chem., Int. Ed.*, vol. **46**, pp. 4434–4440, 2007.

Pavan Kumar, V., Shanthi Priya, S., Harikrishna, Y., Ashish Kumar, and Chary, K.V.R., Catalytic Functionalities of Nano Ruthenium/γ-Al_2O_3 Catalysts for the Vapour Phase Hydrogenolysis of glycerol, *J. Nanosci. Nanotechnol*., vol. **15**, pp. 1–9, 2015.

Sato, S., Akiyama, M., Takahashi, R., Hara, T., Inui, K., and Yokota, M., Vapor-Phase Reaction of Polyols over Copper Catalysts, *Appl. Catal. A*, vol. **347**, pp. 186–191, 2008.

Sharma, R.V., Pardeep Kumar, and Dalai, A.K., Selective Hydrogenolysis of Glycerol to Propylene Glycol by using Cu:Zn:Cr:Zr Mixed Metal Oxides Catalyst, *Appl. Catal. A*, vol. **477**, pp. 147–156, 2014.

Suprun, W., Lutecki, M., Glaser, R., and Papp, H., Catalytic Activity of Bifunctional Transition Metal Oxide Containing Phosphated Alumina Catalysts in the Dehydration of Glycerol, *J. Mol. Catal. A: Chem.*, vol. **342**, pp. 91–100, 2011.

Wang, S. and Liu, H., Selective Hydrogenolysis of Glycerol to Propylene Glycol on Cu-ZnO Catalysts, *Catal. Lett.*, vol. **117**, pp. 62–67, 2007.

Wang, S., Zhang, Y., and Liu, H., Selective Hydrogenolysis of Glycerol to Propylene Glycol on Cu-ZnO Composite Catalysts: Structural Requirements and Reaction Mechanism, *Chem. Asian J.*, vol. **5**, pp. 1100–1111, 2010.

Xiao, Z., Xiu, J., Wang, X., Zhang, B., Williams, C.T., Sub, D., and Liang, C., Controlled Preparation and Characterization of Supported $CuCr_2O_4$ Catalysts for Hydrogenolysis of Highly Concentrated Glycerol, *Catal. Sci. Technol.*, vol. **3**, pp. 1108–1115, 2013.

Yang, Y., Ma, J., and Wu, F., Production of Hydrogen by Steam Reforming of Ethanol over a Ni/ZnO Catalyst, *Int. J. Hydrogen Energy*, vol. **31**, pp. 877–882, 2006.

Yu, W., Xu, J., Ma, H., Chen, C., Zhao, J., Miao, H., and Song, Q., A Remarkable Enhancement of Catalytic Activity for KBH_4 Treating the Carbothermal Reduced Ni/Ac Catalyst in Glycerol Hydrogenolysis, *Catal. Commun.*, vol. **11**, pp. 493–497, 2010.

Yuanqing, L., Nagaraju, P., Kamalakar, G., Garry, L.R., and Flora, T.T.N., Glycerol Hydrogenolysis to 1,2-Propanediol by

Cu/ZnO/Al_2O_3 Catalysts, *Top Catal.*, vol. **57**, pp. 1454–1462, 2014.

Zhengxi, Y., Lei, X., Yingxu, W., Yingli, W., Yanli, H., Qinghua, X., Xinzhi, Z., and Zhongmin, L., A New Route for the Synthesis of Propylene Oxide from Bio-Glycerol Derivated Propylene Glycol, *Chem. Commun.*, vol. **2009**, pp. 3934–3936, 2009.

Zhou, C.H., Beltramini, J.N., Fan, Y.X., and Lu, G.Q., Chemoselective Catalytic Conversion of Glycerol as a Biorenewable Source to Valuable Commodity Chemicals, *Chem. Soc. Rev.*, vol. **37**, pp. 527–549, 2008.

SYNTHESIS OF HIGHLY PURE *L*-3-HYDROXY-γ-BUTYROLACTONE FROM *L*-MALIC ACID AND *L*-ALANINOL FROM ALANINE BY SELECTIVE HYDROGENATION OVER Pt-ReO_X/C CATALYST

Bair S. Bal'zhinimaev,[1,*] Alexey P. Suknev,[1] Eugene A. Paukshtis,[1] & Irina S. Batueva[2]

[1]*Boreskov Institute of Catalysis SB RAS, Prospect Akademika Lavrentieva, 5, 630090 Novosibirsk, Russia*

[2]*Buryat State University, Smolina St. 24a, 670000 Ulan-Ude, Russia*

*Address all correspondence to: Bair S. Bal'zhinimaev, Boreskov Institute of Catalysis SB RAS, Prospect Akademika Lavrentieva, 5, 630090 Novosibirsk, Russia; Tel.: +7 383 330 9770; Fax: + 7 383 330 8056, E-mail: balzh@catalysis.ru

Original Manuscript Submitted: 6/27/2017; Final Draft Received: 1/14/2018

Selective hydrogenation of L-malic acid and L-alanine aqueous solutions, respectively, to L-3-hydroxy-γ-butyrolactone and L-alaninol on a highly dispersed Pt-ReO_x/C catalyst was studied under mild conditions (T = 75°C-110°C). In the low-temperature region, where racemization proceeds by two to three orders of magnitude more slowly than that of hydrogenation, we obtained a chemically (lactone yield > 98%) and optically pure cyclic ester with an enantiomeric excess ee > 99%. In an acid medium (pH < 3.5), L-alanine is in the active state, whereas the carboxyl group is nondissociated and the amine group is protonated. In the region of 3.5 < pH < 7, the structure of the amino acid corresponds to a zwitterion that is characterized by the presence of inactive carboxylate anions. As is the case of malic acid, the appropriate temperature, pH, catalyst loading, and concentration of the acid were found to produce L-alaninol with a yield of 99% and ee > 99%.

KEY WORDS: *L-malic acid, alanine, L-3-hydroxy-γ-butyrolactone, L-alaninol, hydrogenation, chirality, racemization, Pt-ReO_x catalyst*

1. INTRODUCTION

Optically pure *L*-3-hydroxy-γ-butyrolactone (*L*-3-HBL) and *L*-alaninol are widely used in production of cholesterol-reducing drugs (Crestor) and antibiotics (Levofloxacin), agrochemistry for crop protection, and organic synthesis of chiral auxiliaries (Ager et al., 1996; Antons et al., 2001; Muller, 2005; Kutzki et al., 2013). Therewith, chiral centers can be formed during the synthesis of such compounds or are already present in the initial reagents. In the latter case, the simplest method for obtaining 3-HBL and alaninol is catalytic hydrogenation of malic acid and alanine, respectively, that in turn can readily be obtained from renewable sources (biomass). In the literature, only a few examples exist for selective hydrogenation of *L*-malic acid with the use of monometallic and bimetallic heterogeneous catalysts (Rouhi, 2003; Urtel et al., 2007; Antons et al., 2002). In the latter case, the acid was hydrogenated on the Ru-ReO_x catalyst to 1,2,4-butanetriol (1,2,4-BT) with an enantiomeric excess *ee* of ∼ 99%. In addition, optically pure *L*-3-HBL was synthesized via hydrogenation of *L*-malic acid by zinc borohydride (Lee et al., 2008) or direct biosynthesis from glucose (Martin et al., 2013). Similarly, *L*-alanine was hydrogenated to *L*-alaninol by lithium aluminohydride or sodium borohydride (Ager et al., 1996; Antons and Beitzke, 1996). At present, special attention

is drawn to hydrogenation of amino acids to amino alcohols by molecular hydrogen on ruthenium (Jere et al., 2003, 2004; Chen et al., 2007; Pimparkar et al., 2008; Holladay et al., 2004; Bhandare and Vaidya, 2017; Magerlein et al., 2007), rhodium (Tamura et al., 2014, 2015), palladium, and platinum (Tomishige et al., 2017; Studer et al., 2001) catalysts promoted with oxides of groups 6 and 7 metals. Noteworthy is the fact that hydrogenation can proceed only if an amino acid is protonated, that is, the reaction must be carried out in an acid medium in the presence of phosphoric or sulfuric acid (Antons et al., 2001; Jere et al., 2003, 2004; Chen et al., 2007; Pimparkar et al., 2008; Holladay et al., 2004; Bhandare and Vaidya, 2017; Magerlein et al., 2007; Tamura et al., 2014, 2015). Turnover frequency (TOF) values observed in the reaction varied from several h^{-1} for monometallic samples to tens of h^{-1} for bimetallic catalysts; therewith, the yield of alaninol did not exceed 80%–90%, with a conversion of the acid close to 100%. In addition, chirality of the reaction products depended on temperature: At low temperatures, *ee* approached 100%, whereas at higher temperatures ($> 100^{\circ}$C) *ee* decreased substantially due to racemization of chiral molecules (Jere et al., 2003; Magerlein et al., 2007; Tamura et al., 2015). Overall, most of the catalysts under consideration require high (100–200 atm) hydrogen pressures for operation; they have insufficient catalytic activity (a low yield of the target product), so the temperature must be raised, which in its turn leads to racemization of chiral molecules.

In this work, selective hydrogenation of L-malic acid and L-alanine was performed to obtain not only chemically (yield of 98%) but also optically pure L-3-HBL and L-alaninol (*ee* $\geq$ 99%), respectively. The catalyst was represented by highly dispersed Pt-ReO_x species supported on the activated carbon (Suknev et al., 2015; Bal'zhinimaev et al., 2017).

2. EXPERIMENT

2.1 Catalyst Preparation

The catalyst was synthesized using activated carbon Norit SX Ultra (S_{BET} = 1000 m^2/g, pore volume 0.87 cm^3/g, fraction 50–100 μm), and the synthesis method is described in detail elsewhere (Suknev et al., 2015; Bal'zhinimaev et al., 2017). For synthesis, key factors were (1) the sequence of metal introduction, that is, the introduction of ammonium perrhenate before Pt(II) tetraamine complexes under oxygen (air)-free conditions; (2) intermolecular redox decomposition of the ammonium perrhenate (250°C) to form low-valence ReO_x ($x \leq 1$) species strongly bound with the support; and (3) strong redox interaction of Pt(II) complexes (450°C) with highly dispersed ReO_x to form atomically dispersed $Pt^0 - ReO_x$ ($x \leq 1$) active sites on the carbon surface. The best catalyst contained 10% Pt and 20% Re, the latter approximately corresponded to a monolayer coverage of the mesopore surface. According to high-annular dark-field scanning transmission electron hydroscopy and X-ray photoelectron spectroscopy data, the samples contain subnanometer Pt-ReO_x particles (0.5–1 nm), wherein platinum is in the metallic state, and rhenium is in the charged state close to Re^{2+} (Bal'zhinimaev et al., 2017).

2.2 Catalyst Testing

The reduced catalyst was transferred through a dry box (without air access) to the reactor for testing. We carried out catalyst testing in selective hydrogenation of aqueous solutions of both acids in a setup that was thoroughly described elsewhere (Suknev et al., 2015). In particular, the hydrogenation reaction was performed in a titanium 450-mL Parr reactor with a Teflon insert at 75°C–110°C (in some cases, temperature was raised to 130°C and 150°C), hydrogen pressure at 90 atm, catalyst sample weight of 2.6–8.5 g, hydrogen feed rate of 1 L/h, and stirring rate of 700 min^{-1}. Initial concentrations of malic acid were varied from 0.5 to 15 wt%. Malic acid is quite strong, so in the course of its hydrogenation to lactones the concentration of protons in the solution substantially decreases. To keep the pH of the solution constant after changes in acid concentration and to perform the reactions at different but constant pH values, we used a potassium-phosphate buffer ($K_xH_yPO_4$, $x + y = 3$). We performed hydrogenation of malic acid at pH = 1.5, 2, and 3. The use of acid buffer solutions is of special importance for hydrogenation of L-alanine, because the presence of amine and carboxyl groups can lead to the formation of zwitterions that have low reactivity. Therefore, tests were performed at pH = 2, 2.5, 3, and 3.5 with initial alanine concentrations of 0.25, 0.5, 1, and 2 wt%.

Reaction products were analyzed on a high-performance liquid chromatography (HPLC; Shimadzu LC-20 Prominence) system equipped with a PerfectSil Target ODS-3 high-definition column and gas chromatography mass spectroscopy (GC-MS; Agilent 7000B). GC of the gas probe did not reveal the formation of any amount of CO_2 or butane (propane) as gas products of decarboxylation or overhydrogenation processes. In addition, the blank experiments (without catalyst) performed at the same temperatures, concentrations, and pH values did not show any activity toward hydrogenation of acids. Acid conversion (X), selectivity to the products (S_i), and material balance on carbon (N) were calculated as

$$X(\%) = \frac{C^0_{ACID} - C_{ACID}}{C^0_{ACID}} \times 100\%, \quad S_i(\%) = \frac{C_i}{\sum C_i} \times 100\%, \quad N = \frac{C_{ACID} + \sum C_i}{C^0_{ACID}},$$

where C^0_{ACID} and C_{ACID} are the initial and current concentrations of the acid, and C_i is the concentration of the ith reaction product. The initial rate of the reaction (R°) was calculated from the slope of the time dependence of acid concentration (conversion) at reaction onset. TOF was calculated as a ratio of the initial reaction rate to total platinum content in the catalyst.

Chirality of malic acid and reaction products was characterized quantitatively on the same LC-20 Prominence HPLC equipped with a chiral column ORpak CDBS-453 and ultraviolet detector. A mixture of 0.2-M phosphate buffer (70%) and acetonitrile (30%) served as the eluent, and analysis was carried out at 12°C, a flow rate of 0.3 mL/min, and λ_{max} = 190 and 210 nm. *ee* was calculated by

$$ee = (C_\mathrm{L} - C_\mathrm{D})/(C_\mathrm{L} + C_\mathrm{D}),$$

where C_L and C_D are the relative concentrations of L- and D-isomers. Optical purity of the acid and reaction products was determined by polarimetric analysis as well. The specific angle of rotation $[\alpha]_\mathrm{D}$ was measured on a PolAAr 3005 polarimeter equipped with a special quarts cuvette (10 mL) and a tungsten-halogen lamp that served as a source of stable white light. Afterward, the measured angles of rotation were compared with tabular data for the acid and lactones to determine *ee*.

2.3 Fourier Transform Infrared Spectroscopy Study of Malic Acid Association Process in Water

The association of malic acid molecules was investigated using 0.5%, 1%, 2%, 5%, 15%, and 30% solutions in D_2O (98% deuterium enrichment). Infrared (IR) spectra were recorded at room temperature and 90°C. A solution was placed between calcium fluoride windows with an optical length path of 10–30 μm. In high-temperature measurements, a malic acid solution heated to 90°C was deposited onto a calcium fluoride window that was heated to the same temperature and then covered with another window. The windows with a layer of malic acid solution were placed in a solid metallic cuvette that was also heated to the measurement temperature and mounted in the cuvette compartment of spectrometer to prevent cooling of the solution when recording the spectrum. IR spectra were recorded on a Shimadzu FTIR-8300 in the region of 900–4000 cm^{-1}, with a resolution of 4 cm^{-1} and accumulation from 200 scans. We obtained spectra of the acids by subtraction of the D_2O spectra. To compare relative intensities of the absorption bands, these were normalized to the band intensity of the C = O stretch at 1719 cm^{-1}.

To study the structure of L-alanine species in water by IR spectroscopy, we prepared 15% acid solutions that differed in pH from 1.8 (phosphate buffer) to 6.2 (as dissolved). Such a high α-alanine concentration was applied to obtain high-quality spectra, because only the stretching vibration band of carboxyl groups (–COOH) at 1700–1750 cm^{-1} was observed at 2% alanine. A drop of alanine solution was placed between two BaF_2 windows to form a thickness layer of 10–30 μm. Spectra were recorded on the same Shimadzu FTIR-8300 in the range of 700–6000 cm^{-1}, with a resolution of 4 cm^{-1} and scan number of 100 followed by subtracting the water spectrum.

3. RESULTS AND DISCUSSION

3.1 Selective Hydrogenation of L-Malic Acid

Figure 1 displays typical kinetic dependences observed in hydrogenation of L-malic acid. One can see that the main products of the reaction are cyclic esters, that is, lactones, namely, 3-HBL and 2-HBL. The latter is produced in a

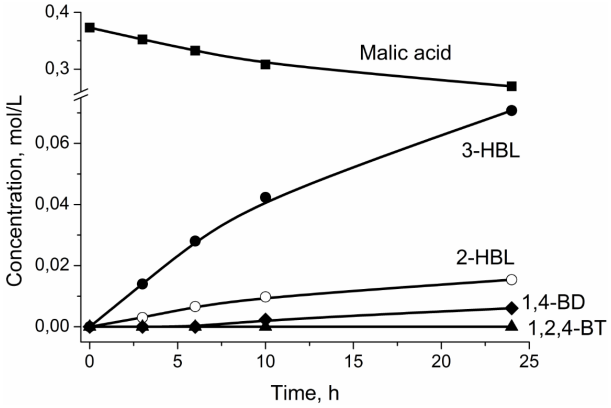

FIG. 1: Time dependences of *L*-malic acid, 3-HBL, 2-HBL, 1,2,4-BT, and 1,4-BD concentrations. Reaction temperature: 90°C, hydrogen pressure: 90 bar, catalyst loading: 2.6 g, initial acid concentration: 5%, and pH: 1.5

much smaller amount, which may be caused by preferential hydrogenation of the carboxylic group adjacent to the electron-withdrawing hydroxyl. In addition, we observed the formation of small amounts of 1,4-butanediol (1,4-BD). Regardless of the reaction temperature, lactones appear immediately, whereas 1,2,4-BT emerges with a considerable delay (induction period), indicating a consecutive conversion of the acid to lactones and then to alcohols. Indeed, as seen on Fig. 2, at a higher temperature (150°C) the induction period of triol disappears and concentration of lactones exceeds the maximum. At the same time, at low temperatures ($\leq$ 90°C) the induction period of alcohols was so extended that 1,2,4-BT appeared in just 24 h.

Similar dependences were obtained under varying concentrations of malic acid (Table 1). At first, reaction rate increases with the rise in concentration and then exceeds the maximum as concentration of malic acid increases. Note that the reaction rate does not increase with acid concentration, as may be expected; moreover, it even starts to decrease at 90°C. On the contrary, selectivity toward lactones increases from 83% to 94%, mostly due to the decreasing formation rate of triol and diol. The initial rates of reaction and TOF values increase with temperature, reaching 6 and 20 h^{-1} at 110°C and 150°C, respectively. Thus, one can say that at low temperatures, only lactones are formed. This testifies to a rapid formation of cyclic esters, mostly 3-HBL, and their extremely slow hydrogenolysis to dihydric and trihydric alcohols. However, the attained conversions of malic acid and hence the yields of products are not high. It can be assumed that increased catalyst loading will enhance conversion of the acid and retain high

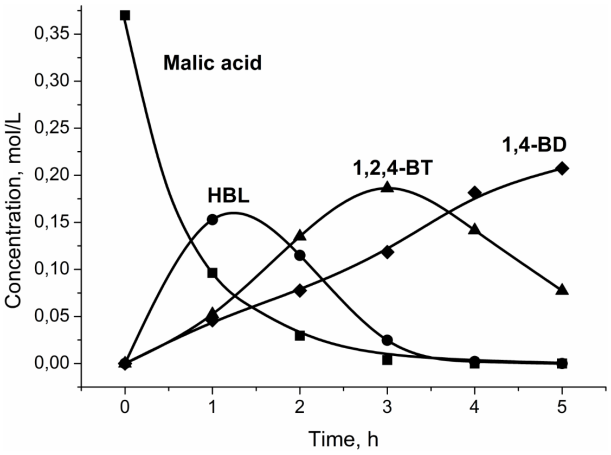

FIG. 2: Time dependences of *L*-malic acid, 3-HBL, 1,2,4-BT, and 1,4-BD concentrations. Reaction temperature: 150°C, hydrogen pressure: 90 bar, catalyst loading: 2.6 g, initial acid concentration: 5%, and pH: 1.5

selectivity for lactone. Indeed, when catalyst weight was increased to 8.5 g, malic acid conversion reached 100% for 10 h, and the acid was quantitatively converted into lactone (Table 1). In other words, 3-HBL with a yield $> 98\%$ can be obtained at low temperatures using the Pt-ReO_x/C catalyst.

Obviously, the sharp decrease in reaction rate with increasing acid concentration, especially at low temperatures, is caused not only by catalytic (chemical) reactions but also by processes of a different nature. Supposedly, among the main causes of the slow hydrogenation of lactones to alcohols is association of acid molecules into large aggregates that are hydrogenated hardly due to steric reasons.

Pt-ReO_x/C showed good stability in hydrogenation of malic acid during three consecutive and identical cycle tests (24 h in total; Bal'zhinimaev et al., 2017). After each test, the malic acid solution was changed to a fresh solution, and the catalyst was filtered from the water solution without washing out and reducing.

3.2 Association of Malic Acid Molecules

It is well known that, due to formation of hydrogen bonds, molecules of C_3–C_4 monocarboxylic acids in water readily dimerize with the enthalpy of ~ 1 kcal/mol per each COOH group (Carson and Rossotti, 1961; Yamamoto and Nishi, 1990). Dimers of carboxylic acids are commonly represented by a cyclic structure comprising two carboxyl groups connected with hydrogen bonds. In the case of malic acid, which is stronger and more dibasic, its association is likely to produce larger aggregates that are connected by two and more hydrogen bonds. Hypothetically, malic acid molecules will form quite extended structures, wherein bent acid molecules are held by a number of H bonds forming a ring-like configuration with closely located terminal carboxyl groups. This configuration implies a fast formation of cyclic esters, when after hydrogenation of one carboxylic group the formed hydroxyl reacts immediately with another carboxylic group to form lactones, mostly 3-HBL. Further hydrogenation/hydrogenolysis of lactone to alcohol is significantly hindered due to the likely low accessibility of active sites to rather large associates of ester molecules.

Figure 3(a) displays the normalized intensity spectra for 1% and 30% solutions of malic acid in D_2O in the range of 1000–1850 cm^{-1}. IR spectra of both solutions have a broad and intensive band near 1711–1717 cm^{-1}, that corresponds to a C = O stretching vibration and the bands at 1065 and 1105 cm^{-1} assigned to the C–OH stretch of the carboxyl group. A shift of the absorption band from 1711 to 1717 cm^{-1} with an increase in acid concentration may be related to a weakening of the hydrogen bonds with the increasing size of associates. However, owing to low energy of the hydrogen bond, loosening of the carbonyl group double bond is not pronounced, so the band shifts toward low frequencies by only 30–35 cm^{-1}. It should be remembered that monomers of carboxylic acids in nonpolar solvents are characterized by a band at 1750 cm^{-1} (Barraza et al., 1987), because the interaction with very weakly basic

TABLE 1: The initial reaction rates (R°), acid concentrations and TOFs at different temperatures, as well as malic acid conversion (X) and lactone selectivity (S) after 5-24 hours of the reaction

T, °C	C°, wt%	R°, mmol/g/h	TOF, h^{-1}	X, %	S, %
90	0.5	0.41	0.5	56	83
	1	0.57	2	95	86
	2	0.66	2	87	88
	5	0.45	0.5	25	94
	5*	**0.44**	**0.5**	**100**	**98**
100	5	1.40	3	76	84
	15	1.44	3	49	90
110	5	2.88	6	93	70

*catalyst loading was increased to 8.5 g.

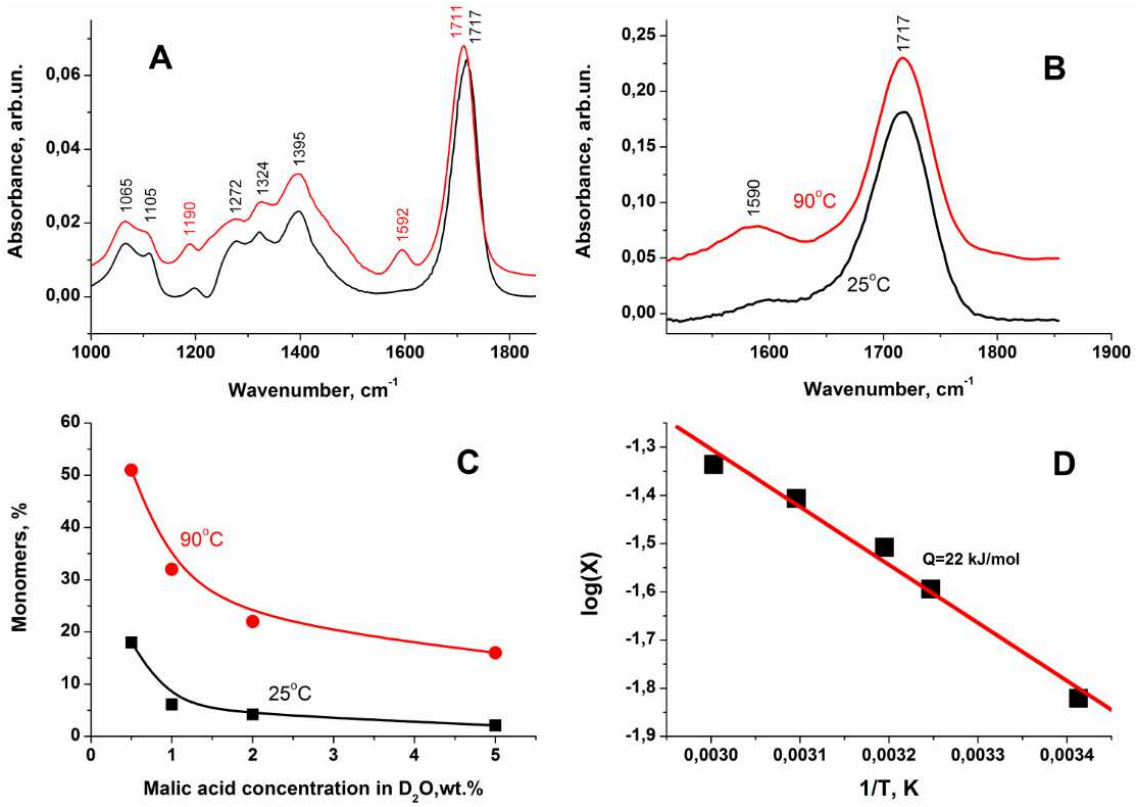

FIG. 3: (A) Normalized IR spectra of 1% (red) and 30% (black) aqueous (D_2O) solutions of *L*-malic acid recorded at room temperature; (B) normalized IR spectra of 5% *L*-malic acid recorded at 25°C and 90°C; (C) dependence of the fraction of acid monomers on its concentration; (D) Arrhenius dependence of the fraction of monomers in a 5% solution of the acid on temperature

molecules of the solvent virtually does not disturb OH and C = O groups in the carboxyl group. Bands in the range of 1272–1395 cm^{-1} can be attributed to bending vibrations of H–C–H, C–C–H, and O–C–H, and two new bands at 1190 and 1590 cm^{-1} correspond to monomeric molecules of malic acid, or more exactly, to symmetric and antisymmetric vibrations of the carboxyl group connected to a water molecule by the hydrogen bond.

One can see in Figs. 3(b) and 3(c) that the relative concentration of malic acid monomers substantially increases with temperature. IR spectra can be used to estimate the concentration of monomers from the relative intensity of the band at 1590 cm^{-1}, assuming that the bands at 1590 and 1711–1717 cm^{-1} have close absorption coefficients. Indeed, absorption coefficients of the band from the stretch of the carboxyl group for monomers and dimers of acids differ by no more than 30% (Barraza et al., 1987). Thus, as the concentration of malic acid increases from 1% to 15%, the fraction of monomers decreases by more than sixfold, whereas the temperature elevation increases by sevenfold at the acid concentration of 5% and only twofold at 0.5% [Fig. 3(c)]. The association heat of malic acid in an aqueous solution is 5 kcal/mol [Fig. 3(d)], which is close to data appearing in the literature (Schrier et al., 1964; Chen et al., 2008). Such an increase in heat may be attributed to the formation of several hydrogen bonds in abovementioned ring-like structures.

3.3 Racemization of *L*-Malic Acid

Malic acid and its hydrogenation product 3-HBL possess chiral properties. Distinctive to heterogeneous hydrogenation, racemization of malic acid in an aqueous solution proceeds homogeneously without the involvement of catalyst.

The rate of this reaction does not depend on the presence of solid catalyst at all of the studied temperatures. In addition, malic acid and its hydrogenation products were shown to have close enantioselectivity at all of the tested temperatures, including high values (130°C and 150°C) and at wide range of acid conversions (Table 2). This means that optical activity is incident only to *L*-malic acid but not to reaction products. As follows from data in Table 2, the racemization process sharply intensifies with increasing temperature. Thus, at 90°C the rate of this reaction is very low and the *ee* value for hydrogenation products is 99%, whereas at higher temperatures *ee* decreases to 82%–84% (130°C), and at 150°C the *ee* for lactone and triol drops to 60%–64%. In addition, as follows from Figs. 4(a) and 4(b), the racemization rate shows linear (first-order) growth with malic acid concentration and increases with the concentration of protons present in the solution (decrease in pH).

The above results thus testify to the fact that racemization proceeds with the involvement of protons by the keto-enol mechanism. During this process, a proton is transferred from an asymmetric carbon atom to a terminal oxygen of the C = O group. The intermediate resonance structure contains a threefold coordinated carbon (with substituents in one plane), so that the proton can equiprobably return to the position above or under the plane with the formation of *L*- and *D*-isomers, respectively. Evidently, according to this mechanism, racemization cannot occur with either *L*-3-HBL or *L*-1,2,4-BT, because the OH group at the asymmetric center does not have an adjacent C = O group to which the proton can be transferred. This was experimentally verified for *L*-3-HBL: The lactone did not show any optical activity even at high temperatures. Keto-enol racemization should proceed quite slowly with high activation energy, due to the implication of proton abstraction and transfer without catalyst participation. Indeed, it follows from the Arrhenius dependence of malic acid racemization rate that the activation energy is $\sim$ 29 kcal/mol, which is more than two times higher than that of the activation energy of hydrogenation at 12 kcal/mol (Fig. 5). Note that the activation

TABLE 2: Chirality of malic acid and reaction products at different temperatures and acid conversions. Initial malic acid concentration is 5%, pH = 1.5

T, °C	Enantiomeric excess *ee*, %			Malic acid
	Malic acid	3-HBL	1,2,4-BT	conversion, %
90	99	98.6	–	25
130	84	n.d.	82	95
150	66	64	60	100
90*	**99**	**99**	**–**	**100**

*catalyst loading was increased to 8.5 g.

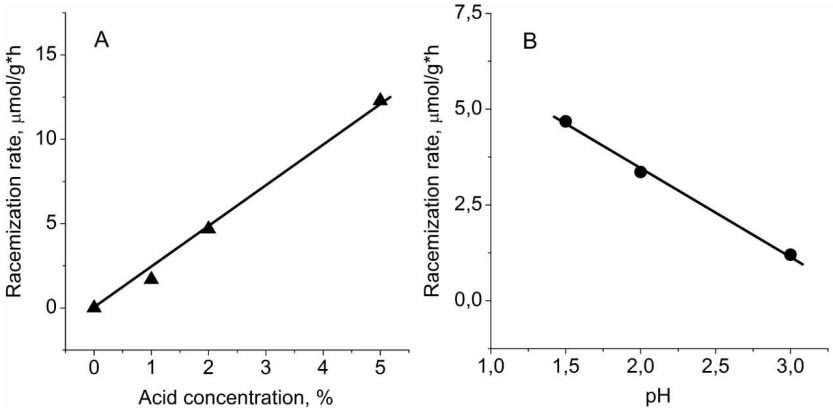

FIG. 4: Dependences of racemization rate on the initial concentration of *L*-malic acid at (A) pH = 1.5 and (B) pH values for 2% *L*-malic acid. Reaction temperature: 90°C

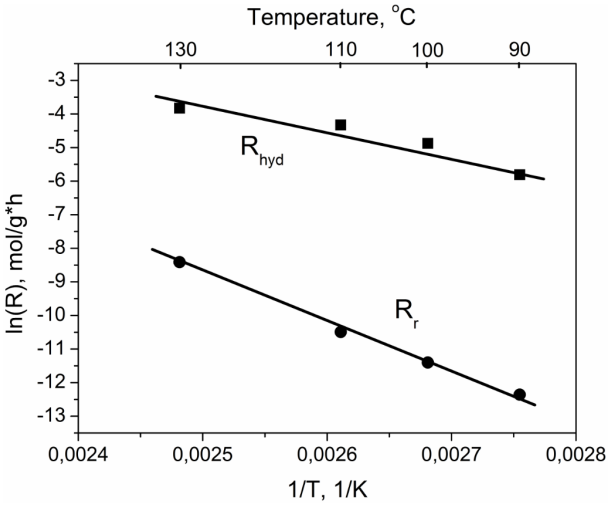

FIG. 5: Arrhenius dependences of initial hydrogenation (R_{hyd}) and racemization (R_r) rates. Initial concentration of L-malic acid: 5%, pH: 1.5

energy of hydrogenation was calculated taking into account the process of the malic acid association. Therefore, in the low-temperature region, the hydrogenation rate of L-malic acid exceeds the racemization rate by two to three orders of magnitude. Because reaction products do not exhibit optical activity (at least at low temperatures), optically pure lactones can be obtained by rapid hydrogenation of the acid. Indeed, in cases of increased catalyst weight, L-malic acid completely converts to L-3-HBL at 90°C (Table 2). In this case, hydrogenation of the acid to 3-HBL occurs too fast to have enough time to undergo noticeable racemization. This thus allows production (at low temperatures) of not only chemically but also optically pure ($ee \geq 99\%$) L-3-HBL.

3.4 Selective Hydrogenation of L-Alanine

As was noted above, an aqueous solution of alanine is almost neutral (pH = 6) due to the presence of an amine group and does not exhibit noticeable activity in the hydrogenation reaction. However, acidification of the alanine solution by phosphoric acid sharply increases reactivity of the acid (causes of the acid activation are discussed below). Table 3 lists data regarding the effect of pH, temperature, and alanine concentration on the reaction rate (TOFs) in hydrogenation of L-alanine. TOF values were determined from the initial rate of the hydrogenation reaction. It is seen that alanine hydrogenation rate increases with temperature, but unlike malic acid, this slightly depends on both alanine concentration and pH value in the range of 2–3.5. Indeed, as pH increases, the reaction rate shows a weak tendency to decrease. A nearly zero order of the reaction with respect to concentration of the acid and lower TOF values may be caused by a stronger adsorption of the amino acid on Pt-ReO_x catalyst in comparison to that of malic acid. We observed a more or less noticeable effect of alanine concentration on reaction rate in only the region of strongly diluted solutions with acid content of 0.25%–0.5%. Hydrogenation of alanine proceeds very selectively (97%–98%); the selectivity for alaninol depends only weakly on pH, slightly increases with decreasing the temperature, and reaches 99% at 75°C (Table 4). The main by-product of the reaction is isopropylamine (the product of hydrogenation of the OH group in alaninol); its concentration increases with temperature and reaches 3%–4% at 150°C. In the course of the reaction, its selectivity slightly decreases due to overhydrogenation of alaninol to isopropylamine.

We obtained quite interesting results after varying the initial pH of the solution, which revealed the key role of protons in activation of the alanine molecule. As illustrated in Fig. 6, at the initial pH of 2 we see a typical behavior of the substance undergoing reduction: alanine conversion increases monotonically with reaction time and reaches 100% in 10 h. At that point, the final pH value increases to only 2.5, and the reaction proceeds in quite an acidic region at a virtually constant pH. However, if the reaction is initiated at pH = 3–3.5, in approximately 4 h (when alanine conversion approaches 50%), hydrogenation sharply slows down and conversion of the acid virtually stops

TABLE 3: Effect of temperature, pH and acid concentration on TOFs in *L*-alanine hydrogenation

T, °C	Acid concentration, %	Initial pH	TOF, h^{-1}
Temperature effect			
110	1	2	2.7
90	1	2	2.0
75	1	2	1.1
pH effect			
90	1	2	2.0
90	1	2.5	2.0
90	1	3	1.9
90	1	3.5	1.9
75	1	2	1.1
75	1	3	1.0
75	1	3.5	1.0
Acid concentration effect			
75	1	2	1.1
75	0.5	2	1.2
75	1	3	1.0
75	0.5	3	0.85
75	0.25	3	0.8

increasing. Therewith, the acid solution becomes nearly neutral (pH = 6–7). Similar dependences in hydrogenation of alanine at different pH values have been observed earlier (Jere et al., 2003, 2004). In weakly acidic and neutral media, the alanine structure is characterized by carboxylate rather than a carboxyl group, and the proton proceeds to the amine group with the formation of a zwitterion; in this case, the amino acid is poorly hydrogenated. Only in a sufficiently acidic medium, wherein the carboxyl group is nondissociated, does alanine begin to hydrogenate. The literature shows that this can be attributed to thermodynamic causes related to endothermicity in the reduction of carboxylate species (Jere et al., 2003; Deakyne et al., 2008; Wyttenbach et al., 2000). In addition, in an acid medium, alanine is protonated, so that the electron-withdrawing NH_3^+ group creates an electron-density deficit at the adjacent carbonyl group, thus facilitating its hydrogenation by hydride ions. Similarly, in the case of malic acid, we observed preferential hydrogenation of the carboxyl group closest in proximity to the electron-withdrawing hydroxyl. And finally, accumulation of alaninol as the reaction product with basic properties increases the pH of the solution, so that the unreacted acid represented by zwitterions can form inactive salt-like species of the NH_3^+-$CH(CH_3)$-COO^- $\cdots$ $^+NH_3$-$CH(CH_3)$-CH_2-OH type.

3.5 Structure of Alanine Molecules in Solutions with Different pHs

It is assumed that the structure of an alanine molecule is determined, to a great extent, by the concentration of protons in an aqueous solution; thus, our study was carried out using IR spectroscopy. Figure 7(a) displays IR spectra of *L*-alanine recorded at a wide range of pH values (1.5–6.2) at room temperature. It can be seen that at pH = 1.5–3.5,

TABLE 4: Reaction products distribution in the course of L-alanine hydrogenation at different temperatures and pH. Initial acid concentration is 1%

T, °C	pH	Time, h	Acid conversion, %	Alaninol, %	Isopropyl amine, %
110	2	3	58	98	2
		6	81	96.5	3.5
90	2	5	70	98.4	1.6
		10	95	97.3	2.7
75	2	3	54	99.5	0.5
		8	86	98.8	1.2
		10	93	98.6	1.4
75	3	4	48	99.4	0.6
		8	55	99.0	1.0
		11	61	98.8	1.2
75	3.5	4	44	99.6	0.4
		8	52	99.2	0.8
		11	55	99.0	1.0

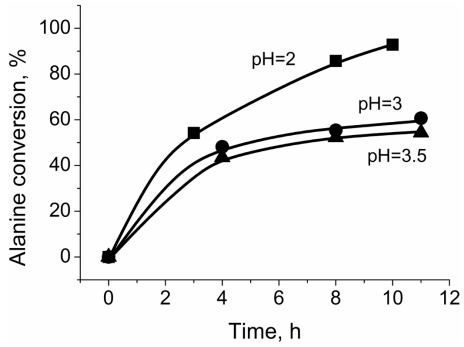

FIG. 6: Time dependences of L-alanine conversion at different pH values. Initial concentration of acid: 1%, T: 75°C

the concentration of protonated amines $R{-}NH_3^+$ absorbing at 1535 and 1630 cm^{-1} (Garcia et al., 2008; Thogersen et al., 2017) remains virtually constant and slightly decreases only when it approaches an almost neutral solution. This may be because in nearly in all of the studied range of pH values, the protonated amines enter the composition of zwitterions and protonated alanine. Moreover, not only is the acid protonated, but the reaction product (alaninol) is pronated as well (Fig. 8). Here, an intense band at 1058 cm^{-1} corresponds to C–O stretching vibrations in alcohol. Only at pH of 6 alaninol deprotonated with the formation of the amine group (the absorption band of 1630–1640 cm^{-1}). Noteworthy is the fact that in the region of pH = 3.5–6.2, the band at 1735 cm^{-1}, which corresponds to the carboxyl group, is absent [Fig. 7(a)]. The simultaneous presence of carboxylate species at $\sim$ 1600 cm^{-1} and protonated amines suggests that under the indicated conditions, alanine occurs as zwitterions. Only starting from a pH of 2.5 the band of the carboxyl group appear in the IR spectrum and grow in intensity as the concentration of protons in the solution increases. At pH = 1.5, the amino acid exists in the protonated form with a nondissociated carboxyl group. Evidently, this is the most active form of the acid during its hydrogenation to alcohol. The dependence

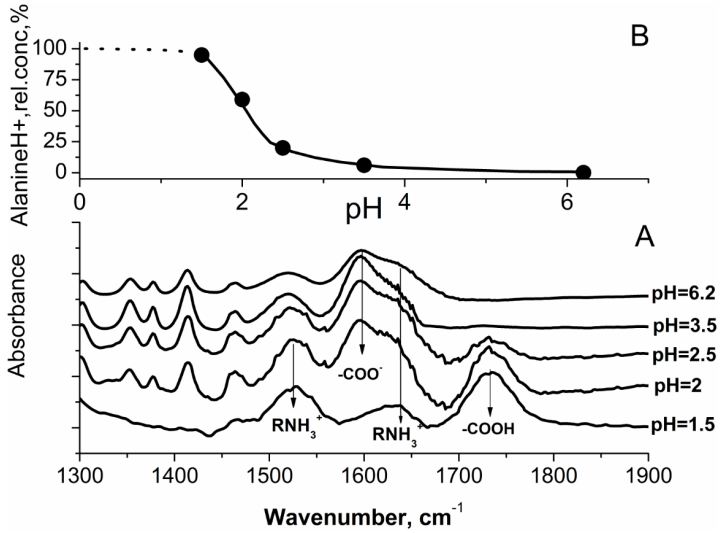

FIG. 7: (A) IR spectra of 5% solutions of *L*-alanine in D_2O recorded at room temperature and at different pH values; (B) dependence of the relative concentration of protonated alanine on pH

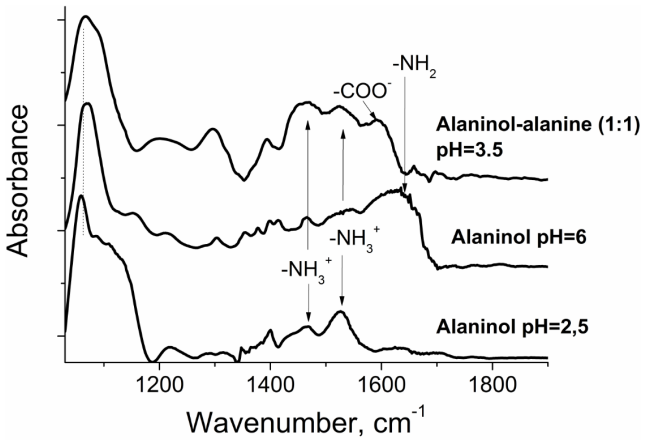

FIG. 8: IR spectra of an alaninol water solution at different pH values and an alanine:alaninol (1:1) salt-like species at pH = 3.5

of the relative concentration of carboxyl groups on pH is displayed on Fig. 7(b), which shows that an increase in pH above 2 decreases the concentration by more than threefold. Although the IR spectroscopy study was performed at room temperature, such regularities can also be observed at higher temperatures. In such a case, equilibrium constants controlling the ratio of different alanine species may shift toward higher pH values.

Thus, the structure of the *L*-alanine molecule and the related activity toward its hydrogenation to alaninol depend on the pH of the solution. In an acid medium (pH $<$ 3.5), the amino acid is in an active state, where the carboxyl group is nondissociated and the amine group is protonated. In the region of 3.5 $<$ pH $<$ 7, the amino acid occurs as zwitterions that are characterized by the presence of inactive carboxylate anions. In addition, according to the IR spectrum of the alanine-alaninol (1:1) solution, not only are the bands of the protonated amine group and carboxylate species present, but a substantial shift of the C–O band in alcohol also occurs, from 1058 to 1069 cm^{-1} (Fig. 8). This may be related to the formation of inactive salt-like species between the carboxylate anion and protonated alcohol. Thus, if an insufficient amount of buffer is used, the accumulation of alaninol possessing basic properties may cause the reaction to cease as a result of the formation of inactive zwitterions or salt-like species.

3.6 Racemization of *L*-Alanine

Both *L*-alanine and the reaction product *L*-alaninol have chiral properties. Table 5 lists the dependences of their enantioselectivity on temperature. One can see that the enantiomeric excess of both substances decreases with increasing temperature; in the case of alaninol, the decrease is sharper in comparison to that with alanine. This means that in contrast to malic acid, both alanine and alaninol undergo racemization. One can also suggest that at low temperatures, racemization of alanine occurs even more quickly than that of alaninol, whereas at high temperatures, alaninol is racemized faster than alanine. In other words, the ratio of acid and alcohol enantiomers changes differently with temperature. As in the case of malic acid, racemization of *L*-alanine proceeds homogeneously without catalyst involvement.

Key factors in the production of chemically and optically pure alaninol include the ratio between *L*-alanine hydrogenation and racemization rates as well as the dependence of this ratio on temperature, concentration of amino acid, and pH value. As seen in Fig. 9, at low temperatures (75°C–90°C) the rate of alanine hydrogenation is nearly three orders of magnitude higher than the rate of its racemization. Activation energy of alanine hydrogenation is estimated to be 7 kcal/mol, whereas for racemization, this value is three times higher and close to 21 kcal/mol. The high activation energy of racemization caused by proton abstraction and transfer without catalyst participation is typical of amino acids (Collins and Riley, 2000; Bada and Schroeder, 1975). At the same time, low activation energy is characteristic of highly selective homogeneous hydrogenation reactions (Zakhariev et al., 1977), where due to the good geometric conformity between active sites and reacting molecules, the entropy term is also low. One can propose that, in our case, satisfactory geometric conformity between Pt-ReO_x species and carboxylic group structure

TABLE 5: Chirality of alanine and alaninol at different temperatures and high acid conversions. Initial acid concentration is 1% and pH = 2

T, °C	Enantiomeric excess *ee*, %		Alanine conversion, %
	Alanine	Alaninol	
75	72	96	93
90	70	94	95
110	64	54	81
130	60	14	98

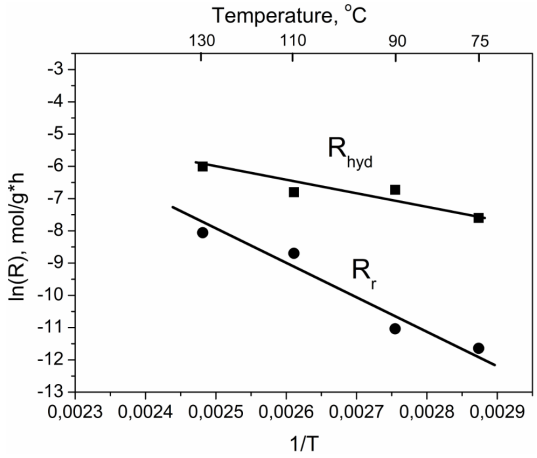

FIG. 9: Arrhenius dependences of initial *L*-alanine hydrogenation (R_{hyd}) and racemization (R_r) rates. Initial concentration of *L*-alanine: 1%, pH: 2

also takes place. Here, the racemization rate of alanine is approximately one order of magnitude higher. We can therefore conclude that alanine hydrogenation must be performed at low temperatures to achieve best optical purity. Because racemization proceeds homogeneously, its rate linearly depends (by first order) on *L*-alanine concentration [Fig. 10(a)]. Alanine hydrogenation is characterized by virtual zero order of the reaction with respect to the acid; thus, the process must be performed in quite a diluted solution to obtain optically pure alaninol. It follows from Fig. 10(b) that the rate of racemization increases nearly linearly with proton concentration in the solution. This means that the racemization reaction in the solution actually occurs with the participation of protons. Thus, in the low-temperature region (75°C–90°C) *ee* of alanine and alaninol increases with pH (Table 6). However, under such conditions, the reaction rates are low, and quite a long time (> 10 h) is needed to reach high conversions of the acid. During this time, a considerable amount of *L*-alaninol transforms into a *D*-isomer. As is the case with malic acid, to reduce the time of full alanine conversion, we increased catalyst loading to 8.5 g. The racemization rate was minimized by reducing the temperature (75°C), alanine concentration (0.5%), and pH (2); at these conditions, we reached a complete alanine conversion for only 3–4 h of the reaction, which yielded very high optical purity of alaninol (*ee* = 99%) and yield of *L*-alaninol (99%). In a period of 3–4 h, the produced *L*-alaninol simply does not have time to be racemized.

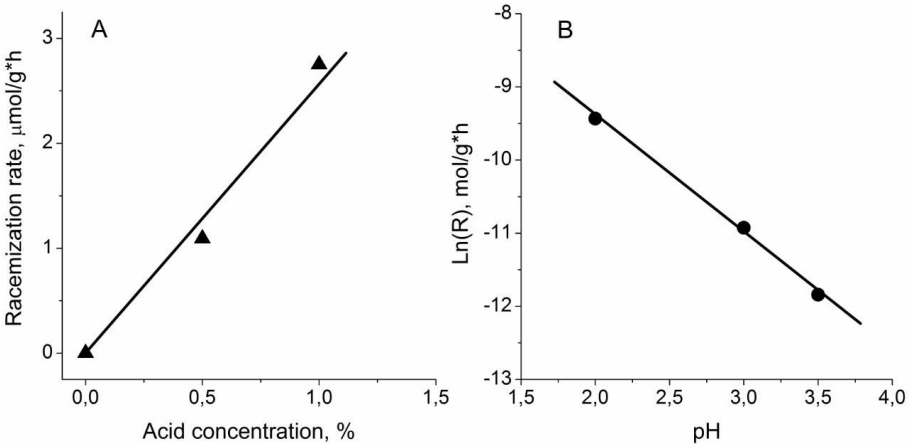

FIG. 10: Dependences of racemization rates on initial alanine concentration at 75°C and pH = 3 (A) and on pH at 75°C and 1% *L*-alanine (B)

TABLE 6: Enantiomeric excess of alanine and alaninol at different acid conversion, pH and temperatures. Initial concentration of alanine is 1%

pH	Enantiomeric excess *ee*, %					
	90°			75°		
	Acid conversion, % (time, h)	Alanine	Alaninol	Acid conversion, % (time, h)	Alanine	Alaninol
2	95 (10)	70	94	93 (10)	72	96
3	73 (8)	86	98.6	61 (11)	90	99.0
3.5	64 (11)	92	99.2	55 (11)	96	99.5
2*	**–**	**–**	**–**	**100 (4)**	**–**	**99.0**

*catalyst loading was increased to 8.5 g.

We observe similar dependences of L-alanine and L-malic acid racemization rate on temperature, pH, and acid concentration. This suggests that racemization of amino acid also proceeds by the keto-enol mechanism. Because alaninol is a stronger base (even at pH = 6, alaninol is partially protonated) than alanine, and so is malic acid, especially, its racemization proceeds at higher pH values. This is clearly seen in Fig. 8, which shows that absorption bands at 1460 and 1530 cm^{-1} correspond to the R-NH_3^+ group in IR spectra of alaninol recorded at pH = 6. Thus, as temperature increases (Table 5), racemization of L-alaninol continues, regardless of the presence of acid. Studies on the structure and energy of protonated amino alcohols and amino acids (Deakyne et al., 2008; Wyttenbach et al., 2000) revealed that the proton can be bound to both nitrogen and oxygen atoms, and the difference in formation energies of these species is insignificant. This enables quick movement of the proton along the carbon chain of L-alaninol and, hence, a fast exchange of all hydrogen atoms on deuterium (Jere et al., 2003). In this case, an intermediate compound with a double C = C bond that is necessary for transformation of L-alaninol to its D-isomer can also form in the absence of the carbonyl group, as in L-alanine.

4. CONCLUSIONS

We studied selective hydrogenation of L-malic acid and L-alanine, respectively, to L-3-HBL and L-alaninol on a highly dispersed Pt-ReO_x/C catalyst under quite mild conditions (T = 75°C–110°C). We found that in the low-temperature region, a considerable portion of malic acid (up to 80%) is present in the form of low-activity associates. As a result, the acid completely (quantitatively) converts to cyclic ester, and the subsequent hydrogenation of lactone to 1,2,4-butanetriol can be neglected. Because only L-malic acid exhibits optical activity and its racemization proceeds by two–three orders of magnitude more slowly than hydrogenation, chemically (with yield $>$ 98%) and optically pure L-3-HBL with *ee* $>$ 99% can be obtained under the indicated conditions.

Owing to the presence of amine (basic) and carboxyl (acid) groups in the L-alanine molecule, the acid has quite a specific structure depending on the pH of the solution. In an acid medium (pH $<$ 3.5), the amino acid is in the active state, whereas the carboxyl group is nondissociated and the amine group is protonated. In the region of 3.5 $<$ pH $<$ 7, the structure of alanine corresponds to zwitterions that are characterized by the presence of inactive carboxylate anions. In the low-temperature region, the racemization rate of L-alanine and L-alaninol is lower by nearly three orders of magnitude compared to the hydrogenation rate of amino acid, which ensures the production of optically pure substances. We found that similar to the case with malic acid, the appropriate pH, catalyst loading, and acid concentration produced L-alaninol with a yield of 99% and *ee* above $>$ 99%.

ACKNOWLEDGMENT

This work was conducted within the framework of budget project no. 0303-2016-0006 for the Boreskov Institute of Catalysis.

REFERENCES

Ager, D.J., Prakash, I., and Schaad, D.R., 1,2-Amino Alcohols and Their Heterocyclic Derivatives as Chiral Auxiliaries in Asymmetric Synthesis, *Chem. Rev*., vol. **96**, pp. 835–875, 1996.

Antons, S. and Beitzke, B., Process for Preparing Optically Active Amino Alcohols, United States Patent US 5536879, July 16, 1996.

Antons, S., Tilling, A.S., and Wolters, E., Method for Producing Optically Active Amino Alcohols, United States Patent US 6310254B1, Oct 30, 2001.

Antons, S., Tilling, A.S., and Wolters, E., Method for Producing Optically Active Alcohols, United States patent US 6355848B1, Mar 12, 2002.

Bada, J.L. and Schroeder, R.A. Amino Acid Racemization Reactions and Their Geochemical Implications, *Naturwissenschaften*, vol. **62**, pp.71–79, 1975.

Bal'zhinimaev, B.S., Paukshtis, E.A., Suknev, A.P., and Makolkin, N.V., Highly Selective/Enantioselective Pt-ReO_x/C Catalyst for Hydrogenation of L-Malic Acid at Mild Conditions, *J. Energy Chem*., 2017. DOI: 10.1016/j.jechem.2017.07.018

Barraza, R., Borschel, E.M., and Buback, M., Dimerization of Carboxylic Acid in Solution up to High Pressures and Temperatures. 2. Bensoic Acid., *Z. Naturforsch.*, vol. **42a**, pp. 406–412, 1987.

Bhandare, S.G. and Vaidya, P.D., Kinetics of Hydrogenation of Serine and Glutamic Acid in Aqueous Solution over a Ru/C Catalyst, *Ind. Eng. Chem. Res*., vol. **56**, pp. 3797–3803, 2017.

Carson, J.D.E. and Rossotti, F.J.C., The Determination of Stability Constants, in S. Kirshner, Ed., *Advances in the Chemistry of the Coordination Compounds*, New York: Macmillan, p. 181, 1961.

Chen, Y., Miller, D.J., and Jackson, J.E., Kinetics of Aqueous-Phase Hydrogenation of Organic Acids and Their Mixtures over Carbon Supported Ruthenium Catalyst, *Ind. Eng. Chem. Res*., vol. **46**, pp. 3334–3340, 2007.

Chen, J., Brooks, C.L., and Scheraga, H.A., Revisiting the Carboxylic Acid Dimmers in Aqueous Solution: Interplay of Hydrogen Bonding, Hydrophobic Interaction, and Entropy, *J. Phys. Chem. B.*, vol. **112**, no. 2, pp. 242–249, 2008.

Collins, M.J. and Riley, M.S., Amino Acid Racemization in Biominerals: The Impact of Protein Degradation and Loss, in G.A. Goodfriend, M.J. Collins, M.L. Fogel, S.A. Macko, and J.F. Wehmiller, Eds., *Perspectives in Amino Acid and Protein Geochemistry*, Oxford: Oxford University Press, pp. 120–142, 2000.

Deakyne, C.A., Liebman, J.F., Vlasov, E.A., and Zavatsky, Y.E., Paradigms and Paradoxes: Analysis of the Site of Protonation of Bifunctional Organic Compounds with the Protonation Energy/Volume Computation Method, *Struct. Chem.*, vol. **19**, pp. 609–611, 2008.

Garcia, A.R., Barros, R.B.D., Lourenco, J.P., and Ilharco, L.M., The Infrared Spectrum of Solid *L*-Alanine: Influence of pH-induced Structural Changes, *J. Phys. Chem. A*, vol. **112**, pp. 8280–8287, 2008.

Holladay, J.E., Werpy, T.A., and Muzatko, D.S., Catalytic Hydrogenation of Glutamic Acid, *Appl. Biochem. Biotechnol*., vol. **113–116**, pp. 857–869, 2004.

Jere, F.T., Jackson, J.E., and Miller, D.J., Kinetics of the Aqueous-Phase Hydrogenation of *L*-Alanine to *L*-Alaninol, *Ind. Eng. Chem. Res.*, vol. **43**, no. 13, pp. 3297–3303, 2004.

Jere, F.T., Miller, D.J., and Jackson, J.E., Stereoretentive C–H Bond Activation in the Aqueous Phase Catalytic Hydrogenation of Amino Acids to Amino Alcohols, *Org. Lett*., vol. **5**, no. 4, pp. 527–530, 2003.

Kutzki, O., Ditrich, K., and Bartsch, M., Process for the Preparation of (S)-2-Amino-1-Propanol (*L*-Alaninol) from (S)-1-Methoxy-2-Propylamine. United States patent US 8344182 B2, 2013 Jan 1.

Lee, S.-H., Park, O.-J., and Uh, H.-S., A Chemoenzymatic Approach to the Synthesis of Enantiomerically Pure (S)-3-Hydroxy-γ-butyrolactone, *Appl. Microbiol. Biotechnol.*, vol. **79**, pp. 355–362, 2008.

Magerlein, W., Dreisbach, C., Hugl, H., Tse, M.K., Klawonn, M., Bhor, S., and Beller, M., Homogeneous and Heterogeneous Ruthenium Catalysts in the Synthesis of Fine Chemicals, *Catal. Today*, vol. **121**, pp. 140–150, 2007.

Martin, C.H., Dhamankar, H., Tseng, H.-C., Sheppard, M.J., Reisch, C.R., and Prather, K.L.J., A Platform Pathway for Production of 3-Hydroxyacids Provides a Biosynthetic Route to 3-Hydroxy-γ-butyrolactone, *Nat. Comm*., vol. **4**, pp. 1414–1422, 2013.

Muller, M., Chemoenzymatic Synthesis of Building Blocks for Statin Side Chains, *Angew. Chem. Int. Ed*., vol. **44**, pp. 362–365, 2005.

Pimparkar, K.P., Miller, D.J., and Jackson, J.E., Hydrogenation of Amino Acid Mixtures to Amino Alcohols, *Ind. Eng. Chem. Res.*, vol. **47**, pp. 7648–7653, 2008.

Rouhi, A.M., Custom Chemicals, *Chem. Eng. News*, vol. **81**, pp. 55–73, 2003.

Schrier, E.E., Pottle, M., and Scheraga, H.A., The Influence of Hydrogen and Hygrophobic Bonds on the Stability of the Carboxylic Acid Dimmers in Aqueous Solution, *J. Am. Chem., Soc*., vol. **86**, no. 17, pp. 3444–3449, 1964.

Studer, M., Burkhardt, S., and Blaser, H.-U., Catalytic Hydrogenation of Chiral α-Amino and α-Hydroxy Esters at Room Temperature with Nishimura Catalyst without Racemization, *Adv. Synth. Catal*., vol. **343**, no. 8, pp. 1–7, 2001.

Suknev, A., Zaikovskii, V., Kaichev, V., Paukshtis, E., Sadovskaya, E., and Bal'zhinimaev, B., The Nature of Active Sites in Pt-ReO_x/TiO_2 Catalysts for Selective Hydrogenation of Carboxylic Acids to Alcohols, *J. Energy Chem.*, vol. **24**, pp. 646–654, 2015.

Tamura, M., Tamura, R., Takeda, Y., Nakagawa, Y., and Tomishige, K., Catalytic Hydrogenation of Amino Acids to Amino Alcohols with Complete Retention of Configuration, *Chem. Commun*., vol. **50**, pp. 6656–6659, 2014.

Tamura, M., Tamura, R., Takeda, Y., Nakagawa, Y., and Tomishige, K., Insight into the Mechanism of Hydrogenation of Amino Acids to Amino Alcohols Catalyzed by a Heterogeneous MoO_x-Modified Rh Catalyst, *Chem. Eur. J.*, vol. **21**, pp. 3097–3107, 2015.

Thogersen, J., Coletta, A., Keiding, S.R., Jensen, F., Jones, N., Hoffman, S.V., and Knak Jensen, S.J., Protonation of Aqueous Alanine by Photoionization of Water, *J. Phys. Chem. Chem. Phys.*, vol. **19**, pp. 1560–1570, 2017.

Tomishige, K., Nakagawa, Y., and Tamura, M., Selective Hydrogenolysis and Hydrogenation using Metal Catalysts Directly Modified with Metal Oxide Species, *Green Chem.*, 2017. DOI: 10.1039/C7GC00620A

Urtel, H., Rosch, M., and Haunert, A., Hydrogenation Method for Producing Optically Active Alcohols or Carboxylic Acids, United States patent US0142648A1, 2007 June 21.

Wyttenbach, T., Witt, M., and Bowers, M.T., On the Stability of Amino Acid Zwitterions in the Gas Phase: The Influence of Derivatization, Proton Affinity and Alkali Ion Addition, *J. Am. Chem. Soc.*, vol. **122**, no. 14, pp. 3458–3464, 2000.

Yamamoto, K. and Nishi, N., Hydrophobic Hydration and Hydrophobic Interaction of Carboxylic Acids in Aqueous Solution: Mass Spectrometric Analysis of Liquid Fragments Isolated as Clusters, *J. Am. Chem. Soc.*, vol. **112**, no. 2, pp. 549–558, 1990.

Zakhariev, A., Petrov, L., and Shopov, D., Kinetics of the Homogeneous Catalytic Hydrogenation of Methacrylic Acid in the Presence of Pentacyanocobaltate (II), *React. Kinet. Catal. Lett.*, vol. **7**, no. 3, pp. 253–259, 1977.

PLATINUM/GRAPHENE AS A RECYCLABLE CATALYST FOR ASYMMETRIC HYDROGENATION OF α-KETOESTERS

Poonam Sharma & Rakesh K. Sharma*

Indian Institute of Technology, Jodhpur, India

*Address all correspondence to: Rakesh K. Sharma, Indian Institute of Technology, Jodhpur, India, E-mail: poonamshrmap6@gmail.com

Original Manuscript Submitted: 6/10/2017; Final Draft Received: 1/15/2018

Asymmetric heterogeneous hydrogenation of the carbonyl group is one of the most important reactions for development of new chiral molecules. This study involves the asymmetric hydrogenation of α-ketoesters using a Pt/graphene support–based heterogeneous catalytic system and cinchonine as a chiral modifier. The catalyst produces high enantioselectivity (> 96.8%) and conversion (99.8%). Recyclability of the catalyst is tested for up to five cycles, and sustainable catalytic activity is found.

KEY WORDS: *heterogeneous catalysis, graphene, platinum, cinchonine*

1. INTRODUCTION

Chirality has a crucial role in pharmaceutical chemistry (Rouhi, 2003). Asymmetric homogenous catalysts have been used extensively for a variety of organic synthesis due to their high reactivity and enantioselectivity (Chen et al., 2013; Li and Zhang, 2013). Despite various benefits, separation, purification of products, and recycling make catalysts less environmentally welcoming (Berthod et al., 2005). But strategic development with homogeneous catalysts, such as immobilization on a solid support, has been carried out to overcome such issues (Mallat et al., 2007). Alumina (Al_2O_3), silica (SiO_2), polymers (Sharma and Sharma, 2017), and titanium oxide (TiO_2) are some conventional supporting materials that have been used in various studies involving asymmetric hydrogenation (Blaser and Jalett, 1993; Wilhelmus, 1993; Blaser et al., 1997, 2000). However, a number of drawbacks still exist for these supports, such as reduced electronic conductivity, higher solubility in acidic medium, low thermal stability, and comparatively small surface area (Tauster et al., 1978). Lately, a new concept of metal nanoparticle (NP)–based heterogeneous catalytic systems has been proposed using carbon as the supporting material (Chen et al., 2011). Carbon allotrope materials prove to be a smart choice due to their extraordinary properties including high specific surface area, electrical conductivity, and good chemical and thermal stability (Britto et al., 1996; Fraga et al., 2002). Among the carbon allotropes, graphene, carbon fibers, activated carbon, and multiwalled carbon nanotubes are some of the key nominees due to their industrial availability and ease of chemical modification. Of these, graphene particularly proves to be an excellent choice due to its extraordinary properties such as conduction, transparency, and material flexibility with high surface area (Allen et al., 2009; Weiss et al., 2012). These properties make it useful in various applications (Guo et al., 2010; Zhou et al., 2014; Xie et al., 2017) such as solar cells, light emitting diodes, touch panels as a support (Li et al., 2009), batteries (Wang et al., 2009), supercapacitors (Zhang et al., 2010), and smart windows or phones. Metal-incarcerated graphene systems are believed to serve as nanoreactors for catalytic conversion. Because pristine graphene is chemically inactive, chemical modification for the attachment of metal NPs for catalytic applications is essential (Carvalho Padilha et al., 2016; Tan et al., 2017). We carried out surface functionalization out using oxidizing agents such as H_2O_2, $KMnO_3$, and HNO_3 and introduced hydroxyl (–OH), carboxyl (–COOH), and carbonyl (–C = O) groups onto the surface of carbon (Sharma and Sharma, 2015). These functional groups have a vital role in

facilitating the binding, embedding, or stacking of NPs on the carbon support (von Arx et al., 2003; Satishkumar et al., 1996; Guo et al., 2009). In an earlier study, we used graphene as the supporting material and compared it to other supporting materials (Sharma and Sharma, 2015). Thus, several impressive methods have been involved in the development of heterogeneous catalytic systems (Chen et al., 2011). Pt/graphene systems are of great interest in catalysis due to their exclusive properties such as high surface area and high temperature resistance (Chen et al., 2011; Sharma and Sharma, 2015). The asymmetric heterogeneous catalysis is related to the use of a chiral modifier; heterogeneity occurs by binding onto the metal catalyst with solid supports (Yoon and Jacobsen, 2003).

For the current study, we prepared highly dispersed, platinum NP–functionalized graphene and tested for hydrogenation of the carbonyl group in an α-ketoester using a chiral modifier (Fig. 1). Cinchonine alkaloid was used as a chiral modifier. Cinchona has great importance in the field of asymmetric synthesis due to cost effectiveness and that fact that it is a naturally occurring source of chirality induction (Marcelli and Hiemstra, 2010). However, brief studies in the literature exist on asymmetric hydrogenation of ethyl pyruvate and methyl pyruvate on Pt/C (Chen et al., 2011; Sharma and Sharma, 2015).

2. MATERIALS AND METHODS

We obtained chloroplatinic acid (H_2PtCl_6), α-ketoesters, and cinchonine from Sigma-Aldrich. Acetic acid (Fisher Scientific) and graphene (commercial grade) were obtained commercially.

2.1 Characterization

Catalysts and products are examined by Fourier-transform infrared (FTIR) spectrosco-py, scanning electron microscopy (SEM), transmission electron microscopy (TEM), energy-dispersive X-ray (EDX) spectroscopy, Brunauer–Emmett–Teller (BET) theory, thermogravimetric analysis (TGA), nuclear magnetic resonance (NMR), high-performance liquid chromatography (HPLC), and polarimetry. SEM-EDX (SEM-EDX, EVO18 Zeiss, 20 KeV) and TEM (FEI Tecnai-G2 T20) are used to characterize the morphology and elemental analysis of Pt/graphene composites. TGA is performed on a TGA-6000 thermal analyzer (Perkin Elmer) under a nitrogen atmosphere (19.8-mL/min flowing nitrogen; temperature range 30–900°C; rate of 10°C/min; pressure, 3 bar) and a heating rate of 10°C min^{-1}. Surface area and pore size measurements of Pt/graphene are carried out on standard adsorption equipment (Quantachrome Autosorb iQ3) using N_2 gas with 99.99% purity. Nuclear magnetic resonance spectra (1H) are recorded on a Bruker 500 spectrometer operating at 500 MHz in $CDCl_3$. High-performance liquid chromatography (HPLC) from Waters Ireland (Dublin) is used to analyze catalytic products under isocratic and isothermal (at 30°C) conditions using a respective mixture of n-hexane/isopropanol/buffer as the mobile phase. Specific rotation is measured with a Rudolph polarimeter (APII/2W). We used the X-ray diffractometer (XRD) D8 advance (Bruker) with Cu Kα1 (λ = 1.54056Å) as a radiation source to ascertain the quality and crystalline nature of samples with tube current and voltage of 40 mA and 40 kV, respectively.

2.2 Preparation of Catalyst

A typical activation of graphene was already performed, in which graphene (0.45 g) is refluxed under constant stirring in 45 mL of (68 wt%) HNO_3 for 12 h at 140°C (Sharma and Sharma, 2015). Activated graphene is extracted by centrifugation at 3000 rpm and washed several times with water, followed by ethanol. The resultant graphene is dried for 24 h at 80°C. The wet chemical method is used to prepare the Pt support on graphene (Fig. 2; Tsang et al., 1994; Satishkumar et al., 1996). To accomplish that, we immersed the activated graphene (0.45 g) in an aqueous solution of Pt metal salt [H_2PtCl_6 (5 wt%)] and sonicated for 3 h. The solution mixture is stirred for 48 h at room temperature and heated for 24 h at 110°C. During this slow drying method, Pt NPs are tinted on graphene layers. Sodium formate (42 mg/mL^{-1}) is used to reduce Pt for 1 h at 100°C, followed by washing with deionized water and drying for 16 h at 80°C.

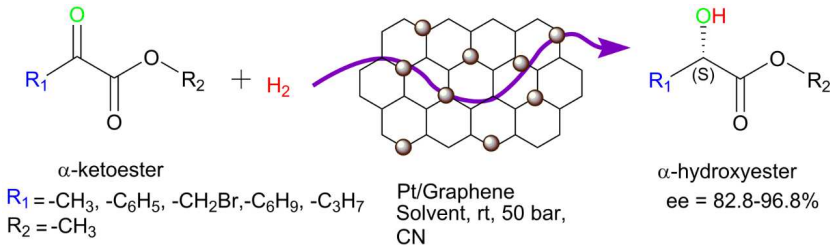

FIG. 1: Pictorial representation of asymmetric hydrogenation of an α-ketoester on the Pt surface

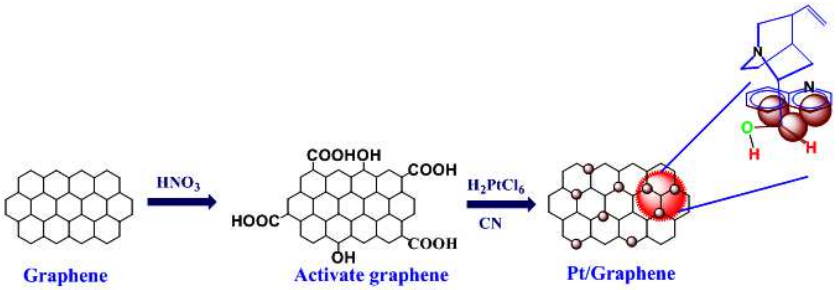

FIG. 2: Typical preparation method of Pt/graphene

2.3 Catalytic Activity

Catalytic activity is tested for asymmetric hydrogenation of α-ketoesters in a pressurized vessel. The percentages of conversion and enantiomeric excess (*ee*) of products are determined by HPLC and NMR [Table 1 (below)]. For this, the Pt/graphene catalyst is pretreated in a tubular furnace under hydrogen flow for 3 h at 300°C before the reaction. In the asymmetric reaction mixture (30 mg) catalyst, (0.01 M) chiral modifier and (17.6 M) acetic acid are premixed in a Teflon vessel under hydrogen. After 10 min, (0.5 mmol) ketoesters are introduced into the reaction mixture. The Teflon vessel is purged with hydrogen two to three times to remove the air and fill to the desired pressure. After completion of the reaction, the catalyst is removed by centrifuge, and the organic product is separated by column chromatography using hexane as the eluent.

3. RESULTS AND DISCUSSION

The morphology, shape, size, and distribution of NPs on graphene are characterized by SEM and TEM imaging. As seen from the SEM images in Fig. 3(b), the Pt NPs uniformly cover the surface of graphene. We can see the petals of graphene before loading the Pt (Fig. 3[a]). The TEM image in Fig. 3(c) shows that the NPs are extremely small, in the range of 2–20 nm, and higher magnification provides information about the shape and allocation of NPs on the surface of graphene (Fig. 3[d]). For qualitative and quantitative examination of the catalyst, EDX spectroscopy is carried out. Figures 3(e) and 3(f) confirm the Pt to be on the surface of graphene.

BET theory is used to determine the surface area, pore volume, and pore size distribution of materials. The BET surface area is performed for the Pt/graphene and is found to be 241.8 m^2/g^{-1} (Fig. 4[a]). Pt/graphene is characterized by XRD and shows an intense peak at 25.90° along with other peaks at 42.70° and 53.50°, corresponding to the graphene 002, 100, and 004 plan reflections, respectively, and three major peaks at 39.68°, 46.4°, and 67.7° corresponding to diffraction from the 111, 200, and 220 planes of the face-centered cubic lattice of Pt (Fig. 4[b]). TGA analyses are carried out for graphene and Pt/graphene (Fig. 4[c]). The oxidized behavior of compounds is studied at up to 900°C under N_2. Weight loss $<$ 400°C is due to the desorption of moisture and volatile impurities; at higher temperature ($\sim$ 610°C), the carbon material loses most of its starting weight, which increases gradually with increasing temperature of the postcarbonization. The thermal behavior of Pt/C is observed at two main mass loss regions: An initial mass loss around 200°C–375°C corresponds to the desorption of structural H_2O, CO_2, and Pt, and the second

TABLE 1: Asymmetric hydrogenation of ketoesters

S Number	Substrate	Conversion (%)	*ee*[1] (%)
1	Ethyl 3-bromo-2-oxopropanoate	80.2	82.8
2	Ethyl 3-methyl-2-oxobutanoate	90.4	$>$ 93.7
3	Ethyl 2-oxo-4-phenylacetate	92.7	92.6
4	Ethyl 2-oxo-2-phenylbutanoate	94.4	93.0
5	Ethyl 2-oxopropanoate	99.8	$>$ 96.8

Proposed reaction conditions: Temperature, 25°C; Pt/graphene, 30 mg; room temperature, 12 h; substrate, 0.5 mmol; CN, 4 mg; acetic acid, 1.5 mL; pressure, 50 bar.
[1]Determined by HPLC analysis using different chiral columns.

peak at $\sim$ 650°C is a result of the oxidative decomposition of carbonaceous materials. Graphene shows more stability and loses 10 wt% at 800°C (Fig. 4[c]). Pt/graphene oxidizes by 10 wt% before reaching 400°C. The next 10 wt% is lost before reaching 650°C, and finally, the graphitized carbon oxidizes after reaching 700°C. Thus, after loading Pt, the catalyst starts to decompose early. The TGA data confirm that Pt is found as a defect in graphene. IR spectra are taken for Pt/graphene under a transmission mode (Fig. 4[d]). In the case of functionalized carbon materials, some characteristic peaks occur at $\sim$ 400 and 700 cm^{-1} due to aromatic C–H bending (699.23 cm^{-1}) and other peaks such as 1547.07, 1696.21, 2356, and 3600–3700 cm^{-1} occur due to C–C stretching, six-member C = O stretching, C = C stretching, and the O–H functional group, respectively (Sharma and Sharma, 2016). The Pt-loaded graphene nanocomposites depict a few new peaks resulting from carboxylic ion binding between NPs and the graphene. Other new peaks at 1727.52 and 3331.11 cm^{-1} may be attributed to aromatic C = C stretching and O–H stretching, respectively. The peak appearing at 839.86 cm^{-1} (Pt-O covalent bond) is a result of the strong bond between Pt and the oxygen-containing group (Sharma and Sharma, 2016). We performed inductively coupled plasma atomic emission spectroscopy to determine leaching of Pt and found 0.1 parts per million after five cycles. To optimize reaction conditions, we performed hydrogenation of ethyl 2-oxopropanoate in acetic acid using 5 wt% Pt/graphene at room temperature by varying the pressure (Table 2).

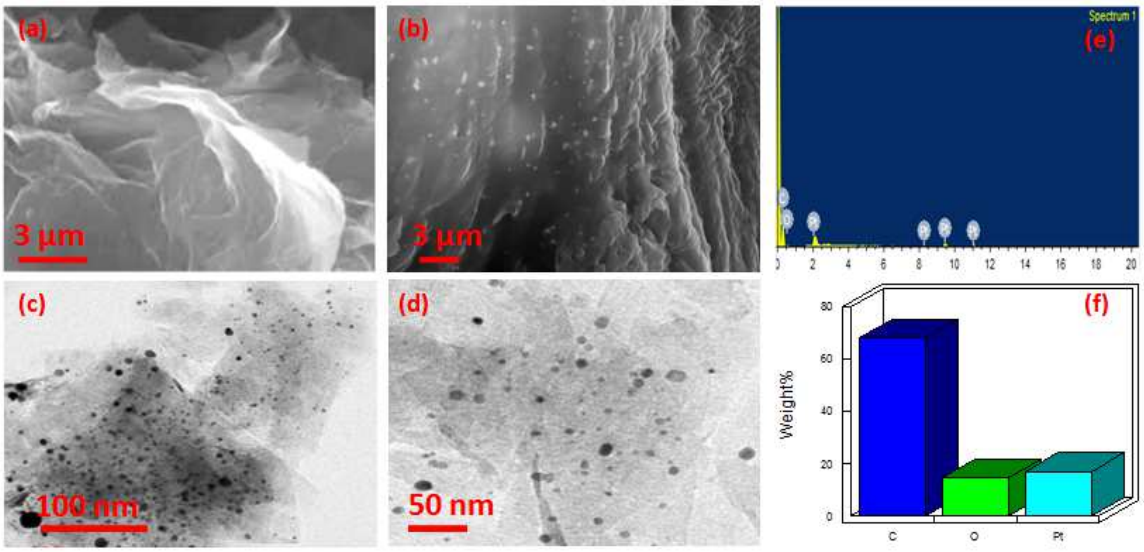

FIG. 3: SEM analyses of (a) graphene and (b) Pt/graphene; (c), (d) TEM analyses of Pt/graphene; (e), (f) EDX analyses of Pt/graphene

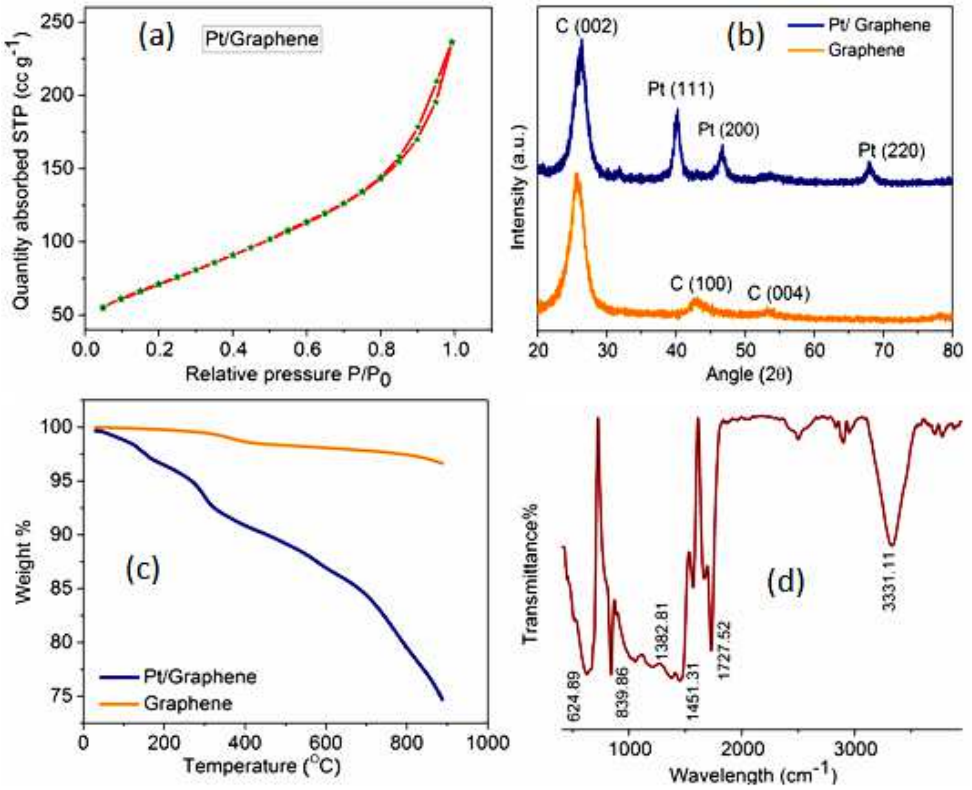

FIG. 4: (a) BET adsorption–desorption isotherms of Pt/graphene; (b) XRD of Pt/graphene and graphene; (c) TGA of Pt/graphene and graphene; (d) FTIR of Pt/graphene

TABLE 2: Optimization of reaction conditions using commercial Pt-loaded graphene (Pt/graphene) for hydrogenation of ethyl 2-oxopropanoate

S Number	Pressure (Bar)	Yield[1] (%)
1	10	68.4
2	20	85.7
3	30	93.0
4	40	96.2
5	50	99.8

[1]Reaction was performed using 5 wt% Pt/graphene (30 mg), ethyl 2-oxopropanoate (0.5 mmol), and acetic acid for 12 h at room temperature. Racemic mixtures of the products were obtained.

Based on these observations, asymmetric catalytic hydrogenation of other ketoesters is studied using Pt/graphene under the optimized reaction conditions (Table 1). Among these ketoesters, ethyl 2-oxopropanoate is found to be the most effective in terms of product yield and enantioselectivity, that is $>$ 96.8% *ee*. The specific rotation of the product is determined using a polarimeter, which confirmed enantioselectivity reduction of the S-enantiomer.

3.1 Substrate–Modifier Interaction

To examine the interaction between substrate and modifier, 1H NMR is recorded in toluene-d8 (Fig. 5). An account of the detailed experimental process and discussion can be found in Sharma and Sharma, 2015. An NMR study reveals the π–π interaction between modifier and substrate. The proton chemical shift of cinchonine suggests the interaction participation of ketoesters. This interaction helps to control the mode of substrate adsorption and chiral induction on the catalyst surface. Thus, cinchonine behaves like a ligand and forms a substrate–modifier complex.

3.2 Recyclability of the Catalyst

In the present case, the stability of Pt/graphene is tested using a recycling process, in which the catalyst is separated out by centrifugation and washed with acetic acid after each reaction cycle. For a new catalytic test, a fresh reactant and cinchonine are added to the reaction mixture and the same steps are repeated for five consecutive cycles. A relatively constant conversion and enantioselectivity are obtained in all cycles. TEM and XRD analyses of recycled Pt/graphene confirmed the catalytic center (Fig. 6).

4. CONCLUSIONS

We used a simple wet chemical method to prepare Pt/graphene. The new composite combines the unique and attractive behavior of graphene and Pt NPs. Asymmetric heterogeneous hydrogenation of α-ketoester is studied using Pt/graphene and is found to exhibit excellent conversion (99.8%) and enantioselectivity ($>$ 96.8%). The supremacy of Pt/graphene is attributed to the high surface area of graphene and well-dispersed Pt NPs on the graphene sheet. NMR studies elucidate the substrate–modifier complex. Catalyst reusability is obtained during up to five cycles without loss of activity.

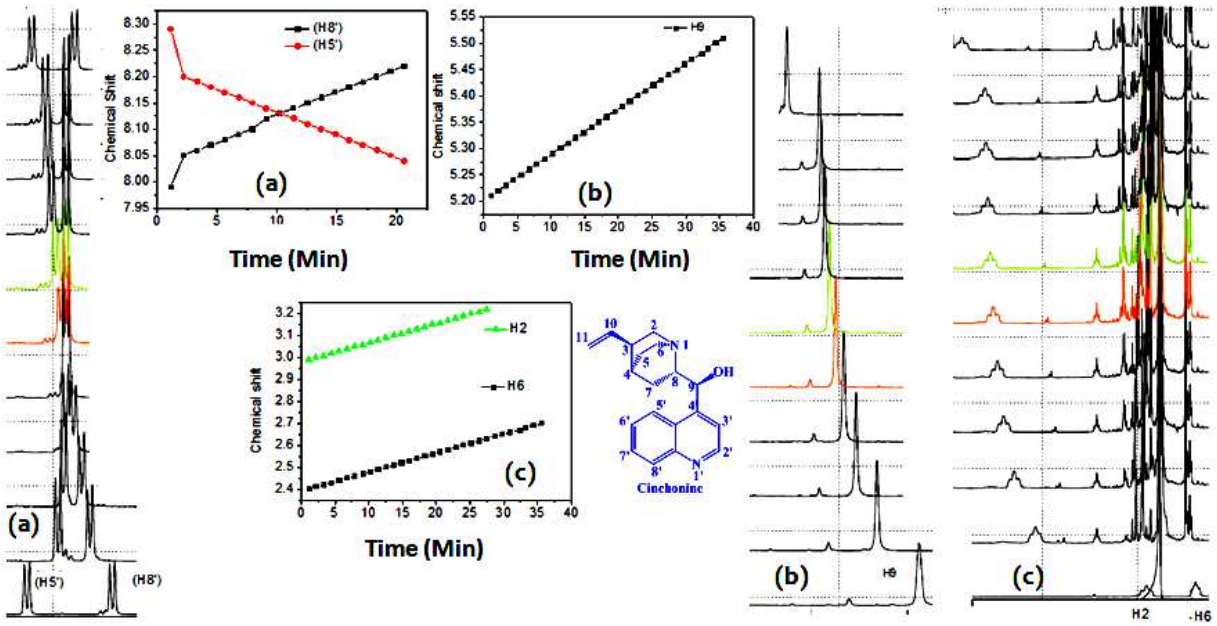

FIG. 5: NMR spectra (Sharma and Sharma, 2015, 2016) of (a) an H5′ and H8′ proton and the corresponding plot of chemical shift versus reaction time; (b) NMR spectra for the H9 proton and the corresponding plot of chemical shift versus reaction time; (c) NMR spectra of H2 and H6 protons and the corresponding plot of chemical shift versus reaction time

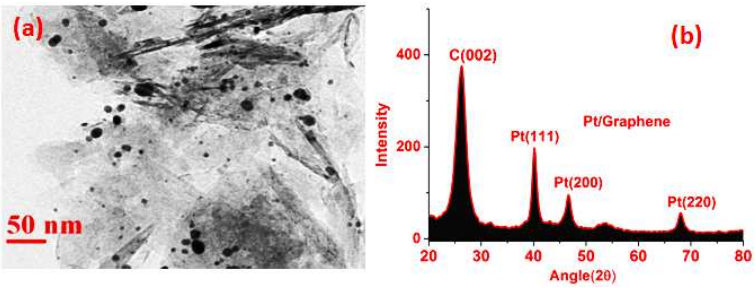

FIG. 6: (a) TEM image and (b) XRD pattern after five catalytic cyclese

ACKNOWLEDGMENTS

We thank the Indian Institute of Technology, Jodhpur, India, for a studentship (to P.S.) and the Department of Science and Technology of the Russian Foundation for Basic Research (Indo-Russian bilateral project INT/RFBR/P-134) for financial support.

REFERENCES

Allen, M.J., Tung, V.C., and Kaner, R.B., Honeycomb Carbon: A Review of Graphene, *Chem. Rev.*, vol. **110**, no. 1, pp. 132–145, 2009.

Berthod, M., Mignani, G., Woodward, G., and Lemaire, M., Modified BINAP: The How and the Why, *Chem. Rev.*, vol. **105**, no. 5, pp. 1801–1836, 2005.

Blaser, H. and Jalett, H., Enantioselective Hydrogenation of α-Ketoacids using Platinum Catalysts Modified with Cinchona Alkaloids, *Stud. Surf. Sci. Catal.*, vol. **78**, pp. 139–146, 1993.

Blaser, H., Jalett, H., Lottenbach, W., and Studer, M., Heterogeneous Enantioselective Hydrogenation of Ethyl Pyruvate Catalyzed by Cinchona-Modified Pt Catalysts: Effect of Modifier Structure, *J. Am. Chem. Soc.*, vol. **122**, no. 51, pp. 12675–12682, 2000.

Blaser, H.-U., Jalett, H.-P., Mller, M., and Studer, M., Enantioselective Hydrogenation of α-Ketoesters using Cinchona Modified Platinum Catalysts and Related Systems: A Review, *Catal. Today*, vol. **37**, no. 4, pp. 441–463, 1997.

Britto, P., Santhanam, K., and Ajayan, P., Carbon Nanotube Electrode for Oxidation of Dopamine, *Bioelectr. Bioenerg.*, vol. **41**, no. 1, pp. 121–125, 1996.

Carvalho Padilha, J., Nol, J.-M., Bergamini, J.-F., Rault-Berthelot, J., and Lagrost, C., Functionalization of Carbon Materials by Reduction of Diazonium Cations Produced in Situ in a Br⊘nstedt Acidic Ionic Liquid, *Chem. Electro. Chem.*, vol. **3**, no. 4, p. 572, 2016.

Chen, Z., Guan, Z., Li, M., Yang, Q., and Li, C., Enhancement of the Performance of a Platinum Nanocatalyst Confined within Carbon Nanotubes for Asymmetric Hydrogenation, *Angew. Chem. Int. Ed.*, vol. **50**, no. 21, pp. 4913–4917, 2011.

Chen, Q.-A., Ye, Z.-S., Duan, Y., and Zhou, Y.-G., Homogeneous Palladium-Catalyzed Asymmetric Hydrogenation, *Chem. Soc. Rev.*, vol. **42**, no. 2, pp. 497–511, 2013.

Fraga, M., Mendes, M., and Jordao, E., Examination of the Surface Chemistry of Activated Carbon on Enantioselective Hydrogenation of Methyl Pyruvate over Pt/C Catalysts, *J. Mol. Catal. A Chem.*, vol. **179**, no. 1, pp. 243–251, 2002.

Guo, S., Dong, S., and Wang, E., Three-Dimensional Pt-on-Pd Bimetallic Nanodendrites Supported on Graphene Nanosheet: Facile Synthesis and Used as an Advanced Nanoelectrocatalyst for Methanol Oxidation, *ACS Nano*, vol. **4**, no. 1, pp. 547–555, 2009.

Guo, S., Wen, D., Zhai, Y., Dong, S., and Wang, E., Platinum Nanoparticle Ensemble-on-Graphene Hybrid Nanosheet: One-Pot, Rapid Synthesis, and Used as New Electrode Material for Electrochemical Sensing, *ACS Nano*, vol. **4**, no. 7, pp. 3959–3968, 2010.

Li, W. and Zhang, X., Asymmetric Hydrogenation of Imines, in *Stereoselective Formation of Amines*, Heidelberg: Springer, pp. 103–144, 2013.

Li, Y., Tang, L., and Li, J., Preparation and Electrochemical Performance for Methanol Oxidation of Pt/Graphene Nanocomposites, *Electrochem. Comm.*, vol. **11**, no. 4, pp. 846–849, 2009.

Mallat, T., Orglmeister, E., and Baiker, A., Asymmetric Catalysis at Chiral Metal Surfaces, *Chem. Rev.*, vol. **107**, no. 11, pp. 4863–4890, 2007.

Marcelli, T. and Hiemstra, H., Cinchona Alkaloids in Asymmetric Organocatalysis, *Synthesis*, vol. **2010**, no. 8, pp. 1229–1279, 2010.

Rouhi, A.M., Chiral Business, *Chem. Eng. News*, vol. **81**, no. 18, pp. 45–55, 2003.

Satishkumar, B., Vogl, E.M., Govindaraj, A., and Rao, C., The Decoration of Carbon Nanotubes by Metal Nanoparticles, *J. Phys. D Appl. Phys.*, vol. **29**, no. 12, p. 3173, 1996.

Sharma, P. and Sharma, R.K., Platinum Functionalized Multiwall Carbon Nanotube Composites as Recyclable Catalyst for Highly Efficient Asymmetric Hydrogenation of Methyl Pyruvate, *RSC Adv.*, vol. **5**, no. 124, pp. 102481–102487, 2015.

Sharma, P. and Sharma, R.K., Asymmetric Hydrogenation of α-Ketoesters on the Pt (111) Surface, *New J. Chem.*, vol. **40**, no. 11, pp. 9038–9041, 2016.

Sharma, P. and Sharma, R.K., Platinum Functionalized Chiral Polyamides: Efficient Heterogeneous Catalyst for Solvent Free Asymmetric Hydrogenation of Ethyl 2-Oxo-4-Phenylbutanoate, *Chem. Select*, vol. **2**, no. 1, pp. 513–520, 2017.

Tan, J.L., De Jesus, A.M., Chua, S.L., Sanetuntikul, J., Shanmugam, S., Tongol, B.J.V., and Kim, H., Preparation and Characterization of Palladium-Nickel on Graphene Oxide Support as Anode Catalyst for Alkaline Direct Ethanol Fuel Cell, *Appl. Catal. A Gen.*, vol. **531**, pp. 29–35, 2017.

Tauster, S., Fung, S., and Garten, R.L., Strong Metal-Support Interactions. Group 8 Noble Metals Supported on Titanium Dioxide, *J. Am. Chem. Soc.*, vol. **100**, no. 1, pp. 170–175, 1978.

Tsang, S., Chen, Y., Harris, P., and Green, M., A Simple Chemical Method of Opening and Filling Carbon Nanotubes, *Nature*, vol. **372**, pp. 159–162, 1994.

von Arx, M., Dummer, N., Willock, D., Taylor, S.H., Wells, P.B., and Hutchings, G.J., Observation of High Enantioselectivity for the Gas Phase Hydrogenation of Methyl Pyruvate using Supported Pt Catalysts Pre-Modified with Cinchonidine, *Chem. Comm. (Cambridge)*, vol. **15**, pp. 1926–1927, 2003.

Wang, D., Choi, D., Li, J., Yang, Z., Nie, Z., Kou, R., Hu, D., Wang, C., Saraf, L.V., and Zhang, J., Self-Assembled TiO_2–Graphene Hybrid Nanostructures for Enhanced Li-Ion Insertion, *ACS Nano*, vol. **3**, no. 4, pp. 907–914, 2009.

Weiss, N.O., Zhou, H., Liao, L., Liu, Y., Jiang, S., Huang, Y., and Duan, X., Graphene: An Emerging Electronic Material, *Adv. Mater.*, vol. **24**, no. 43, pp. 5782–5825, 2012.

Wilhelmus, A., New Enantioselective Reactions Catalysed by Cinchonidine-Modified Platinum, *J. Am. Chem. Soc., Chem. Comm.*, no. 13, pp. 1053–1054, 1993.

Xie, Y., Wang, J., Huang, X., Luo, B., Yu, W., and Shao, L., Palladium Nanoparticles Supported on Graphene Sheets Incorporating Boron Oxides (B_xO_y) for Enhanced Formic Acid Oxidation, *Electrochem. Comm.*, vol. **74**, pp. 48–52, 2017.

Yoon, T.P. and Jacobsen, E.N., Privileged Chiral Catalysts, *Science*, vol. **299**, no. 5613, pp. 1691–1693, 2003.

Zhang, K., Zhang, L.L., Zhao, X., and Wu, J., Graphene/Polyaniline Nanofiber Composites as Supercapacitor Electrodes, *Chem. Mater.*, vol. **22**, no. 4, pp. 1392–1401, 2010.

Zhou, H., Chen, Q., Li, G., Luo, S., Song, T.-B., Duan, H.-S., Hong, Z., You, J., Liu, Y., and Yang, Y., Interface Engineering of Highly Efficient Perovskite Solar Cells, *Science*, vol. **345**, no. 6196, pp. 542–546, 2014.

EPOXIDATION OF CANOLA OIL FOR THE PRODUCTION OF BIOLUBRICANTS USING SILICA-TITANIA TiSBA-15 HETEROGENEOUS CATALYSTS

C.S. Madankar,[1,2,3,] R.V. Sharma,[1] A.K. Dalai,[1] & S.N. Naik[2]*

[1]*Catalysis and Chemical Reaction Engineering Laboratory, Department of Chemical and Biological Engineering, University of Saskatchewan, Saskatoon, SK S7N 5A9, Canada*

[2]*Centre for Rural Development and Technology, Indian Institute of Technology, Hauz Khas, New Delhi 110016, India*

[3]*Department of Oils, Oleochemicals, and Surfactants Technology, Institute of Chemical Technology, N.P. Marg, Matunga, Mumbai 400019, India*

*Address all correspondence to: C.S. Madankar, Department of Oils, Oleochemicals, and Surfactants Technology, Institute of Chemical Technology, N.P. Marg, Matunga, Mumbai 400019; Tel.: + 91 22 33612557, E-mail: chandumadankar@gmail.com

Original Manuscript Submitted: 12/12/2017; Final Draft Received: 1/9/2018

We focus on the preparation and use of mesoporous TiSBA-15 (Santa Barbara Amorphous) material with different Si/Ti mass ratios. Catalysts with different Si/Ti mass ratios were prepared and characterized by several techniques including X-ray powder diffraction, Fourier-transform infrared (FTIR) spectroscopy, and Brunauer–Emmett–Teller surface area analysis. N_2 adsorption and desorption isotherms revealed that all of the catalysts have large surface areas ($\sim$ 900 m^2/g) and pore diameters in the range of mesopores ($\sim$ 7 nm), making them suitable catalysts for bulky molecular transformation reactions. Catalyst activity was examined for the preparation of a biolubricant from the epoxidation of canola oil. Canola oil epoxidation was carried out at 70°C, with a canola oil–to–hydrogen peroxide molar ratio of 1:14 and catalyst loading of 5 wt%. TiSBA-15 with a mass ratio of 20 resulted in 88% conversion based on unsaturation. The oxirane oxygen content of the product was 1.66, and the formation of an epoxide product of canola oil was confirmed by FTIR, ^1H nuclear magnetic resonance (NMR), and ^{13}C NMR spectral analysis. These studies showed that TiSBA-15 with the mass ratio of 20 shows promise for the preparation of epoxidized canola oil that can act as a starting material for lubricant formulation. On the basis of these results, we conclude that this system could have great potential for industrial use.

KEY WORDS: *canola oil, epoxidation, biolubricant, solid catalyst, epoxidized canola oil*

1. INTRODUCTION

Research on the synthesis of environmentally friendly biolubricants has attracted wide attention. Each year, $\sim 9 \times 10^6$ metric tons of lubricants are used by industry, especially the automobile industry, and the amount is increasing. Petroleum-based lubricants generate a significant amount of waste, increasing concern about pollution, thus necessitating further development (Salimon et al., 2010). Vegetable oil–based lubricants are preferred over petroleum-based synthetic fluids because they are renewable, nontoxic, and biodegradable. Most vegetable oils, including rapeseed, soybean, palm, palm kernel, olive, and *Jatropha*, have been used as precursors for biolubricants. Viscosity, viscosity index, oxidative stability, thermal stability, flash point, low-temperature fluidity, corrosiveness, wear resistance, biodegradability, and nontoxicity are the main properties of lubricants that determine their range of application.

A lubricant must remain in the liquid state over a wide range of temperature. This property can be evaluated by pour point at lower temperature and flash point at higher temperature. Vegetable oils with high oleic content are considered to be potential substitutes for conventional mineral oil–based lubricants and synthetic esters (Hwang and Erhan, 2001). The poor oxidative stability of lubricants is due to the double bonds present in fatty acid chains of the triglyceride molecule. Most triglyceride-based vegetable oils contain unsaturated fatty acids, therefore producing greater levels of unsaturation; the greater the number of double bonds, the more susceptible is the oil to oxidation and decreased oxidation stability. Oxidation of a biolubricant results in insoluble deposits and increased oil acidity and viscosity (Jayadasa et al., 2007). Studies of low-temperature properties have also revealed that most vegetable oils undergo cloudiness, precipitation, and solidification at colder temperatures (Schuster et al., 2008). A few reports are available on ester and estolide biolubricant preparation from castor, *Lesquerella*, and meadowfoam oils through chemical modification (Erhan et al., 1993; Isbell et al., 2006; Madankar et al., 2013). Epoxidized vegetable oil can also be used as a high-temperature lubricant, and products obtained from the ring opening of epoxidized oil can be used in low-temperature lubricants (Hang and Yang, 1999). Epoxidized vegetable oils can also act as promising intermediates for the use of vegetable oils that may be easily functionalized. Erhan et al. (2008) reported an acid-catalyzed epoxy ring-opening reaction between epoxidized soybean oil and different alcohols. The researchers esterified the resulting hydroxyl group with an acid anhydride and also reported a method for preparing biolubricant from dihydroxylated soybean oil, which is obtained using acid hydrolysis of the epoxide group followed by esterification (Adhvaryu et al., 2005; Sharma et al., 2006). Sharma et al. (2015) reported on the production of biolubricants from canola biodiesel, stating that this lubricant has low cloudiness and pour point properties, better friction, and antiwear characteristics. Salimon and Salih (2010) reported on the oxirane ring opening of epoxidized oleic acid using behenic acid and p-toluenesulfonic acid as catalyst followed by the esterification reaction with 1-octanol and 2-ethylhexanol to form diesters. The remaining free hydroxyl group reacted with oleic and stearic acid to yield trimesters (Salimon and Salih, 2010). Tinia et al. used an alkaline-based catalyst to prepare biolubricant from *Jatropha* oil. These authors used a two-step process as follows: (1) transesterification of *Jatropha* oil produced *Jatropha* methylester (JME) and (2) transesterification of JME with trimethylolpropane (TMP) occurred in the presence of an alkaline-based catalyst under reduced pressure. Sinadinovic-Fiser et al. (2001) reported the kinetics of soybean oil epoxidation in the presence of an ion exchange resin (as the catalyst) and peracetic acid, which were generated in situ due to the reaction of acetic acid and hydrogen peroxide. Canada is the largest exporter of canola oil in the world and the second-largest producer of canola oil seeds. Saskatchewan province is responsible for $\sim$ 38% of the total canola oil production in western Canada (Kulkarni et al., 2006). The chemical application of canola oil is limited to biodiesel production (no other chemical derivatives are made from canola oil) (Mungroo et al., 2008). Canola oil has a unique composition of $\sim$ 60% oleic fatty acid; it is therefore a perfect candidate for epoxidation.

Epoxidized canola oil (ECO) may be a promising source for biolubricating oil and renewable feedstock for the chemical industry. The objective of our research was to study the epoxidation of canola oil to produce ECO (Mungroo et al., 2011). Percarboxylic acids and organic and inorganic peroxides can be used as reagents for epoxidation of vegetable oils, but these generate significant amount of chemical waste. However, a cleaner process can be designed using heterogeneous catalysts instead of traditional homogeneous mineral acid (Capanella et al., 2004). The main goal of our work is to investigate the feasibility of producing biolubricants via heterogeneous catalytic transformation of canola oil. Mesoporous materials such as TiSBA-15 (Santa Barbara Amorphous) have the advantage of larger surface area compared with that of amorphous Ti–SiO_2, which is suitable for bulky molecular transformation reactions.

2. EXPERIMENT

2.1 Material

Canola oil was supplied by Loblaws Co. Ltd. (Montreal, Canada). Sources of other chemicals include glacial acetic acid (100%), 33% HBr in acetic acid, poly(ethylene glycol)-block-poly(propylene glycol)-block-poly(ethylene glycol), titanium isopropoxide, and tetraethyl orthosilicate: EMD Chemicals Inc. (Darmstadt, Germany); formic acid (88%): Sigma-Aldrich (St. Louis, MO); hydrogen peroxide (30 wt%): EMD Chemicals Inc. (Gibbstown, NJ); iodine monochloride and Wijs solution: VWR (San Diego, CA).

2.2 Catalyst Preparation

TiSBA-15 with different Si/Ti ratios was synthesized using poly(ethylene glycol)-block-poly(propylene glycol)-block-poly(ethylene glycol) as a structure-directing agent and titanium isopropoxide and tetraethyl orthosilicate as titanium and silica sources, respectively (Vinu et al., 2006). The molar gel composition of the mixture is 0.988 TEOS (Tetra Ethyl Orthosilicate):0.012−0.05 Ti(-OiPr)$_4$:0.016 P123:0.46 HCl:127 H_2O. In a typical TiSBA-15 synthesis, 9.28 g of pluronic P123 were added to 228.6 g of water. After stirring for 2 h, a clear solution was obtained, 4.54 g of HCl (37%) was added, and the solution was stirred for another 2 h. Then, 20.6 g of tetraethyl orthosilicate and the required amount of the Ti source were added, and the resulting mixture was stirred for 24 h at 40°C. The solid product was recovered by filtration, washed several times with water, and dried overnight at 100°C. The resulting gel was transferred to a polypropylene bottle and kept in an air oven for 48 h at 100°C. Finally, the product was calcined at 550°C to remove the template. The samples were labeled TiSBA-15(x), where (x) denotes the Si/Ti mass ratio (Soni et al., 2012).

2.3 Characterization

2.3.1 N_2 Adsorption–Desorption Isotherms

Nitrogen physisorption isotherms were obtained using a Micromeritics ASAP 2000 analyzer. Before analysis, the catalyst was out-gassed in a vacuum at 200°C until the static pressure remained $< 6.6 \times 10^{-4}$ Pa. The Brunauer–Emmett–Teller (BET) method was used to calculate surface area in the range of relative pressures between 0.01 and 0.20. Pore diameters (Pd) and pore size distributions (P/P_0) were calculated from the adsorption and desorption branches of the isotherms using the Barrett–Joyner–Halenda (BJH) method. The mesopore volume was determined from the N_2 adsorbed at a P/P_0 of 0.4. The total pore volume (Vp) was calculated from the amount of nitrogen adsorbed at P/P_0 of 0.95, assuming that adsorption on the external surface was negligible compared with that in pores. In all cases, correlation coefficients > 0.999 were obtained.

2.3.2 X-Ray Diffraction Analysis

Catalysts were analyzed by small-angle X-ray scattering to ascertain their crystal structures. Diffraction patterns were recorded with a Bruker Smart 6000 charge-coupled-device detector on a three-circle D8 goniometer using a Rigaku RU 200 Cu rotating anode generator fitted with parallel focusing cross-coupled mirrors and a 0.5-mm pinhole collimator. Data were obtained using a still data collection (SMART: Bruker Software) with an exposure time of 300 s in the 0°–10.0° range. Broad-angle X-ray diffraction (XRD) patterns of all SBA-15–supported catalysts were recorded on a Rigaku diffractometer using Cu-K radiation.

2.3.3 Fourier-Transform Infrared Spectroscopy

Fourier-transform infrared (FTIR) spectra were recorded in the range of a 400 to 4000 cm^{-1} wave number with a Perkin-Elmer Spectrum GX instrument (Wellesley, MA), equipped with a deuterated triglycine sulfate detector and a KBr beam splitter. Spectra for each analysis were averaged from 16 scans with a nominal 4-cm^{-1} resolution using a spectroscopic-grade potassium bromide (KBr) cell.

The pyridine FTIR adsorption experiment was performed to ascertain Lewis and Brønsted acid sites. Before the analysis, samples were dried at 500°C and maintained under vacuum (10^{-7} bar) for 3 h. Pyridine was then injected into the sample by saturating the carrier gas helium for 30 min at room temperature, followed by degassing and evacuation at 250°C. The spectra were detected using the Perkin-Elmer Spectrum-GX spectrophotometer with a 1400–1700 cm^{-1} wavelength.

2.3.4 Scanning Electron Microscopy

To assess catalyst particle and surface morphology, we used scanning electron microscopy (Zeiss EVO Series, model EVO 50).

2.3.5 Experimental Setup and Procedure

All experiments were carried out in a 50-cm^3-capacity borosilicate glass reactor with a 5-cm internal diameter. The reactor was equipped with four equally spaced baffles, a standard six-blade pitched turbine impeller, and a reflux condenser. The reaction temperature was maintained by means of a thermostatic oil bath with an accuracy of $\pm$ 1°C. The side neck of the flask was connected to a reflux condenser, and a thermometer was introduced through the other side neck to record reaction-mixture temperature. The mixture was stirred using the six-blade pitched turbine impeller through the central neck of the flask. We placed 10 g of canola oil into the reactor and added the necessary amounts of tert-butanol (10 g) and catalyst (catalyst loading is expressed as wt% of canola oil; here, the value was 5 wt%). The mixture was continuously stirred for 5 min, after which 18 g of 30% aqueous hydrogen peroxide (3 mol hydrogen peroxide per mole of ethylenic unsaturation) were added in a dropwise fashion to the reaction mixture at a rate such that the hydrogen peroxide addition was completed within 30 min. After the complete addition of hydrogen peroxide, the reaction continued for 24 h with 1000-rpm stirring. Constant stirring was maintained throughout the experiment so that a fine dispersion of oil could be achieved. After 24 h, the reaction mixture was cooled to 25°C and then immediately extracted with diethyl ether in a separating funnel, washed with cold and slightly hot water (successively), and analyzed for oxirane content and iodine value.

2.3.6 Analysis of Product

The oxirane oxygen content of each sample was determined using a direct method with hydrobromic acid solution in acetic acid, and the iodine value was determined using a Wijs solution (May, 1973; Paquot, 1979). Any excess periodate and iodic acid that was formed was reduced with potassium iodide, and the liberated iodine was titrated with sodium thiosulfate. ^{1}H NMR and ^{13}C NMR spectra were recorded using a Bruker (Ettlingen, Germany) AMX-500 FT spectrometer. From the oxirane content, the percentage of relative conversion to oxirane (RCO) was determined using the following formula:

$$\text{RCO} = (OO_{ex}/OO_{th}) \times 100,$$

where OO_{ex} is the experimentally determined content of oxirane oxygen, and OO_{th} is the theoretical maximum oxirane oxygen content in 100 g of oil, determined using the following expression (Petrovic et al., 2002):

$$OO_{th} = \{(Iv_o/2A_i)/[100 + (Iv_o/2A_i)A_o]\} \times A_o \times 100,$$

where A_i (126.9) and A_o (16.0) are the atomic weights of iodine and oxygen, respectively, and IV_o is the initial iodine value of the oil sample. Some of the experimental runs were repeated under identical conditions to determine the percentage of deviation between the two experimental results, and the deviation was found to be 1.0%–3.0%. The pour point was measured according to the American Society for Testing and Materials (ASTM) D-97, using a K46100 cloud point and pour point apparatus. Sample viscosity was measured at 40°C using the Brookfield model RVTDCP cone and plate viscometer (Brookfield Engineering Laboratories, Stoughton, MA).

3. RESULTS AND DISCUSSION

3.1 Characterization of Catalyst

3.1.1 Low-Angle XRD

The catalysts obtained after hydrothermal synthesis and calcinations were analyzed by low-angle XRD, and the resulting diffractograms of SBA-15 and TiSBA-15 with various Si/Ti ratios are shown in Fig. 1. Calcined siliceous SBA-15 and TiSBA-15 material showed a three-peak pattern consisting of a sharp, low-angle peak at $\sim 2\theta = 0.80$ and two weak peaks at $2\theta = 1.4$ and 1.6. These diffraction peaks are related to the long-range two-dimensional hexagonal order of a p6mm symmetry structure. The peak position slightly shifted to higher angles, and the unit cell parameter (a_o) increased from 9.6 nm for SBA-15 to 10.3 nm for TiSBA-15 (80) and 11.4 nm for TiSBA-15 (20), with increasing Ti content in the structure. The shift of unit cell parameter signifies longer Ti–O bond length compared

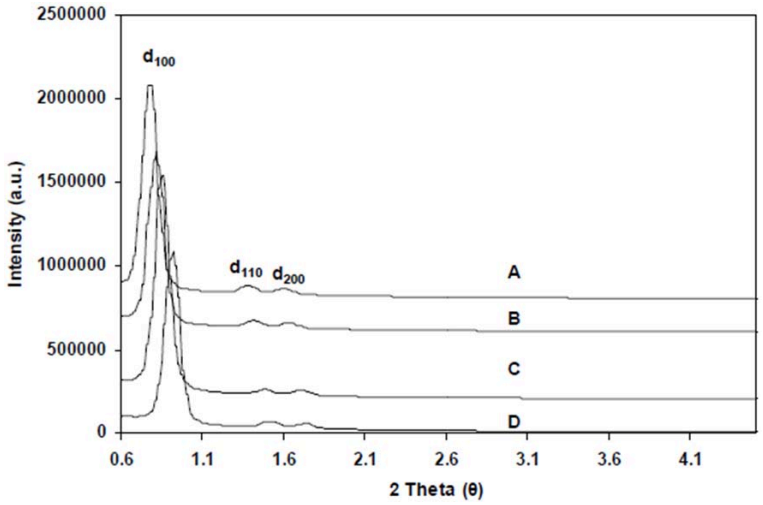

FIG. 1: Low-angle XRD pattern of TiSBA-15 catalysts with various Si/Ti ratios. Lines A–D represent TiSBA-15 (20), (B) TiSBA-15 (40), (C) TiSBA-15 (80), and (D) SBA-15, respectively.

to that of the Si–O bond. Such an observation indicates successful incorporation of Ti into the SBA-15 structure. These results are in agreement with the work of Chen et al. (2004). We estimated the pore-wall thickness (δ) of these materials by subtracting the pore-diameter value from the hexagonal unit cell dimension (a_o), which increases with increasing Ti content, indicating structure stability for all of the Ti content.

3.1.2 FTIR Spectroscopy

The framework vibration of Ti in the silica catalyst was examined using FTIR spectroscopy. The FTIR spectrum of TiSBA-15 with different Si/Ti ratios is given in Fig. 2. The band at 966 cm^{-1} in the spectra was due to Si-O-Ti vibrations, which are clearly visible in the TiSBA-15 catalyst spectra compared to that of pure SBA-15 (Choudhary

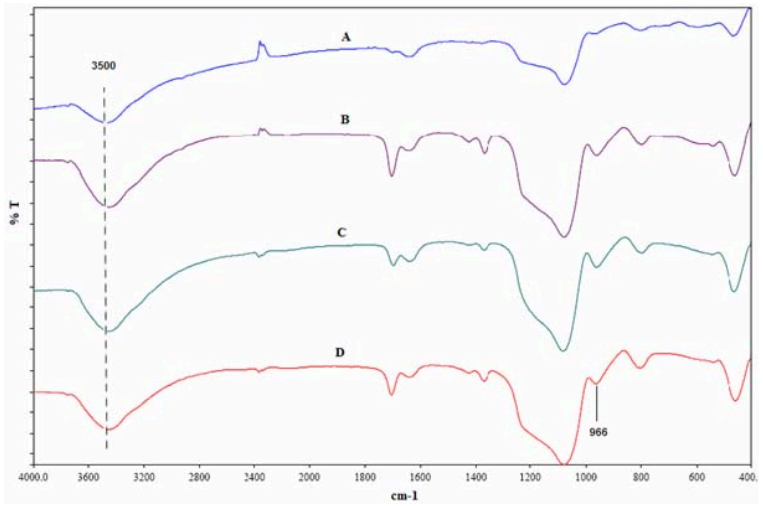

FIG. 2: FTIR spectra of SBA-15 and catalysts with different Si/Ti ratios ratios. Lines A–D: SBA-15, (B) TiSBA-15 (20), (C) TiSBA-15 (40), and (D) TiSBA-15 (80), respectively.

et al., 2001). The intensity of this band increases with increasing Ti content in the framework and indicates the successful incorporation of Ti ions inside the silica framework. We detected a broad band in the hydroxyl region of 3700–3300 cm^{-1} for all samples, due to surface hydroxyl groups that can be attributed to silanol groups interacting via hydrogen bonding, υOH (Si–O–H). The intensity of this band was higher in the case of TiSBA-15 and continuously increased as Ti content increased. Therefore, it can be seen that the more intense the band in Ti-containing samples, the more that hydrogen bonding is available in the Ti-containing SBA-15 samples, due to the presence of more defective sites (Boahene et al., 2011).

3.1.3 N_2 Adsorption–Desorption Isotherms and Pore Size Analysis

The N_2 adsorption–desorption isotherms, pore size distribution, and textural properties of TiSBA-15 with catalysts are given in Fig. 3 and Table 1, respectively. The isotherm of TiSBA-15 samples gives a clear H1-type hysteresis loop at high relative pressure, suggesting that the TiSBA-15 samples possess very regular mesoporous channels despite their large pore sizes; this is proven by the narrow Gaussian pore size distribution. These results clearly indicate that the structure remains unchanged after Ti addition during the synthesis process, which agrees with the XRD results shown in Fig. 1. The values of specific surface area (S; SBET), Vp, and Dp of supports are listed in Table 1. We noted that with an increase in Ti content, the BET surface area, Vp, and Vd of the TiSBA-15 catalyst increased, but the increment was unremarkable. Specific S increased with titanium content, following the order of SBA-15 < TiSBA-15 (20) < TiSBA-15 (80) < TiSBA-15 (40). These results suggest that the introduction of a large amount of Ti does not destroy the hexagonal structure of the support. The surface area of TiSBA-15 (20) is smaller than that of other Ti-containing SBA-15 material, due to the increased Dp of TiSBA-15 (20). The pore size of TiSBA-15 continuously increases with Ti loading, indicating high Ti incorporation in the framework of the silica material. This effect can occur due to greater bond length of Ti–O–Si rather than that of Si–O–Si, causing a greater pore size of TiSBA-15 (20) compared to other supports. This type of behavior has also been reported by Nava et al. (2007) for the case of TiSBA-15. The catalysts were also characterized for BJH pore size distribution, and that data as a function of Si/Ti ratio are given in Table 1. It can be seen that a sharp distribution centered around ∼ 7 nm is obtained for all cases. Dp for TiSBA-15 catalysts gradually increases in the following order: SBA-15 < TiSBA-15 (80) < TiSBA-15 (40) < TiSBA-15 (20).

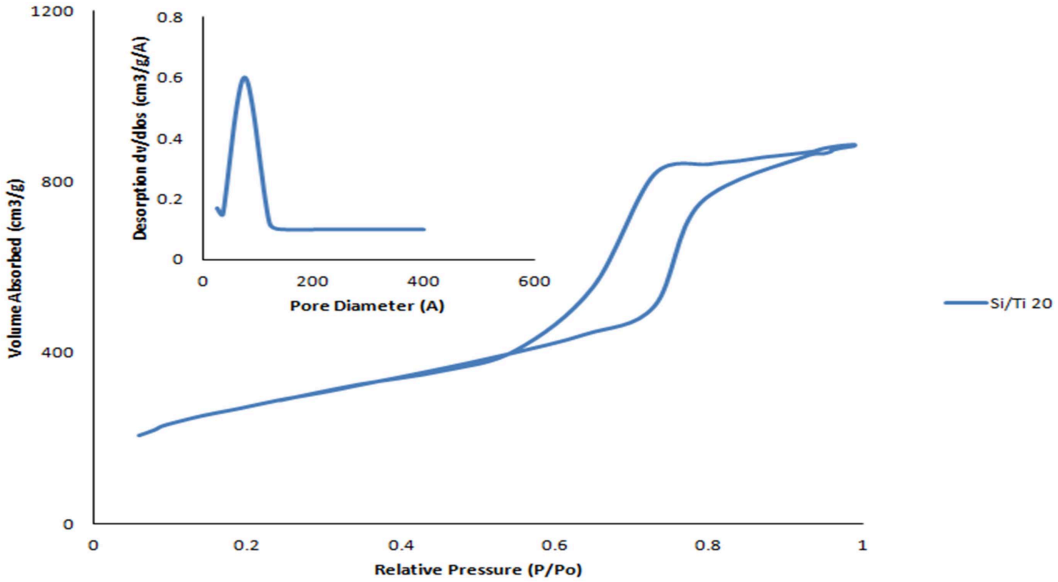

FIG. 3.

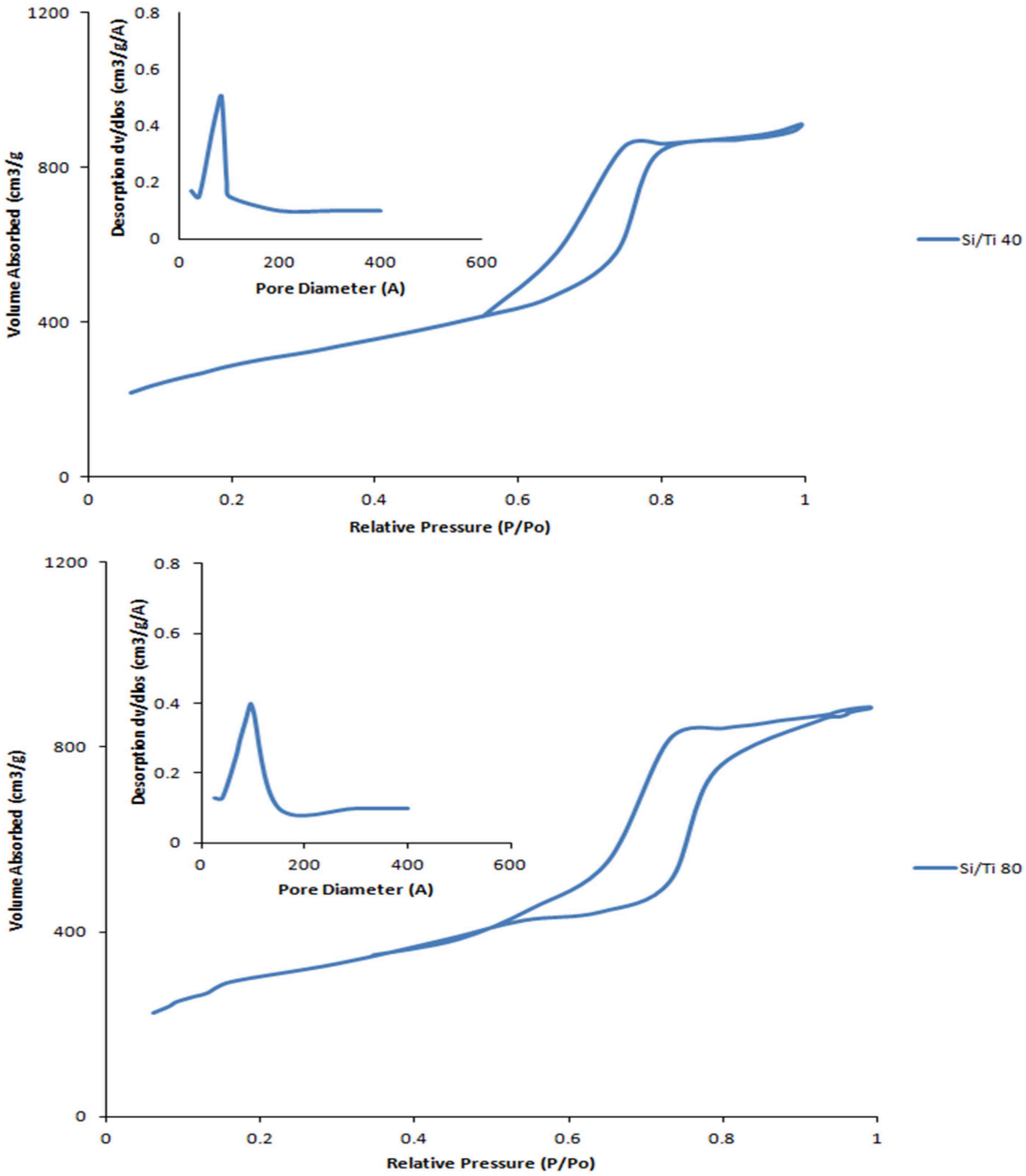

FIG. 3: N_2 Adsorption–desorption isotherm and BJH pore size distribution of TiSBA-15 with different Si/Ti ratio ratios. (Top) TiSBA-15 (20), (middle) TiSBA-15 (40), and (bottom) TiSBA-15 (80)

3.1.4 Scanning Electron Microscopy

As described in the literature, pure SBA-15 has bundled, rope-like units in a highly ordered structure (Zhao et al., 1998; Lopez-Munoz et al., 2005). Moreover, the regular silica morphology is maintained in the case of Ti-SBA-15 (80), but the hexagonal, highly ordered structure of the TiSBA-15 sample with a Si/Ti ratio of 20 is partially destroyed (Fig. 4).

TABLE 1: Textural characterization of SBA-15 and TiSBA-15 with different Si/Ti ratios (in parentheses)

Sample	BET (m^2/g) SBET	Dp (nm)	Vp (cm^3/g)	a_0 (nm)
SBA-15	767	6.40	0.86	9.6
TiSBA-15 (20)	898	7.47	1.26	11.4
TiSBA-15 (40)	928	7.19	1.59	11.0
TiSBA-15 (80)	919	6.70	0.87	10.3

BET, Brunauer–Emmett–Teller; Db, pore diameter, SBET, specific surface area calculated by the Brunauer–Emmett–Teller method; Vp, pore volume.
The normalized SBET (NSBET) can be calculated using $NSBET = (SBET$ of the catalysts)/$(1 - x)$. Vp is determined by nitrogen adsorption at a relative pressure of 0.98, Dp is the mesopore diameter corresponding to the maximum of the pore size distribution obtained from the adsorption isotherm using the Barrett–Joyner–Halenda method, and a_o is the unit cell parameter estimated from the position of the (100) diffraction line $a_o = 2d100/\sqrt{3}$ (pore wall thickness $= a_o - Dp$).

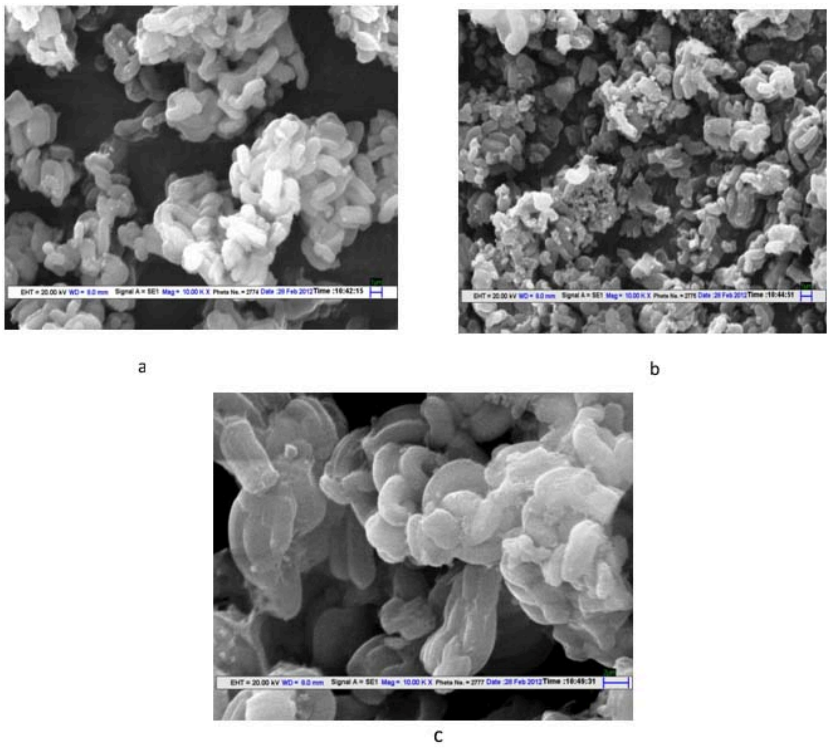

FIG. 4: Scanning electron micrographs for TiSBA-15 supported with different Si/Ti loadings. (a) TiSBA-15 (20), (b) TiSBA-15 (40), and (c) TiSBA-15 (80)

3.1.5 Catalytic Activity Studies

Oxidation activity of all of the prepared catalysts was studied by carrying out epoxidation of canola oil using hydrogen peroxide as the oxidant. We found that TiSBA-15 (20) has better activity than TiSBA-15 (40) and TiSBA-15 (80), because the titania content in TiSBA-15 (20) is greater. It is well documented that titania induces acidity to catalysts. Table 2 shows the oxirane oxygen content of ECO. Catalyst TiSBA-15 (20), with a 1.66 oxirane oxygen content,

TABLE 2: Oxirane oxygen content of ECO with different catalysts

Catalyst	Oxirane Oxygen Content
SBA-15	0.24
TiSBA-15 (20)	1.66
TiSBA-15 (40)	0.44
TiSBA-15 (80)	0.23

Reaction condition: Canola oil (10 g), 30% H_2O_2 (18 g), tert-butanol (10 g), temperature (70°C), time (24 h), and rpm (1000).

shows better activity than the other catalysts. Table 3 lists the iodine values for ECO; the value for pure canola oil is 119.50. Among all of the catalysts, the ECO iodine value for the catalyst TiSBA-15 (20) is the lowest, showing that most of the double bonds are converted into oxirane linkages. Figure 5 introduces the percentage of canola oil conversion based on unsaturation. TiSBA-15 (20) has the greatest conversion in comparison to the other catalysts. The TiSBA-15 (20) catalyst has a greater Si–O–Ti linkage, which is responsible for the activity: The linkage helps to generate nascent oxygen from hydrogen peroxide, producing which further reaction with canola oil through a catalyst surface reaction mechanism.

3.1.6 FTIR Spectroscopy for Product Analysis

The characteristic peak of canola oil at 3007 cm^{-1} can be attributed to C–H stretching of the double C = C–H. The peak at 3007 cm^{-1} disappeared after the reaction, indicating that almost all of the C = C bonds took part in the epoxidation reaction (Fig. 6). The new peaks appearing at 823 cm^{-1} are attributed to the epoxy group. Another new peak at 3463 cm^{-1} is a result of hydroxyl O–H stretching, indicating that the epoxy group is open. The intensity of the 3463-cm^{-1} band illustrates the extent of the ECO hydroxyl group. Vlcek and Petrovic (2006) reported the presence of epoxy groups at 822–833 cm^{-1}, which agrees well with this spectrum, where the epoxy group was detected at 823 cm^{-1}.

3.1.7 NMR Spectroscopy Analysis

^{1}H NMR and ^{13}C NMR confirmed the formation of an epoxide product of canola oil. ECO shows the epoxy group to be present in the 2.98–3.1 parts per million (ppm) region. The peaks at this region represent a CH–proton attached to the oxygen atom of both epoxy groups. A chemical shift in the epoxy group was observed at 2.98–3.1 ppm in ECO.

TABLE 3: Iodine value of ECO with different catalysts

Catalyst	Iodine Value
SBA-15	103.96
TiSBA-15 (20)	14.42
TiSBA-15 (40)	92.11
TiSBA-15 (80)	105.16
Canola oil	119.5

Reaction condition: Canola oil (10 g), 30% H_2O_2 (18 g), tert-butanol (10 g), temperature (70°C), time (24 h), and rpm (1000).

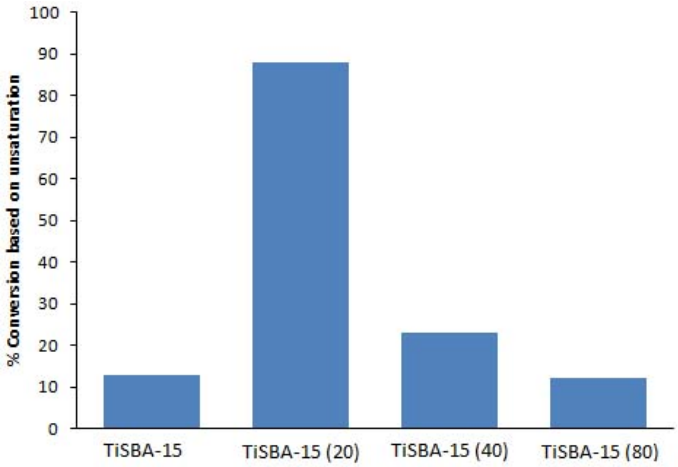

FIG. 5: Percentage of canola oil conversion based on unsaturation. Reaction conditions: Canola oil (10 g), 30% H_2O_2 (18 g), tert-butanol (10 g), temperature (70°C), time (24 h), rpm (1000)

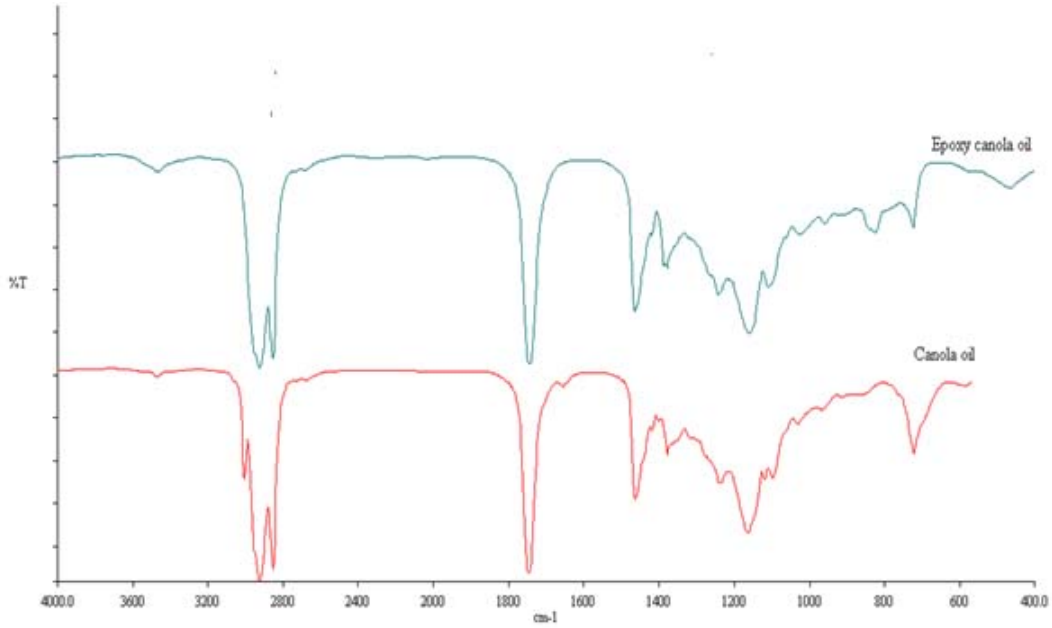

FIG. 6: FTIR spectroscopy analysis of epoxy canola oil (top) and canola oil (bottom)

Olefinic hydrogens (CH = CH) of canola oil are present at 5.2–5.4 ppm. Their partial appearance in ECO suggests that C = C is not completely converted to epoxide (Fig. 7). As seen in Fig. 5, the conversion percentage of the reaction is 88%. The ^{13}C NMR spectra of canola oil and ECO that are shown in Fig. 7 reveal the complete disappearance of the olefin carbon atom between 100 and 150 ppm in the final product, compared its presence in the canola oil beforehand. In addition, ECO shows signals between 53 and 60 ppm, and the glycerol carbon signals at 68 and 62 ppm for β and α atoms, respectively. These additional peaks, which are completely absent in the nonreacted canola oil, are due to the epoxy or glycol carbon of the ECO.

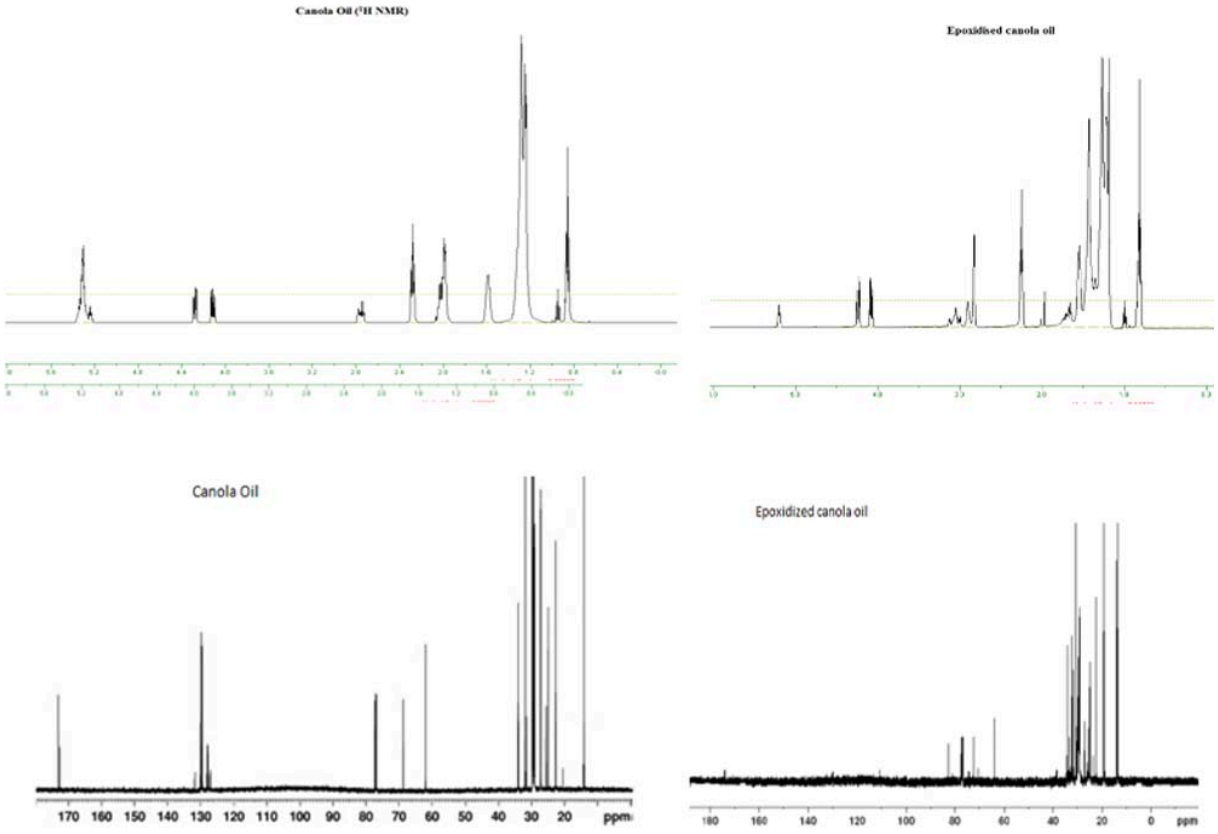

FIG. 7: ^{1}H NMR (top panels) and ^{13}C NMR (bottom panels) spectroscopy analyses of canola oil and ECO

3.1.8 Physical and Chemical Properties of ECO

The physicochemical properties of ECO, defined in accordance with ASTM D-6751 standard methods, are kinematic viscosity, density, acid value, pour point, cloud point, and total glycerol content. These analyses can be seen in Table 4. The lubricity of the ECO was evaluated using a high-frequency reciprocating rig (HFRR) (PCS Instruments, UK) according to the standard EN ISO 12 156-1. The HFRR test involves the use of a steel ball and static steel disk that are submerged in a tested fuel at a temperature of 60°C. The test ball oscillates against the disk with a

TABLE 4: Physicochemical properties of ECO with catalyst TiSBA-15 (20)

Property	Value
Kinematic viscosity (mm^2/s)	162
Density (kg/m^3)	942
Pour point (°C)	8
Cloud point (°C)	12
Acid value (mg KOH/g oil)	4.1
Total glycerol content (mol/100 g oil)	0.08
Lubricity HFRR wear (μm)	216

ECO, Epoxidized canola oil; HFRR, high-frequency reciprocating rig.

constant frequency of 50 Hz for 75 min. The wear scar diameter left on the ball after the test is then measured with a microscope. ECO was tested twice at a 1.0% concentration, in reference to low lubricity diesel fuel (LLDF). Initially, the wear scar diameter of LLDF was 614 μm and after the addition of 1% ECO, it improved to 216 μm; thus, the addition of the small amount of ECO significantly improved the lubricity of LLDF. The kinematic viscosity of ECO is greater, which is an advantage for a lubricant. The cloud point and pour point of ECO are 12°C and 8°C, respectively, due to the polar nature of the structure and greater viscosity.

4. CONCLUSIONS

In this study, a TiSBA-15 catalyst with Si/Ti mass ratios of 20, 40, and 80 were used for epoxidation of canola oil to produce ECO. The high surface area ($\sim$ 900 m^2/g) and Dp in the range of mesopores ($\sim$ 7 nm) make these suitable catalysts for bulky molecular transformation reactions. The catalysts were characterized by various characterization tools including XRD, FTIR, and the BET surface area analyzer. The presence of Si–O–Ti bands in the IR spectra of oxide catalysts indicates the successful incorporation of Ti inside the silica framework. Catalyst activity was investigated by performing epoxidation of canola oil, which we found to occur at 70°C. The canola oil to hydrogen peroxide molar ratio was 1:14, and catalyst loading for canola oil was 5 %wt. TiSBA-15 (20) showed an 88% conversion based on unsaturation and a 1.66 oxirane oxygen content of the product. The formation of an epoxide adduct of canola oil was confirmed by FTIR and ^{1}H NMR spectral analysis. This study showed that a TiSBA-15 (20) catalyst has good activity for preparation of ECO, which acts as a starting material for lubricant formulation. ECO shows excellent antiwear and lubrication properties, and due to greater viscosity, has potential use in biolubricants.

ACKNOWLEDGMENTS

We gratefully acknowledge the financial support of the Agriculture Development Fund, Saskatchewan Ministry of Agriculture, for this work.

REFERENCES

Adhvaryu, A., Liu, Z., and Erhan, S.Z., Synthesis of Novel Triacylglycerol Molecule with Improved High and Low Temperature Behavior, *Ind. Crops Prod*., vol. **21**, pp. 113–119, 2005.

Boahene, P.E., Soni, K., Dalai, A.K., and Adjaye, J., Hydrotreating of Coker Light Gas Oil on Ti-Modified HMS Supports using Ni/HPMo Catalysts, *Appl. Catal. B,* vol. **101**, pp. 294–305, 2011.

Capanella, A., Baltanas, M.A., Capel-Sanchez, M.C., Campos-Martin, J.M., and Fierro, J.L.G., Soybean Oil Epoxidation with Hydrogen Peroxide using an Amorphous Ti/SiO_2 Catalyst, *Green Chem*., vol. **6**, pp. 330–334, 2004.

Chen, S.Y., Jang, L.Y., and Cheng, S., Synthesis of Zr-Incorporated SBA-15 Mesoporous Materials in a Self-Generated Acidic Environment, *Chem. Mater.*, vol. **16**, pp. 4174–4180, 2004.

Choudhary, K., Bal, R., Srinivas, D., Chandwalkar, A.J., and Sivasankar, S., Redox Behaviour and Selective Oxidation Properties of Mesoporous Titano- and Zirconosilicate MCM-41 Molecular Sieves, *Micropor. Mesopor. Mater.*, vol. **50**, pp. 209–218, 2001.

Erhan, S.Z., Sharma, B.K., Liu, Z., and Adhvaryu, A., Lubricant Basestock Potential of Chemically Modified Vegetable Oils, *J. Agric. Food Chem.*, vol. **56**, pp. 8919–8925, 2008.

Erhan, S.Z., Kleiman, R., and Isbell, T.A., Estolides from Meadowfoam Oil Fatty Acids and Other Monounsaturated Fatty Acids, *J. Am. Oil Chem. Soc*., vol. **70**, pp. 461–465, 1993.

Hang, X. and Yang, H., Model for a Cascade Continuous Epoxidation Process, *J. Am. Oil Chem. Soc.*, vol. **76**, pp. 89–92, 1999.

Hwang, H. and Erhan, S.Z., Modification of Epoxidized Soybean Oil for Lubricant Formulations with Improved Oxidative Stability and Low Pour Point, *J. Am. Oil Chem. Soc.*, vol. **78**, pp. 1179–1184, 2001.

Isbell, T.A., Lowery, B.A., DeKeyser, S.S., Winchell, M.L., and Cermak, S.C., Physical Properties of Triglyceride Estolides from *Lesquerella* and Castor Oils, *Ind. Crops Prod.*, vol. **23**, pp. 256–263, 2006.

Jayadasa, N.H., Nair, K.P., and Ajithkumar, G., Tribiological Evalution of Coconut Oil as an Environment-Friendly Lubricant, *Tribol. Int.*, vol. **40**, pp. 350–354, 2007.

Kulkarni, M.G., Dalai, A.K., and Bakhshi, N.N., Utilization of Green Seed Canola Oil for Biodiesel Production, *J. Chem. Technol. Biotechnol*., vol. **81**, pp. 1886–1893, 2006.

Lopez-Munoz, M.J., van Grieken, R., Aguado, J., and Marugan, J., Role of the Support on the Activity of Silica-Supported TiO_2 Photocatalysts: Structure of the TiO_2/SBA-15 Photocatalysts, *Catal. Today*, vol. **101**, pp. 307–314, 2005.

Madankar, C.S., Pradhan, S., and Naik, S.N., Parametric Study of Reactive Extraction of Castor Seed (*Ricinus Communis L.*) for Methyl Ester Production and its Potential Use as Bio Lubricant, *Ind. Crops Prod.*, vol. **43**, pp. 283–290, 2013.

May, C.A., *Epoxy Resins: Chemistry and Technology*, New York: Marcel Dekker, pp. 672–673, 1973.

Mungroo, R., Goud, V.V., Pradhan, N.C., and Dalai, A.K., Modification of Epoxidized Canola Oil for Lubricant Formulations, *Asia-Pac. J. Chem. Eng*., vol. **6**, pp. 14–22, 2011.

Mungroo, R., Pradhan, N.C., Goud, V.V., and Dalai, A.K., Epoxidation of Canola Oil with Hydrogen Peroxide Catalyzed by Acidic Ion Exchange Resin, *J. Am. Oil Chem. Soc.*, vol. **85**, pp. 887–896, 2008.

Nava, R., Ortega, R.A., Alonsa, G., Ornelas, C., Pawelec, B., and Fierro, J.L.G., CoMo/Ti-SBA-15 Catalysts for Dibenzothiophene Desulfurization, *Catal. Today*, vol. **127**, pp. 70–84, 2007.

Paquot, C., *Standard Methods for the Analysis of Oils, Fats and Derivatives*: *Part I*, 6th ed., Oxford: Pergamon Press, pp. 66–70, 1979.

Petrovic, A.S., Zlatanic, A., Lava, C.C., and Sinadinovic-Fiser, S., Epoxidation of Soya Bean Oil in Toluene with Peroxoacetic Acid and Peroxoformic Acids-Kinetics and Side Reactions, *Eur. J. Lipid Sci. Technol*., vol. **104**, pp. 293–299, 2002.

Salimon, J. and Salih, N., Chemical Modification of Oleic Acid Oil for Biolubricant Industrial Applications, *Aust. J. Basic Appl. Sci*., vol. **4**, pp. 1999–2003, 2010a.

Salimon, J. and Salih, N., Modification of Epoxidized Ricinoleic Acid for Biolubricant Base Oil with Improved Flash and Pour Points, *Asian J. Chem.*, vol. **22**, pp. 5468–5476, 2010b.

Salimon, J., Salih, N., and Yousif, E., Biolubricants: Raw Materials, Chemical Modifications and Environmental Benefits, *Eur. J. Lipid Sci. Technol*., vol. **112**, pp. 519–530, 2010.

Schuster, H., Rios, L.A., Weckes, P.P., and Hoelderich, W.F., Heterogeneous Catalysts for the Production of New Lubricants with Unique Properties, *Appl. Cat. A Genl.*, vol. **348**, pp. 266–270, 2008.

Sharma, B.K., Adhvaryu, A., Liu, Z., and Erhan, S.Z., Chemical Modification of Vegetable Oils for Lubricant Applications, *J. Am. Oil Chem. Soc*., vol. **83**, pp. 129–136, 2006.

Sharma, R.V., Somidi, A.K.R., and Dalai, A.K., Preparation and Properties Evaluation of Biolubricants Derived from Canola Oil and Canola Biodiesel, *J. Agric. Food Chem*., vol. **63**, pp. 3235–3242, 2015.

Sinadinovic-Fiser, S., Jankovic, M., and Petrovi, Z.S., Kinetics of in Situ Epoxidation of Soybean Oil in Bulk Catalyzed by Ion Exchange Resin, *J. Am. Oil Chem. Soc.*, vol. **78**, pp. 725–731, 2001.

Soni, K.K., Mouli, K.C., Dalai, A.K., and Adjaye, J., Effect of Ti Loading on the HDS and HDN Activity of KLGO on NiMo/TiSBA-15 Catalysts, *Micropor. Mesopor. Mater*., vol. **152**, pp. 224–234, 2012.

Vinu, A., Srinivasu, P., Miyahara, M., and Ariga, K., Preparation and Catalytic Performances of Ultralarge-Pore TiSBA-15 Mesoporous Molecular Sieves with Very High Ti Content, *J. Phys. Chem. B*, vol. **110**, pp. 801–806, 2006.

Vlcek, T. and Petrovic, Z.S., Optimization of the Chemoenzymatic Epoxidation of Soybean Oil, *J. Am. Oil Chem. Soc*., vol. **83**, pp. 247–252, 2006.

Zhao, D., Feng, J., Huo, Q., Melosh, N., Fredrickson, G.H., Chmelka, B.F., and Stucky, G.D., Triblock Copolymer Syntheses of Mesoporous Silica with Periodic 50 to 300 Angstrom Pores, *Science*, vol. **279**, pp. 548–552, 1998.

WET AIR OXIDATION OF BISPHENOL-A, ISOPHORONE, p-HYDROXYBENZOIC ACID, AND p-TOLUIDINE OVER AN Ru/C CATALYST

Shrikant Y. Vemula & Prakash D. Vaidya*

Department of Chemical Engineering, Institute of Chemical Technology, Nathalal Parekh Marg, Matunga, Mumbai-400019, India

*Address all correspondence to: Prakash D. Vaidya, Department of Chemical Engineering, Institute of Chemical Technology, Nathalal Parekh Marg, Matunga, Mumbai-400019, India, E-mail: pd.vaidya@ictmumbai.edu.in

Original Manuscript Submitted: 8/1/2017; Final Draft Received: 1/9/2018

Wet oxidation is a candidate wastewater-treatment technique, especially suitable when biological oxidation and incineration are inappropriate. In the present study, we investigate subcritical wet air oxidation (WAO) and catalytic WAO (CWAO) of four model compounds bearing different functional groups. Bisphenol-A, p-hydroxybenzoic acid, isophorone, and p-toluidine were the four chosen substrates representing classes of compounds phenols, carboxylic acids, ketones, and amines, respectively. Temperature and pressure were varied in the 423–473-K and 0.69–2.07-MPa ranges. A heterogeneous 5% Ru/C catalyst was used for CWAO. This catalyst was characterized using scanning electron microscopy, X-ray diffraction, Brunauer–Emmett–Teller analysis, and H_2 chemisorption methods. The performance of Ru/C for oxidative destruction of total organic carbon (TOC) was encouraging. Using TOC versus time data collected in the slurry reactor, kinetics of the reaction with isophorone were described using heterogeneous power law and Langmuir–Hinshelwood-type kinetic models. Our research has the potential to aid environmental engineers in effectively treating contaminated wastewater by WAO.

KEY WORDS: *wet oxidation, total organic carbon, bisphenol-A, isophorone, p-hydroxybenzoic acid, p-toluidine*

1. INTRODUCTION

The unrestrained discharge of harmful chemicals into bodies of water has led to an alarming increase in pollution levels. Wet air oxidation (WAO) is a candidate wastewater treatment technique, especially suitable when biological oxidation and incineration are inappropriate. In this advanced oxidation process, organic and some oxidizable inorganic pollutants are oxidized in the liquid phase at high temperature (398–593 K) and pressure (0.5–20 MPa) using air or oxygen. Often, catalysts are used to reduce the severity of reaction conditions (Bhargava et al., 2006; Mishra et al., 1995; Luck, 1999). There is much academic and industrial interest in the catalytic WAO (CWAO) process, for example, for the treatment of distillery effluents (Dhale and Mahajani, 1999; Padoley et al., 2012), and refinery spent caustic (Mishra et al., 1995; Jagushte and Mahajani, 1999) and nitrogenous organic pollutants (Oliviero et al., 2003).

In the present work, we investigate WAO and CWAO in four model compounds: bisphenol-A (BPA), isophorone, *p*-hydroxybenzoic acid (PHBA), and *p*-toluidine. These substrates represent the general classes of compounds phenol, ketone, carboxylic acid, and amine, respectively (see Fig. 1). BPA is mainly used as a raw material for manufacturing epoxy resins, polycarbonates, and food packaging. Its biodegradation is slow, so finding more effective treatment options is essential. Isophorone is widely used as a solvent and chemical intermediate in organic synthesis. It is classified as a possible human carcinogen; hence, its effective degradation in polluted wastewaters is important. PHBA is an intermediate found in toxic olive-oil wastewaters, whereas *p*-toluidine is a nitrogenous compound that is toxic to aquatic life.

NOMENCLATURE

C_i	concentration of species i in the liquid phase	O_2	concentration of oxygen in the bulk liquid phase (kg/m^3)
D_{ei}	effective diffusivity of species i	P_{O_2}	partial pressure of oxygen (MPa)
H_A	Henry's constant for oxygen (kg/[m^3 MPa])	r	initial rate of disappearance of TOC, kg/(m^3 min)
K_{O_2}	adsorption equilibrium constant for oxygen		
k_s	surface reaction rate constant ([m^3]^2/kg/[kg$_{cat}$]/min)		
k'	rate constant in Eq. (4) ([m^3]^n kg^{1-n}/[kg$_{cat}$]/min/MPa^m)	**Greek Symbols**	
K_{TOC}	adsorption equilibrium constant for total organic carbon (TOC)	Φ	Thiele modulus
L	characteristic length of catalyst particle	ΔH_{ad}	heat of adsorption (kJ/mol)
m	order with respect to oxygen	$\eta\Phi_i^2$	observable modulus for species i
n	order with respect to TOC	ω	catalyst loading (kg/m^3)
		ρ_p	density of catalyst (g/cm^3)

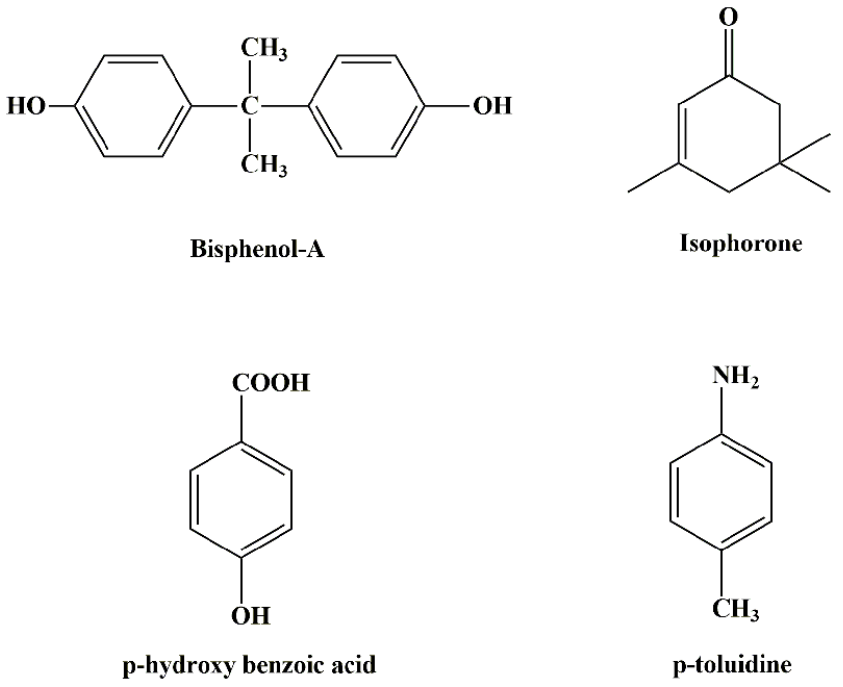

FIG. 1: Structures of model compounds used in this study

Noble metals are an important class of catalysts for WAO, and the performance of ruthenium is especially encouraging (Imamura et al., 1988). For instance, Hammedi et al. (2005) reported that Ru does not leach into aqueous solutions during CWAO of PHBA. Duprez et al. (1996) found that Ru/C is very effective and stable for the oxidation of phenol and acetic acid. For these reasons, we anticipated that Ru/C would be an effective catalyst for CWAO of the chosen model compounds.

In a slurry reactor, we tested the activity of a commercial Ru/C catalyst. Temperature and pressure were varied in the 423–473-K and 0.69–2.07-MPa ranges. The performance of Ru/C for oxidative destruction of total organic

carbon (TOC) was encouraging. Using TOC versus time data collected in the slurry reactor, kinetics of the reaction with isophorone were described using heterogeneous power law and Langmuir–Hinshelwood-type kinetic models.

2. EXPERIMENT

2.1 Materials and Methods

The oxygen gas cylinder (purity 99.5%) was purchased from Inox Air Products Ltd., Mumbai, India. The Ru/C catalyst (Ru = 5 wt%) was procured from Sigma-Aldrich, Mumbai, India (product number, 206180). BPA (purity 97%), p-toluidine (purity 98%), and PHBA (purity 99%) were procured from S.D. Fine Chemicals, Mumbai, India. Isophorone (purity 95%) was purchased from High Purity Laboratory Chemicals, Mumbai, India. Titanium dioxide for TOC analysis was supplied by SGE International Ltd., Melbourne, Australia. Perchloric acid (70% concentration) of analytical reagent grade was purchased from Qualigens Fine Chemicals, Mumbai, India, and used for adjusting the pH of the TiO_2 suspension to a value of 3.

2.2 Setup

An autoclave made of SS316 (capacity 1 dm^3; Parr Instruments, Moline, IL) was used for the oxidation studies. Mounted on the head of the reaction vessel were a variable-speed magnetic drive, turbine agitator, gas-charging inlet, sample withdrawal port, gas-release valve, cooling water feed line with solenoid, pressure gauge, and rupture disk. An electrically heated jacket was provided to work at the desired temperature and ensure isothermal conditions. The temperature and speed of agitation were controlled using a Parr 4842 controller. The liquid sample line and thermocouple well were immersed in the reaction mixture. We fitted a water condenser at the end of the sampling valve to avoid flashing of the sample. We ensured that the entire setup had no leaks. The experimental setup is shown elsewhere (Vaidya and Mahajani, 2002).

2.3 Procedure

The reactor was charged with 0.5 dm^3 of substrate solution. Nitrogen was used to flush out all of the oxygen inside the reactor and solution, enabling the maintenance of an inert atmosphere. The desired temperature was achieved by heating the jacket surrounding the reactor. The stirrer speed was set to 1200 rpm to enable proper agitation in the liquid phase. Before adding oxygen ($t = 0$), we withdrew the first sample. During the reaction, $\sim$ 1 mL of liquid sample was withdrawn at three equal time intervals of 10 min. and three further time intervals of 30 min. The pressure drop during the oxidation process was offset by charging additional oxygen into the reactor. After performing the experiment for 2 h, the reactor was cooled. In every experiment, we maintained the system at isobaric and isothermal conditions. For CWAO, we added 0.01 kg/m^3 of 5% Ru/C catalyst. To check whether the catalyst could be reused, three repeated runs were performed (one with the fresh catalyst and two with the same used catalyst) with PHBA at $T = 473$ K. In all runs, the conversion of TOC after 2 h was identical, thereby suggesting that the catalyst activity did not deteriorate under the conditions used in this work.

2.4 Product Analysis

TOC concentration was measured using a TOC analyzer (ANATOC Series II; SGE, Melbourne, Australia), and TOC measurements were repeated three times, resulting in an error $<$ 3%. Rates of TOC destruction were found from plots of TOC versus time data. Residual BPA concentration was found using high-performance liquid chromatography (HPLC; Agilent Technologies, Santa Clara, CA). The mobile phase was a 75:25 methanol–water mixture, and flow rate of this phase was 0.7 mL/min. Other details of HPLC analysis include values for the C_{18} column (3.5 μm $\times$ 4.6 mm $\times$ 100 mm) and ultraviolet light (wavelength 210 nm). Similarly, residual isophorone concentration was found using HPLC (mobile phase 70:30 methanol–water, flow rate 1 mL/min, wavelength 243 nm). We used mass spectrometry (MS; Thermo Finnigan, San Jose, CA) and gas chromatography (GC)-MS (Thermo Fisher Scientific, Waltham, MA) to identify the products of wet oxidation.

2.5 Catalyst Characterization

Catalyst Brunauer–Emmett–Teller (BET) surface area (2941 m^2/g) and pore volume (0.72 cm^3/g) were determined with a BET apparatus using the N_2 adsorption–desorption technique (Micromeritics model ASAP 2010; Norcross, GA). Useful surface metallic atom features such as dispersion (2.7%) and active particle diameter (94 nm) were investigated by H_2 chemisorption in a Micromeritics Autochem II 2920 (Norcross, GA) instrument. A typical scanning electron micrograph (SEM) of the fresh catalyst is shown in Fig. 2; a honeycomb-like monolithic structure is evident. SEM analysis was performed on a JEOL (Peabody, MA) JSM-6380 LA instrument. The elemental analysis of the fresh (Ru = 4.96 wt%) and spent (Ru = 4.93 wt%) catalysts was performed using energy-dispersive X-ray (EDX) analysis. Ruthenium content of the treated water samples was under detection limits, thereby suggesting that metal leaching did not occur. These results are in line with those of Hammedi et al. (2005). A Rigaku miniflex powder diffractometer (purchased in Mumbai, India) with Cu K radiation was used to obtain X-ray diffraction (XRD) patterns of the fresh and spent catalyst (Fig. 3). The diffraction pattern exhibited by both samples was similar. The spent catalyst did not display new diffraction lines, thus indicating that no new phase is formed in the catalyst after reaction. We attributed the sharp peak at $\sim 28^\circ$ to RuO_2 (Maeder et al., 1999). For the spent catalyst, this peak shifted due to possible changes in interlayer spacing and the crystalline phase. The peak for RuO_2 in the spent catalyst looks sharper, probably due to further oxidation of ruthenium. Ru^0 species show diffraction peaks at $2\theta = 43.8^\circ$. The carbon support shows an unresolved peak at $\sim 26^\circ$. Using the Debye–Scherrer relation [Eq. (1)], we found that the Ru crystallite size was in the 10–30-nm range.

$$d_{XRD} = \frac{0.90\,\lambda}{\beta \cos O}, \tag{1}$$

where d_{XRD} is the crystallite size (in nanometers), λ is the wavelength (0.154 nm), β is the corrected full width at half maximum (in radians), and θ is the Bragg angle (in radians).

3. RESULTS AND DISCUSSION

CWAO is a heterogeneous reaction system. According to Doraiswamy and Sharma (1984), such reactions involve both diffusion and chemical reaction. First, the gaseous reactant oxygen travels from the bulk gas phase into the liquid phase. Next, dissolved oxygen and the reactant in liquid travel to the external surface of the catalyst, and then, still deeper inside the catalyst. After adsorption on the active sites of the catalyst, surface reaction, and product desorption (from the inner surface of the catalyst to its exterior, and further, into the liquid and gas phases), the process

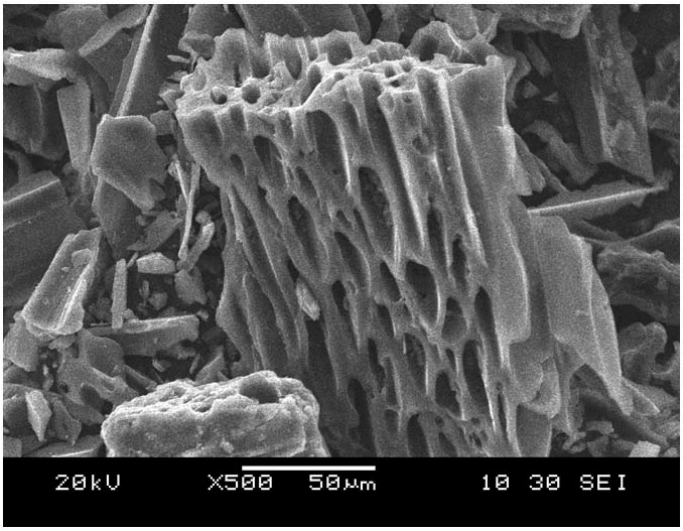

FIG. 2: Scanning electron micrograph of 5% Ru/C catalyst

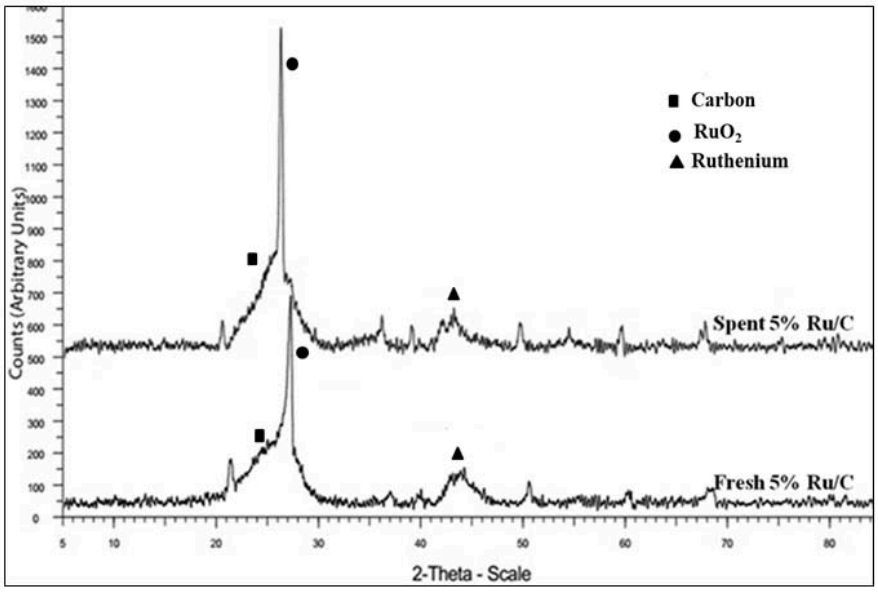

FIG. 3: XRD image of 5% Ru/C

is complete. The rate of the reaction can be influenced by any of the mass transfer processes (external and internal). It is essential to ensure the absence of mass transfer limitations to determine the kinetic parameters.

3.1 Mass Transfer Considerations

Because we performed all runs with pure oxygen, we neglected the gas-side mass transfer resistance. This was justified because of the high diffusivity of oxygen in the gas phase and the low solubility in liquid. In a slurry reactor, the catalyst is kept in suspension by intense agitation, and the extent of turbulence in the liquid phase can be varied by changing the speed of agitation. We studied the effect of impeller speed on the reduction in TOC in the 300–1200-rpm range at $T = 473$ K and $P_{O_2} = 0.69$ MPa (here, P_{O_2} denotes oxygen partial pressure). We observed that above an impeller speed of 1000 rpm, the percentage of TOC reduction after 2 h was independent of the speed of agitation (see Fig. 4). This proved that both gas–liquid and liquid–solid mass transfer resistances were absent. All further experiments were carried out at 1200 rpm. The significance of intraparticle diffusion resistance was estimated using the Weisz–Prater criterion (Fogler, 2010). The parameter $\eta\Phi_i^2$ was calculated as follows:

$$\Phi_i^2 = \frac{r\omega L^2}{C_i De_i}. \tag{2}$$

Because the external diffusion resistances were negligible above 1000 rpm, the concentration of the gas at the surface (C_i) was deemed to be equal to the oxygen solubility in water. We found that the parameter $\eta\Phi_i^2$ was less than unity for both oxygen and substrates; hence, pore diffusion resistance was neglected. Clearly, diffusion resistances were absent, and the system belonged to the kinetics-control reaction regime. Reddy and Mahajani (2005) investigated CWAO of aniline in a slurry reactor and observed that the rate of destruction of chemical oxygen demand (COD) was independent of the speed of agitation greater than impeller speed of 800 rpm. Similarly, Gunale and Mahajani (2008) studied CWAO of morpholine over an Ru/TiO_2 catalyst and found that diffusion limitations were absent at high speed (1000 rpm).

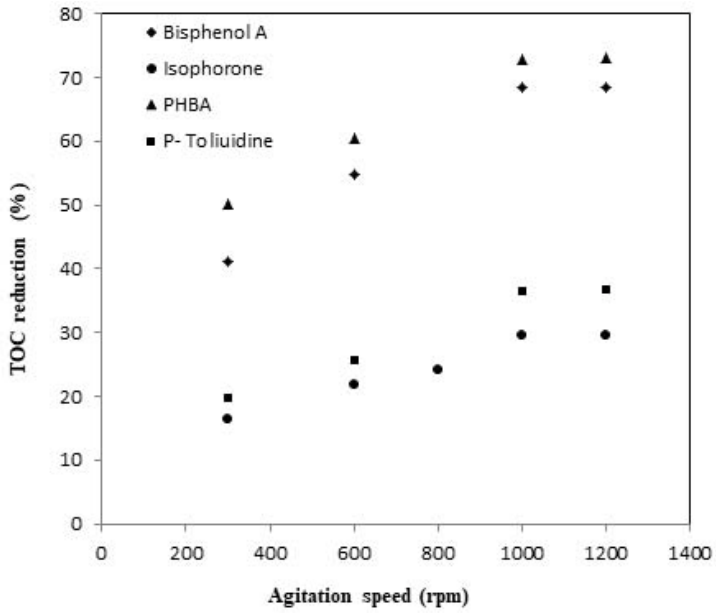

FIG. 4: Effect of speed of agitation on percentage of TOC reduction during CWAO of BPA, isophorone, PHBA, and p-toluidine in the 300–1200-rpm range (initial BPA concentration 0.05 kg/m^3 and catalyst loading 0.01 kg/m^3; initial isophorone concentration 0.1 kg/m^3 and catalyst loading 0.01 kg/m^3; initial PHBA concentration 0.5 kg/m^3 and catalyst loading 0.05 kg/m^3; initial p-toluidine concentration 0.1 kg/m^3 and catalyst loading 0.01 kg/m^3; $T = 473$ K; oxygen partial pressure = 0.69 MPa; reaction time = 120 min)

3.2 Effect of Catalyst Loading

We studied the influence of catalyst loading (ω, kg/m^3) on the destruction of TOC. Experiments were performed with BPA, isophorone, p-toluidine, and PHBA at $T = 458$ K and $P_{O_2} = 0.69$ MPa. The respective substrate concentration in feed solutions was 0.05, 0.1, 0.1, and 0.5 kg/m^3. The reaction was expectedly faster with the rise in catalyst loading in the range studied. For example, TOC conversion after 2 h of reaction with PHBA increased from 68.3% to 93.9% when catalyst loading rose to 0.2 from 0.05 kg/m^3. The rate of disappearance of TOC increased from 0.56 to 2.26 kg/(m^3 min), correspondingly. Similar trends were observed during reactions with BPA and isophorone, for which TOC conversion rates were markedly higher at greater catalyst loading. The respective TOC conversion values for the reaction with p-toluidine were 28.1% (at $\omega = 0.01$ kg/m^3) and 34.6% (at $\omega = 0.03$ kg/m^3). In a previous study, Gunale and Mahajani (2008) reported a similar influence of the loading of Ru/TiO_2 catalyst in the 0.33–1.32-kg/m^3 range for CWAO of morpholine at $T = 483$ K.

3.3 Effect of Temperature

We studied the effect of temperature on the percentage of TOC destruction during the reactions with the four chosen model compounds. In all runs, TOC versus time data were collected at 423, 448, 458, and 473 K. Oxygen partial pressure, initial substrate concentration, and catalyst loading were held constant. The results, represented in Fig. 5, are discussed below.

3.3.1 BPA

For the case of the phenolic substrate BPA (feed concentration 0.05 kg/m^3), the reaction proceeded even when no catalyst was used. Several oxidized organic intermediates such as phenol, hydroquinone, benzoquinone, p-hydroxyaceto-

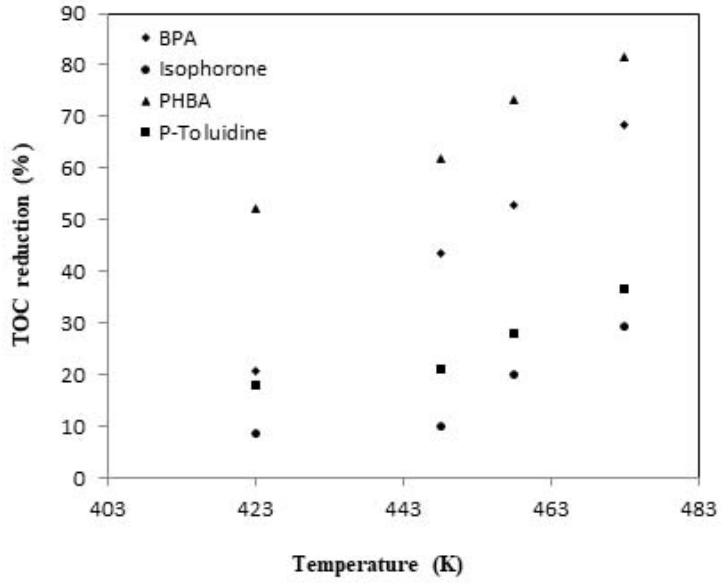

FIG. 5: Effect of temperature on percentage of TOC reduction during CWAO of BPA, isophorone, PHBA, and *p*-toluidine (initial BPA concentration 0.05 kg/m^3 and catalyst loading 0.01 kg/m^3; initial isophorone concentration 0.1 kg/m^3 and catalyst loading 0.01 kg/m^3; initial PHBA concentration 0.5 kg/m^3 and catalyst loading 0.05 kg/m^3; initial *p*-toluidine concentration 0.1 kg/m^3 and catalyst loading 0.05 kg/m^3; oxygen partial pressure = 0.69 MPa; reaction time = 120 min)

phenone, PHBA, maleic acid, succinic acid, and oxalic acid were formed during wet oxidation. Both noncatalytic and catalytic routes for BPA oxidation can be found in previously published work (Erjavec et al., 2013). The reaction pathway was also reported by other researchers (Han et al., 2015; Li et al., 2008). When Ru/C catalyst was used (loading 0.01 kg/m^3), the percentage of TOC destruction after 2 h at $P_{O_2} = 0.69$ MPa was 20.8% and 68.4% at 423 and 473 K. As evident from Fig. 5, the elevation in temperature expectedly resulted in increased TOC disappearance.

3.3.2 Isophorone

We also investigated the reaction with the ketonic model compound isophorone (0.1 kg/m^3) at $P_{O_2} = 0.69$ MPa in the 423–473-K range. When no catalyst was used, 6.4% TOC disappearance was reported after 2 h at $T = 423$ K. Using a catalyst at low loading (0.01 kg/m^3) marginally improved this value (8.7%). At high temperature (473 K), noncatalytic and catalytic reactions yielded 20.1% and 29.5% TOC conversion values, respectively. These results are shown in Fig. 5. Approximately 27.6% of isophorone was destroyed during the catalytic reaction at $T = 473$ K. The oxidation of isophorone yielded unsaturated ketonic intermediates. Clearly, TOC destruction during the reaction with isophorone was slower in comparison to the trend observed during the reaction with BPA. As reported earlier by Dasari and Rodrigues (2007), this may be due to the low solubility of isophorone and oxygen in aqueous solutions and the reduced generation of active oxygen species for propagation of the oxidation reaction. Figure 6 shows plots of residual fractional TOC versus time for the reaction with isophorone at different temperatures.

3.3.3 PHBA

At $T = 473$ K, 81.5% TOC was converted after 2 h when the catalyst loading was 0.05 kg/m^3. The value of P_{O_2} was 0.69 MPa, whereas the concentration of PHBA in feed was 0.5 kg/m^3. When no catalyst was used under similar conditions, TOC conversion was just 37.5%. To identify the major reaction intermediates, we used the GC-MS method. The formation of low- molecular-weight organic acids such as acetic, oxalic, maleic, formic, and succinic was confirmed.

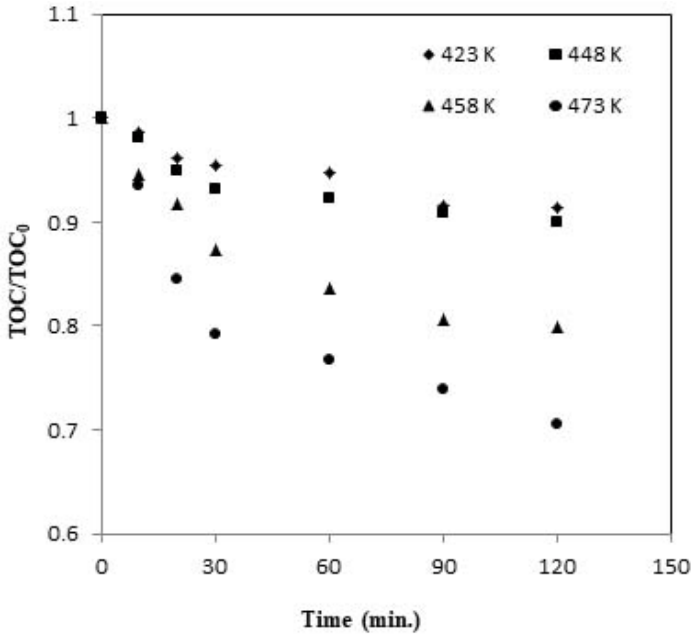

FIG. 6: Influence of temperature on residual TOC during CWAO of isophorone (initial isophorone concentration 0.1 kg/m^3 and catalyst loading 0.01 kg/m^3; oxygen partial pressure = 0.69 MPa; reaction time = 120 min)

3.3.4 p-Toluidine

Reactions with this amine were studied at $P_{O_2} = 0.69$ MPa using feed solutions at a concentration 0.1 kg/m^3. In the absence of the catalyst, TOC conversion after 2 h increased from 12.8% to 30.3% when the temperature rose from 423 to 473 K (see Fig. 5). At low concentration (0.01 kg/m^3) of Ru/C, the corresponding values were 18.1% ($T =$ 423 K) and 36.7% ($T = 473$ K). 4,4′-Dimethylazobenzene is the major intermediate during oxidation of p-toluidine (Croston et al., 2002).

3.3.5 General Remarks

For the sake of comparison, trends in TOC conversion after 2 h at the intermediate temperature $T = 458$ K were represented in Fig. 7. The respective concentrations of substrate and catalyst were 0.1 and 0.01 kg/m^3, and the value of P_{O_2} was 0.69 MPa. The degree of TOC conversion decreased in the order of PHBA $>$ BPA $>$ p-toluidine $>$ isophorone.

3.4 Effect of Oxygen Partial Pressure

Runs were performed with BPA in the 0.69–2.07-MPa oxygen partial pressure range at $T = 448$ K, catalyst loading was 0.01 kg/m^3, and BPA concentration in the feed solution was 0.05 kg/m^3. As anticipated, the increase in oxygen partial pressure resulted in improved conversions. For example, TOC destruction after 2 h was maximized (66.7%) at $P_{O_2} = 2.07$ MPa (against a value of 43.6% at 0.69-MPa pressure). When isophorone was the substrate (concentration 0.1 kg/m^3), the maximum conversion of TOC and isophorone at $P_{O_2} = 2.07$ MPa was 25% and 26% after 2 h. In the absence of a catalyst under similar conditions, these values were 18% and 12%, correspondingly. Reactions with PHBA (feed solution 0.5 kg/m^3) were performed at $T = 448$ K, and catalyst loading was low (0.01 kg/m^3). At $P_{O_2} =$ 2.07 MPa, 80.2% TOC conversion was observed after 2 h (against 61.9% at 0.69-MPa pressure). This was significantly higher than that of the noncatalytic reaction (52.3%). For the runs with feed solutions containing 0.1 kg/m^3 toluidine,

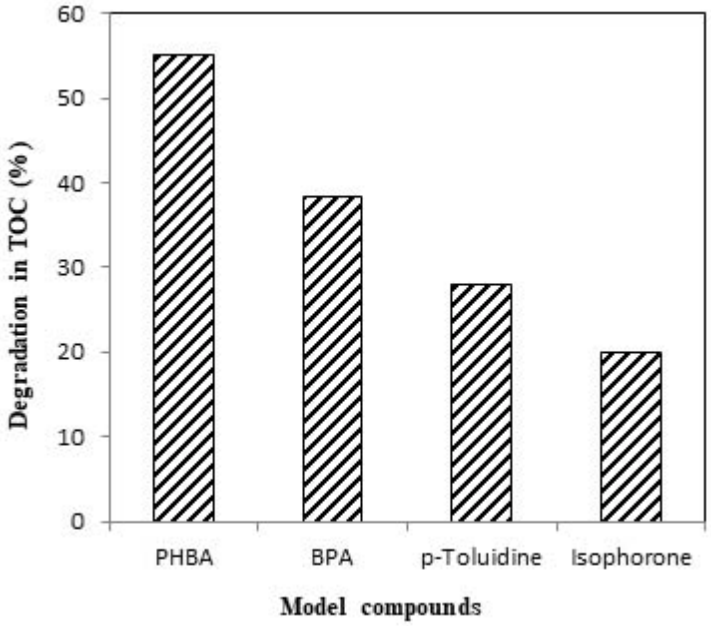

FIG. 7: Comparison of degradation pattern of the model compounds at $T = 458$ K (initial substrate concentration 0.1 kg/m^3 and catalyst loading 0.01 kg/m^3; oxygen partial pressure = 0.69 MPa; reaction time = 120 min)

TOC conversion values for the noncatalytic and catalytic reactions were 25.4% and 36.1%, respectively. In a previous work, Vaidya and Junghare (2011) reported enhanced TOC conversion at high oxygen partial pressures during CWAO of piperazine. Plots of initial rates of TOC conversion versus oxygen partial pressure are shown in Fig. 8. It is evident that the reaction order with respect to oxygen is fractional (between 0 and 1), and oxygen is strongly adsorbed on the catalyst surface.

3.5 Effect of Substrate Concentration in Feed

In Fig. 9, the effect of substrate concentration in feed on TOC conversion is shown (conditions: $T = 458$ K, $P_{O_2} =$ 0.69 MPa, time = 2 h). As the initial reactant concentration increased, the destruction of TOC diminished. For example, the percentage of TOC conversion during the reaction with BPA ($\omega = 0.01$ kg/m^3) was 73.7% and 38.3% for a respective BPA concentration in feed of 0.025 and 0.1 kg/m^3. A similar trend was observed for the reaction with isophorone: 31.5% and 10.8% for initial isophorone concentrations of 0.05 and 0.2 kg/m^3. Such behavior was also seen for the case of p-toluidine. Finally, when the initial PHBA concentration increased from 0.25 to 1 kg/m^3, the percentage of TOC destruction diminished from 89.6% to 35.4% (not shown in Fig. 9). In another work on CWAO of phenol in a trickle-bed reactor, Yang et al. (2008) reported that COD destruction reduced from 83% to 60% as the feed concentration was raised from 1 to 5 kg/m^3.

3.6 Study of Reaction Kinetics for CWAO of Isophorone

From the TOC versus time record, lumped kinetics of the reaction with isophorone was described using heterogeneous power law and Langmuir–Hinshelwood (L-H)-type kinetic models. Isophorone, which was most resistant to oxidation among the investigated model compounds, was especially chosen for the kinetic modeling exercise. First, a power law model of the type shown in Eq. (3) was used for data fitting:

$$r = k\,[O_2]^m\,[TOC]^n\,. \tag{3}$$

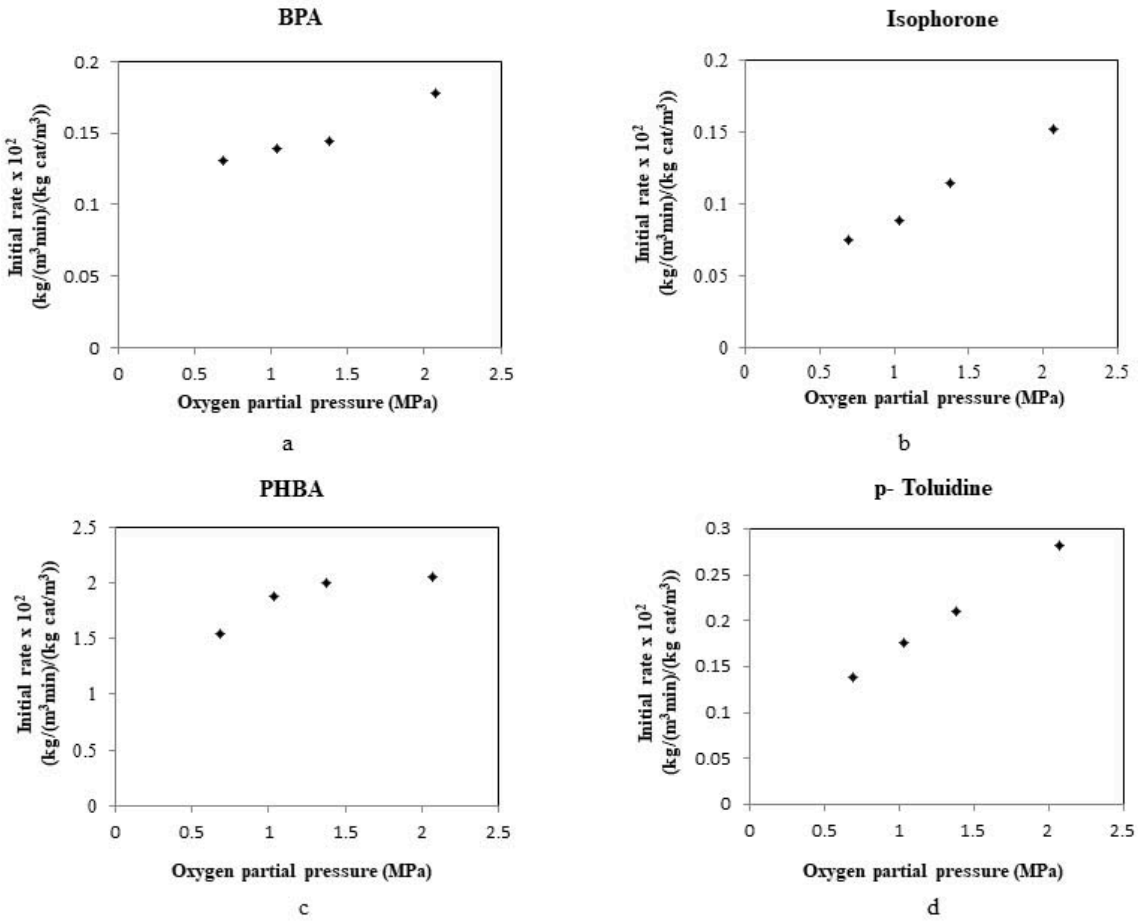

FIG. 8: Effect of pressure on initial rate of reaction for CWAO of (a) BPA, (b) isophorone, (c) PHBA, and (d) *p*-toluidine (initial BPA concentration 0.05 kg/m^3 and catalyst loading 0.01 kg/m^3; initial isophorone concentration 0.1 kg/m^3 and catalyst loading 0.01 kg/m^3; initial PHBA concentration 0.5 kg/m^3 and catalyst loading 0.05 kg/m^3; initial *p*-toluidine concentration 0.1 kg/m^3 and catalyst loading 0.05 kg/m^3; $T = 448$ K; reaction time = b120 min)

Equation (3) was rewritten as follows, using Henry's law (here, $k' = k[H_{O_2}]^m$):

$$r = k[H_{O_2}P_{O_2}]^m\,[TOC]^n = k'[P_{O_2}]^m\,[TOC]^n. \tag{4}$$

The kinetic data were fitted to Eq. (4) and the values of k', m, and n are reported in Table 1. Next, a dual-site, competitive L-H–type hyperbolic model was chosen to provide further insight into adsorption–desorption features. Such models were used earlier in past work on WAO (Reddy and Mahajani, 2005; Maugans and Akgerman, 1997). In the proposed pathway, oxygen was dissociatively adsorbed on the catalyst surface, which is usually the case with diatomic gases such as oxygen on noble metals. The organic substrate was adsorbed on the same types of active sites as oxygen. A surface reaction between the adsorbed organic compound (responsible for TOC) and dissociatively adsorbed oxygen was assumed to be rate controlling. The rate expression is represented by

$$r = \frac{k_s K_{O_2}^{0.5} K_{TOC}\,[H_{O_2}]^{0.5}\,[P_{O_2}]^{0.5}\,[TOC]}{\left(1 + K_{O_2}^{0.5}\,[H_{O_2}]^{0.5}\,[P_{O_2}]^{0.5} + K_{TOC}\,[TOC]\right)^2}. \tag{5}$$

Equation (5) provides a good fit of the data, and the values of all parameters in Eq. (5) are represented in Table 2. When the nondissociative adsorption of oxygen was considered, data fitting was not as satifactory. The good agreement

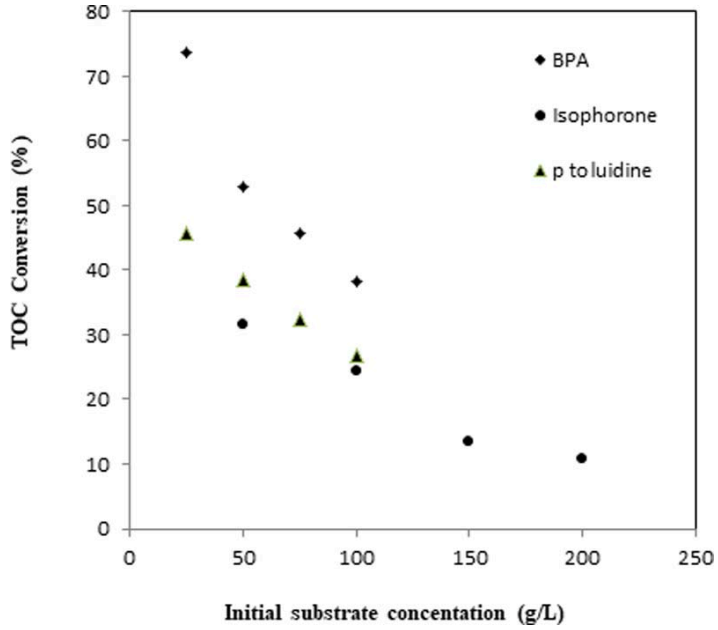

FIG. 9: Effect of initial concentration of BPA, isophorone, and p-toluidine on percentage of TOC reduction during CWAO ($T =$ 458 K; oxygen partial pressure $=$ 0.69 MPa; reaction time $=$ 120 min)

TABLE 1: Rate constants and reaction orders in the power law model

T (K)	$k' \times 10^3$ ($[m^3]^n$ $kg^{-n}/(kg_{cat})$/min/MPa^m)	m	n
423	20.0 ± 0.5	0.50 ± 0.6	0.97 ± 0.20
448	36.1 ± 0.6	0.52 ± 0.7	0.98 ± 0.18
458	57.3 ± 0.4	0.54 ± 0.61	0.98 ± 0.15
473	87.00 ± 0.3	0.56 ± 0.21	1.01 ± 0.16

TABLE 2: Parameters for dissociative L-H model

T (K)	k_s	$K_A \times 10^4$	$K_{TOC} \times 10^3$	Residual sum of squares (RSS)
423	21.38 ± 0.31	32.77 ± 0.65	17.28 ± 0.31	9.56×10^{-7}
448	47.72 ± 1.1	29.59 ± 0.4	14.24 ± 0.33	1.41×10^{-7}
458	86.2 ± 0.2	25.6 ± 0.4	13.2 ± 0.2	3.98×10^{-7}
473	156.3 ± 0.52	18.1 ± 1.10	12.5 ± 0.52	7.15×10^{-7}
—	ΔH_{ad} (kJ/mol)	18.38	11.07	—

between predicted and experimental rates of TOC destruction for the dissociative L-H model is shown in the parity plot of Fig. 10.

4. CONCLUSIONS

In this work, we studied noncatalytic WAO and CWAO of four model compounds in a batch-operated stirred reactor. We selected BPA, PHBA, isophorone, and p-toluidine to represent various organic contaminants in industrial

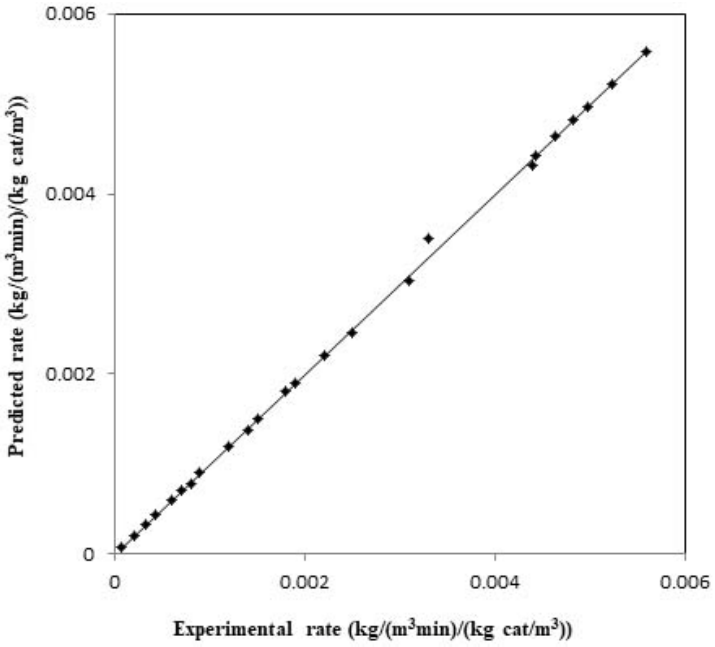

FIG. 10: Parity plot of dissociative L-H model

wastewaters. The performance of the heterogeneous Ru/C catalyst on destruction of TOC was studied between 423 and 473 K and 0.69- and 2.07-MPa oxygen partial pressure. On the whole, the model compound isophorone was most resistant to oxidation. Contrarily, the reaction with BPA, PHBA, and *p*-toluidine occurred more quickly. The catalyst could be reused at least three times without any adverse effect on performance. The analysis of the unused and used catalysts was performed using SEM, XRD, and H_2 chemisorption techniques. Kinetics of the disappearance of TOC during the reaction with isophorone was described using power law and L-H models. Data fitting to a power law model provided fractional reaction orders. The prevailing L-H mechanism was a rate-controlling surface reaction between chemisorbed TOC and atomic oxygen.

ACKNOWLEDGMENTS

Shrikant Y. Vemula is thankful to the University Grants Commission (USC), New Delhi, India, for providing financial assistance in the form of a UGC–Basic Scientific Research Fellowship.

REFERENCES

Bhargava, S.K., Tardio, J., Prasad, J., Foger, K., Akolekar, D.B., and Grocott, S.C., Wet Oxidation and Catalytic Wet Oxidation, *Ind. Eng. Chem. Res.*, vol. **45**, pp. 1221–1258, 2006.

Croston, M., Langston, J., Sangoi, R., and Santhanam, K.S.V., Catalytic Oxidation of *p*-Toluidine at Multiwalled Functionalized Carbon Nanotubes, *Int. J. Nanosci.*, vol. **1**, pp. 277–283, 2002.

Dasari, K. and Rodrigues, A.E., Catalytic Oxidation of Isophorone to Ketoisophorone over Ruthenium Supported Mg Al-Hydrotalcite, *Catal. Commun.*, vol. **8**, pp. 1156–1160, 2007.

Dhale, A.D. and Mahajani, V.V., Treatment of Distillery Waste after Bio-Gas Generation: Wet Oxidation, *Ind. J. Chem. Technol.*, vol. **7**, pp. 11–18, 1999.

Doraiswamy, L.K. and Sharma, M.M., *Heterogeneous Reactions: Analysis, Examples and Reactor Design*, New York: Wiley and Sons, 1984.

Duprez, D., Delanoe, F., Barbier, Jr., J., Isnard, P., and Blanchard, G., Catalytic Oxidation of Organic Compounds in Aqueous Media, *Catal. Today*, vol. **29**, pp. 317–322, 1996.

Erjavec, B., Kaplan, R., Djinovic, P., and Pintar, A., Catalytic Wet Air Oxidation of Bisphenol-A Model Solution in a Trickle-Bed Reactor over Titanate Nanotube-Based Catalysts, *Appl. Catal. B Environ*., vol. **342**, pp. 132–133, 2013.

Fogler, H.S., *Elements of Chemical Reaction Engineering*, 4th Edition, New Delhi: Prentice-Hall, 2010.

Gunale, T.L. and Mahajani, V.V., Studies in Wet Air Oxidation of Aqueous Morpholine over Ru/TiO_2 Catalyst: An Insight into the Fate of the "N" Atom, *J. Chem. Technol. Biotechnol.*, vol. **83**, pp. 1154–1162, 2008.

Hammedi, T., Triki, M., Alvarez, M.G., Chimentao, R.J., Ksibi, Z., Ghorbel, A., Llorca, J., and Medina, F., Total Degradation of *p*-Hydroxy Benzoic Acid by Ru-Catalysed Wet Air Oxidation: A model for Waste Water Treatment, *Environ. Chem. Lett.*, vol. **13**, pp. 481–486, 2005.

Han, Q., Wang, H., Dong, W., Liu, T., Yin, Y., and Fan, H., Degradation of Bisphenol-A by Ferrate (VI) Oxidation: Kinetics, Products and Toxicity Assessment, *Chem. Eng. J.*, vol. **262**, pp. 34–40, 2015.

Imamura, S., Fukuda, I., and Ishida, S., Wet Oxidation Catalyzed by Ruthenium Supported on Cerium (IV) Oxides, *Ind. Eng. Chem. Res.*, vol. **27**, pp. 718–721, 1988.

Jagushte, M.V. and Mahajani, V.V., Insight into Spent Caustic Treatment on Wet Oxidation of Thiosulfate to Sulfate, *J. Chem. Technol. Biotechnol.*, vol. **74**, pp. 437–444, 1999.

Li, C., Li, X.Z., Graham, N., and Gao, N.Y., The Aqueous Degradation of Bisphenol A and Steroid Estrogens by Ferrate, *Water Res.*, vol. **42**, pp. 109–120, 2008.

Luck, F., Wet Air Oxidation: Past, Present and Future, *Catal. Today*, vol. **53**, pp. 81–91, 1999.

Maeder, T., Muralt, P., and Sagalowicz, L., Growth of (111)-Oriented PZT on RuO_2(100)/Pt(111) Electrodes by In-Situ Sputtering, *Thin Solid Films*, vol. **345**, pp. 300–306, 1999.

Maugans, C.B. and Akgerman, A., Catalytic Wet Oxidation of Phenol over Pt/TiO_2 Catalyst, *Water Res.*, vol. **31**, pp. 3116–3124, 1997.

Mishra, V.S., Mahajani, V.V., and Joshi, J.B., Wet Air Oxidation, *Ind. Eng. Chem. Res.*, vol. **34**, no. 1, pp. 2–48, 1995.

Oliviero, L., Barbier, Jr., J., and Duprez, D., Wet Air Oxidation of Nitrogen-Containing Organic Compounds and Ammonia in Aqueous Media, *Appl. Catal. B Environ.*, vol. **40**, pp. 163–184, 2003.

Padoley, K.V., Tembhekar, P.D., Saratchandra, T., Pandit, A.B., Pandey, R.A., and Mudliar, S.N., Wet Air Oxidation as a Pretreatment Option for the Selective Biodegradability Enhancement and Biogas Generation Potential from Complex Effluent, *Biores. Technol.*, vol. **120**, pp. 157–164, 2012.

Reddy, G.R. and Mahajani, V.V., Insight into Wet Oxidation of Aqueous Aniline over a Ru/SiO_2 Catalyst, *Ind. Eng. Chem. Res.*, vol. **44**, pp. 7320–7328, 2005.

Vaidya, P.D. and Junghare, R., Acceleration of the Wet Oxidation Reaction of Piperazine by Heterogeneous Ru/TiO_2 Catalyst, *Chem. Eng. Commun.*, vol. **198**, pp. 992–1003, 2011.

Vaidya, P.D. and Mahajani, V.V., Insight into Sub-Critical Wet Oxidation of Phenol, *Adv. Environ. Res.*, vol. **6**, pp. 429–439, 2002.

Yang, S., Zhu, W., Wang, J., and Chen, Z.J., Catalytic Wet Air Oxidation of Phenol over CeO_2-TiO_2 Catalyst in Batch Reactor and the Packed-Bed Reactor, *Hazard. Mater.*, vol. **153**, pp. 1248–1253, 2008.

SELECTIVE TRANSESTERIFICATION OF GLYCEROL TO GLYCEROL CARBONATE OVER SrO-ZrO_2 BASE CATALYSTS

Ganji Parameswaram,[1] Ambati Srivani,[1] Chenna Sumana,[2] Gollapalli Nageswara Rao,[3] & Nakka Lingaiah[1,*]

[1]*Catalysis Laboratory, I&PC Division*

[2]*Chemical Engineering Division, CSIR-Indian Institute of Chemical Technology, Hyderabad-500 007, Telangana, India*

[3]*Department of Chemistry, Andhra University, Vishakhapatnam, 530017, A.P. India*

*Address all correspondence to: Nakka Lingaiah, Catalysis Laboratory, I&PC Division, Tel.: +91-40-27191722, E-mail: nakkalingaiah@iict.res.in

Original Manuscript Submitted: 6/7/2017; Final Draft Received: 10/28/2017

Glycerol carbonate was prepared selectively by transesterification of glycerol with dimethyl carbonate over heterogeneous strontium-zirconium mixed oxide base catalysts. These catalysts were prepared by coprecipitation method with varying Sr to Zr molar ratio and characterized by Brunauer-Emmett-Teller (BET) surface area, X-ray diffraction, and temperature programmed desorption of CO_2. The catalysts' activity was varied with variation in the Sr to Zr ratio and the catalysts with the ratio of 3:1 exhibited the highest activity towards glycerol carbonate. The characterization results suggested that the activity of the catalysts depended on the amount of basic sites present in the catalysts and the basicity was dependent on the Sr to Zr ratio and treatment temperature. The effect of reaction parameters on the yield of glycerol carbonate was studied and also the kinetic expression was derived. The catalyst showed consistent activity upon reuse.

KEY WORDS: *glycerol, dimethyl carbonate, glycerol carbonate, strontium oxide, zirconium oxide, transesterification*

1. INTRODUCTION

Glycerol, a by-product in biodiesel production can be converted into several valuable chemicals, fuel additives such as acrolein, glyceric acid, esters of glycerol, propane diols, and glycerol carbonate, etc. (Pagliaro et al., 2007; Behr et al., 2008; Zhou et al., 2008). Among various possible products from glycerol, glycerol carbonate (GLC) is a significant chemical as it has a lot of applications. Glycerol carbonate is an attractive starting material as it is a low-flammable, less-toxic, biodegradable fuel and contains two functional groups. This makes it as an attractive chemical to use as a substitute for ethylene carbonate, environmentally friendly solvent, electrolyte for lithium and lithium-ion batteries, an ingredient for cosmetics, and a precursor for glycidol (Olga et al., 2009; Sonnati et al., 2013; Liu et al., 2015; Rokicki et al., 2005). GLC can also be used for the synthesis of functional polymers such as polycarbonates, polyesters, or polyurethanes (Rokicki et al., 2005; Guan et al., 2011).

Glycerol carbonate can be prepared from glycerol using different carbonate sources such as urea (Aresta et al., 2009), phosgene (Teles et al., 1994), CO and O_2 (Hu et al., 2010), carbon dioxide (George et al., 2009), and dialkyl carbonate (Takagaki et al., 2010). Among all these, the route based on transesterification of glycerol with dialkyl carbonate is one of the promising approaches for industrial application due to its mild reaction conditions. The use of dimethyl carbonate (DMC) as carbonating agent is preferred since the severity of the process is less and the coproduct methanol can be easily separated (Sonnati et al., 2013; Climent et al., 2010; Shaikh and Sivaram, 1996).

Transesterification of glycerol can be carried out under basic or acidic conditions. Base catalysts are more promising and have been investigated for the synthesis of glycerol carbonate (Ochoa-Gomez et al., 2009). Mixed metal oxides have been widely applied as heterogeneous base catalysts due to their strong basic property and surface area compared to that of mono metal oxides (Takagaki et al., 2010; Parameswaram et al., 2013). Different heterogeneous base catalysts such as CaO (Ochoa-Gomez et al., 2009), Mg/La (Simanjuntak et al., 2013), LDO (Liu et al., 2013), Mg/Ca (Khayoon and Hameed, 2013), $NaOH/Al_2O_3$ (Bai et al., 2013), and K_2CO_3/MgO (Du et al., 2012) were reported for transesterification of glycerol reaction. Teng et al. (2015) recently reviewed all the homogeneous and heterogeneous catalyst systems for the synthesis of glycerol carbonate from glycerol and DMC.

Among the different solid base catalysts MgO based mixed oxide catalysts were better for the transesterification of glycerol (Malyaadri et al., 2011). However, their selectivity to glycerol carbonate was limited as decarbonylation of glycerol carbonate to glycidol takes place on strong basic sites of the catalysts (Parameswaram et al., 2013). Strontium oxide based catalysts are attractive base catalysts as these possess moderate basic strength (Take et al., 1971). Moreover, strontium based compounds are not toxic (Yang and Xie, 2007). It is anticipated that the strontium based mixed oxide catalysts may lead to moderate base catalysts when combined with MgO. The high basicity of MgO-SrO may lead to selective preparation of glycerol carbonate during glycerol transesterification. The selectivity in the transesterification of glycerol depends on the nature of basic sites and their strengths. There is a need to develop stable solid base catalysts with high selectivity towards glycerol carbonate and MgO-SrO mixed oxide catalyst may be a suitable catalytic system to obtain a high yield of glycerol carbonate.

In the present study, a series of strontium and zirconium mixed oxide catalysts were prepared by varying their molar ratios and evaluated for the transesterification of glycerol with dimethyl carbonate. The variation in the textural and structural characteristics of the catalysts with the change in their composition and calcination temperature was investigated. The effect of reaction parameters on the yield of glycerol carbonate was also studied.

2. EXPERIMENTAL

2.1 Materials and Catalyst Preparation

The precursors $Sr(NO_3)_2$ and $ZrO(NO_3)_2{\cdot}H_2O$ were purchased from Sigma-Aldrich. Analytical grade glycerol and dimethyl carbonate were obtained from SD Fine Chem., India. Glycerol carbonate was supplied by Tokyo Chemical Industries, Japan. All the reagents were used as received without further purification.

The mixed metal oxide SrO-ZrO_2 (SZ) catalysts were synthesized by the coprecipitation method. In a typical preparation method for the synthesis of SZ binary mixed oxide with a molar ratio of 3:1, the required quantities of Sr $(NO_3)_2$ (12.6 g) and $ZrO(NO_3)_2{\cdot}H_2O$ (4.62 g) were dissolved in de-ionized water and allowed to precipitate using KOH (0.1 M) solution. Alkaline solution was slowly added dropwise to the mixture until to a pH of 9–10 was obtained. The precipitate was aged for about 12 h at 80°C. The precipitate was filtered and washed with an excess of water to remove alkali ions. The thus obtained white solid was dried at 110°C for 12 h. Samples were calcined in air at 650°C with a heating rate of 5°C/min for 4 h. The SrO-ZrO_2 catalysts were represented as SZ-11, SZ-21, and SZ-31 where the numbers indicate the molar ratios of SrO and ZrO_2, respectively.

2.2 Characterization of Catalysts

The Brunauer-Emmett-Teller (BET) surface area of the catalyst samples were obtained by N_2 adsorption at liquid N_2 temperature on an Autosorb-1 Quantachrome instrument.

X-ray powder diffraction (XRD) patterns of the catalysts were recorded on a Rigaku Miniflex diffractometer using Cu $K\alpha$ radiation (1.5406 Å) at 40 kV and 30 mA. The measurements were obtained in steps of 0.045° with account time of 0.5 s and in the 2θ range of 10°–80°.

Temperature programmed desorption of CO_2 (TPD-CO_2) was carried out to measure the basicity of the catalysts. The catalyst sample was pretreated in He flow at 300°C for 1 h and then cooled to 50°C prior to the adsorption of CO_2 at this temperature. After the adsorption of CO_2 for 1 h the sample was flushed with He for 1 h at 100°C in order to remove physisorbed CO_2 from the catalyst surface. The CO_2 desorption profile was recorded during a temperature

program from 100°C to 800°C at a heating rate of 10°C min^{-1}. The evolved CO_2 was monitored by an online gas chromatograph provided with a thermal conductivity detector (TCD).

2.3 Transesterification of Glycerol

The transesterification of glycerol with dimethyl carbonate was carried using Sr-Zr catalysts at atmospheric pressure. In a typical experiment, glycerol (2 g), DMC (9.78 g), and 0.3 g of catalyst were charged into a 50-ml round-bottom (RB) flask equipped with a reflux condenser. The reaction was carried out at a reaction temperature of 90°C. After completion of the reaction or stipulated time the catalyst was removed by centrifugation. The products were analyzed using a gas chromatograph (Shimadzu, 2010) equipped with a flame ionization detector over an INNOWax capillary column (diameter: 0.25 mm; length: 30 m). The products were also identified by GC-MS (Shimadzu, GCMS-QP2010S) analysis.

3. RESULTS AND DISCUSSION

3.1 Characterization of Catalysts

The catalysts showed relatively low surface area. Bulk SrO was found to have a low surface area of 0.6 $m^2 \cdot g^{-1}$ and the pure ZrO_2 surface area was 41 $m^2 \cdot g^{-1}$. The catalysts SZ-11, 21, and 31 exhibited surface areas of 23, 48, and 72 $m^2 \cdot g^{-1}$, respectively. These catalyst surface areas increased with increase in the Sr to Zr molar ratio. The surface area of the catalysts increased from 23 to 72 $m^2 \cdot g^{-1}$ with increase in Sr content.

XRD patterns of the catalysts are shown in Fig. 1. The patterns of both SrO and ZrO_2 were also shown for comparison. Bulk strontium oxide showed the presence of SrO and $Sr(OH)_2$ phases. Zirconia was present predominantly in its monoclinic phase. The Sr-Zr mixed oxide catalysts exhibited patterns mainly related to the crystalline phase of strontium-zirconium oxide ($SrZrO_3$) along with less intense patterns of $SrO/Sr(OH)_2$ (Parameswaram et al., 2013). The catalysts with Sr to Zr ratio of 1:1 and 2:1 showed the presence of $SrZrO_3$ and t-ZrO_2 phases. The presence of the tetragonal phase even after calcination at high temperature (650°C/4 h) suggests the strong interaction between ZrO_2 and SrO. In the case of the catalyst with Sr to Zr ratio of 3:1, formation of $SrZrO_3$ was observed as a major phase along with t-ZrO_2. The formation of the $SrZrO_3$ phase is expected as these mixed oxide catalysts were prepared by the coprecipitation method (Lima et al., 2012).

The basicity of the catalysts was estimated by temperature programmed desorption of CO_2 and the corresponding profiles are shown in Fig. 2. The patterns suggest that the basicity of the catalysts varied with change in the Sr to Zr

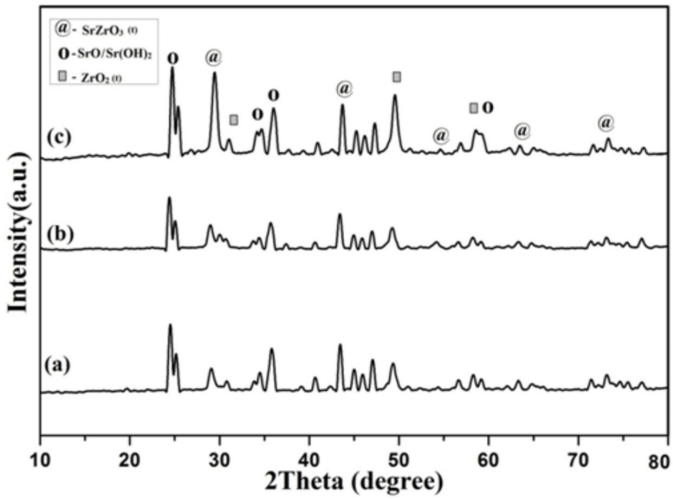

FIG. 1: XRD patterns of Sr/Zr catalysts (a) SZ-11, (b) SZ-21, and (c) SZ-31

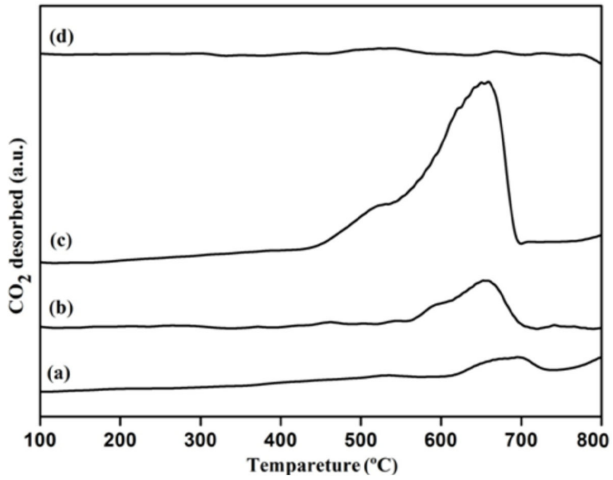

FIG. 2: CO_2-TPD profiles of Sr/Zr catalysts (a) SZ-11, (b) SZ-21, (c) SZ-31, and (d) SZ-31 without CO_2

ratio. The SZ-11 and 21 catalysts exhibited broad desorption peaks with less intensity in the temperature range of 450°C–700°C. The SZ-31 catalyst showed an intense and high-temperature desorption peak at 670°C along with a small peak at 550°C. The desorption band at high temperature might be assigned to the strong basic sites mainly associated to oxygen in M^{2+}–O^{2-} pairs (Gerpen et al., 2005; Hoydonckx et al., 2004; Albuquerque et al., 2008). The high basicity of the SZ-31 catalyst was related to the availability of a higher number of oxygen anions of alkali-earth strontium oxide which is present in a high ratio in the sample.

The base catalysts are prone to adsorb atmospheric CO_2. Strontium based catalysts may form the $Sr(CO_3)_2$ phase and the desorption of CO_2 may also arise from this phase during TPD of CO_2. In order to confirm this, a separate TPD run was carried out on the SZ-31 catalyst without adsorption of CO_2, and the profile is shown in Fig. 2(d). The TPD patterns suggested that there was no desorption of CO_2. This indicates that desorption peaks in the samples are related to the CO_2 adsorbed on basic sites during TPD analysis only.

3.2 Catalytic Activity for Glycerol Transesterification

The Sr-Zr catalysts were evaluated for the transesterification of glycerol with DMC; the results are shown in Table 1. The transesterification of glycerol was also carried in the absence of a catalyst and gave about 5% yield of GLC. The activities of SrO and ZrO_2 oxides are also included in Table 1 for comparison. The activities of individual SrO and ZrO_2 are low compared to the Sr-Zr mixed oxide catalysts. SrO and ZrO_2 gave about 24% and 4% yield of GLC, respectively. In the presence of Sr-Zr mixed oxide catalysts, conversion of glycerol and selectivity to GLC improved significantly. The glycerol conversion is found to be increased from 31% to 92% with increase in the Sr to Zr molar ratio from 1:1 to 3:1. This result indicates that the transesterification activity is significantly dependent on the mole ratio of Sr to Zr. The activity profiles of these catalysts can be explained based on their physicochemical characteristics. The transesterification activity of the catalysts is mainly related to the catalyst basicity (Gerpen et al., 2005; Hoydonckx et al., 2004). The increased number of basic sites with increase in the amount of Sr in SZ catalysts with reasonable surface area might be responsible for the high activity of the SZ-31 catalyst. The increase in basicity for the SZ-31 catalyst may be due to the existence of $SrZrO_3$ as a major phase. The high basicity associated with the $SrZrO_3$ phase might be the possible active species for the transesterification reaction (Lima et al., 2012). Zhang et al. (2015) reported that Lewis basic sites were favorable for the synthesis of glycerol carbonate. It is important to note that the present SZ-31 catalyst has exhibited 100% selectivity to GLC. The present catalyst is advantageous as there was no formation of other by-products like glycidol (Simanjuntak et al., 2013). The formation of glycidol is observed when the catalysts contain a very high amount of strong basic sites (Parameswaram et al., 2013; Malkemus et al., 1958; Yoo et al., 2001). The reason for high selectivity of SZ catalysts might be due to their moderate basic sites.

TABLE 1: Transesterification of glycerol with DMC using SZ catalysts

Catalyst	Conversion (%)	Yield of GLC (%)
SZ-11	30	30
SZ-21	65	65
SZ-31	92	92
SrO	24	24
ZrO_2	4	4
Without catalyst	5	5

Reaction conditions: glycerol: 21.73 mmol; DMC: 108.5 mmol; catalyst weight: 0.3 g; temperature: 90°C; time: 90 min.

3.3 Effect of Calcination Temperature

In order to know more about the relation between surface-structural characteristics of SZ catalysts and that of transesterification activity, the active SZ-31 catalyst was treated at different temperatures from 450°C to 750°C. These catalyst samples are studied for transesterification activity; the results are shown in Table 2. The calcination temperature has a significant effect on the catalytic activity. The uncalcined SZ-31 catalyst showed very low (10% yield of GLC) transesterification activity. The yield of GLC increased from 71% to 92% with increase in catalyst calcination temperature from 450°C to 650°C. With further increase in calcination temperature to 750°C the activity was found to be decreased marginally.

In order to understand the variation in activity of the catalysts calcined at different temperatures, these catalysts were characterized further.

XRD patterns of the SZ-31 catalyst calcined at different temperatures are presented in Fig. 3. The patterns suggest the crystalline nature of the catalysts. The catalysts calcined at 450°C and 550°C showed the presence of $SrZrO_3$ and $SrO/Sr(OH)_2$ phases along with a low intense peak of t-ZrO_2. With the increase in calcination temperature to 650°C, the formation of $SrZrO_3$ was observed. This might be due to strong interaction between t-ZrO_2 and SrO oxides at high calcination temperature. With further increase in calcination temperature up to 750°C, less intense patterns related to $SrZrO_3$ phase were observed.

The basicity of the SZ-31 catalyst calcined at different temperatures was estimated by TPD of CO_2 and the basicity values are presented in Table 2. The values indicate that basicity was increased from 0.12 to 0.24 mmol/g with increase in calcination temperature from 450°C to 650°C. With further increase in calcination temperature to 750°C, the basicity of the catalysts was decreased to 0.09 mmol/g. From these results it can be concluded that the catalyst calcined at 650°C contains a greater number of basic sites. From the above discussion based on XRD and TPD results, it is concluded that 650°C is the favorable calcination temperature for the SZ-31 catalyst to have a significant number of active sites.

TABLE 2: Influence of catalyst calcination temperature on the transesterification of glycerol activity

Calcination Temperature (°C)	Conversion (%)	Yield of GLC (%)	TON[a]	Basicity (mmol•g^{-1})
450	71	71	22.4	0.12
550	80	80	25.4	0.15
650	92	92	29.1	0.24
750	66	66	20.7	0.09

Reaction conditions: glycerol: 21.73 mmol; DMC: 108.5 mmol; catalyst weight: 0.3g; temperature: 90°C; time: 90 min.
[a]TON (mol converted glycerol/mol cat).

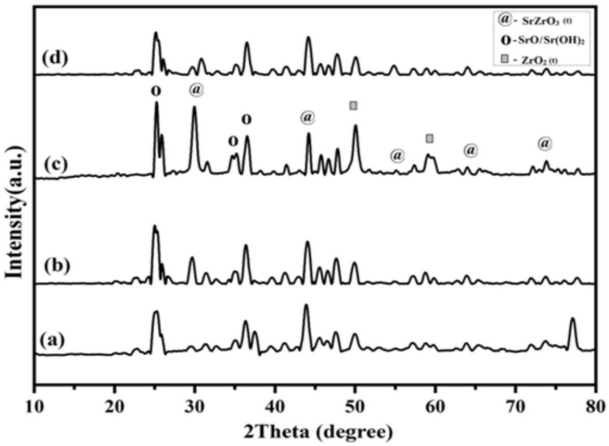

FIG. 3: XRD patterns of SZ-31 catalyst calcined at different temperatures. (a) 450°C (b) 550°C (c) 650°C and (d) 750°C

The characterization results demonstrated that the calcination temperature of the Sr-Zr mixed oxides has an influence on the transesterification of glycerol activity. The surface-structural properties varied with calcination temperature. These properties influence the basicity of the catalysts and thereby affect catalytic activity. These results strongly indicate that the calcination temperature is an important factor in the preparation of mixed oxide base catalysts.

3.4 Influence of Reaction Parameters on Transesterification Reaction

The influence of reaction parameters like temperature, time, glycerol to DMC mole ratio, and catalyst concentration was studied over the SZ-31 catalyst to optimize the reaction conditions to obtain a high yield of GLC.

3.4.1 Influence of Reaction Temperature

The effect of reaction temperature on the transesterification of glycerol was studied; the results are shown in Fig. 4. The conversion of glycerol is found to be continuously increased with the increase in reaction temperature from 50°C to 90°C. The conversion was found to increase noticeably with the increase in temperature from 70°C to 90°C. Transesterification of glycerol is a reversible reaction and reaction temperature is a critical parameter related to chemical equilibrium. The increase in reaction temperature within the range of 40°C to 80°C led to the attainment of chemical equilibrium which in turn resulted in enhancement of the reaction rate (Teng et al., 2015). As expected, the yield of GLC increased with temperature and reached a maximum of 92% at 90°C. There was not much further improvement in yield with further increase in temperature to 110°C. These results indicate that 90°C is the most suitable reaction temperature for the synthesis of GLC over the SZ-31 catalyst.

3.4.2 Influence of Reaction Time

In general, the conversion rate of glycerol and the yield of GLC increase with reaction time in a catalyzed transesterification reaction. The transesterification of glycerol with DMC over the SZ-31 catalyst was studied by varying the reaction period from 30 to 120 min; the results are presented in Fig. 5. The results suggest that the activity increased gradually with increase in reaction time from 30 to 90 min and remained constant with further increase in reaction time. About 43% of glycerol conversion was observed even at 30 min and reached a maximum of 92% within 90 min. The base catalyzed transesterification reaction carried out at long reaction times ($>$ 60 min) led to the formation of glycidol by decarbonylation of GLC (Parameswaram et al., 2013). Interestingly, in the present case there was no formation of glycidol even after the reaction time of 120 min. These results justify that the present SZ-31 catalyst is highly active and selective within short reaction times.

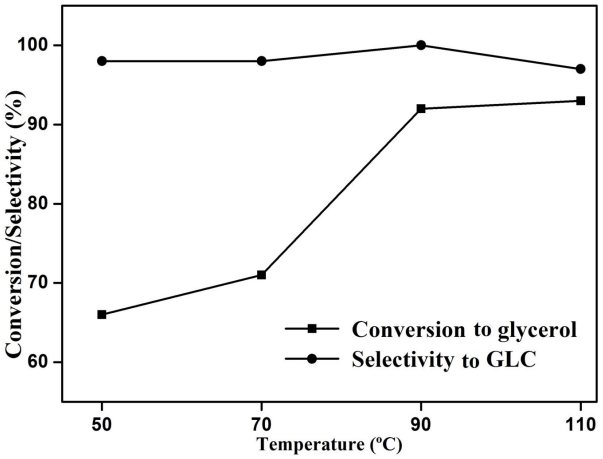

FIG. 4: Effect of reaction temperature on glycerol transesterification with DMC. Reaction conditions: glycerol: 21.73 mmol; DMC: 108.5 mmol; catalyst weight: 0.3 g; time: 90 min

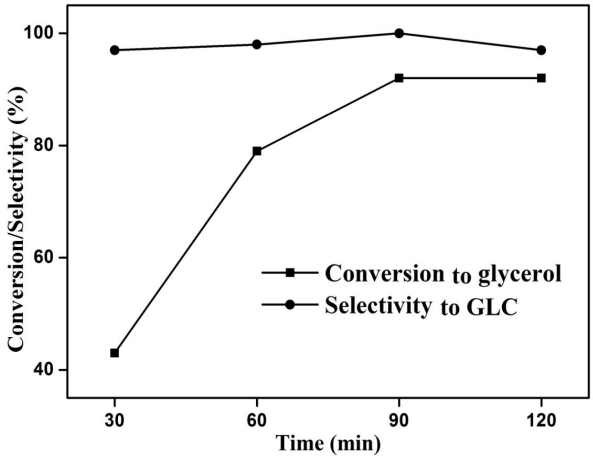

FIG. 5: Influence of reaction time on the transesterification glycerol with DMC. Reaction conditions: glycerol: 21.73 mmol; DMC: 108.5 mmol; catalyst weight: 0.3 g; temperature: 90°C

3.4.3 The Role of Reactants' Molar Ratios

The ratio for transesterification of glycerol with DMC requires 1 mole each to produce 1 mole of GLC. In general, an excess of DMC is required as glycerol is hydrophilic and not miscible with hydrophobic DMC. In order to have homogeneity in the reaction excess DMC or solvent is used. The transesterification reaction carried with varying the glycerol to DMC ratio; the results are shown in Fig. 6. The glycerol to DMC molar ratio had a noticeable effect on glycerol conversion and GLC yield. The yield of GLC improved from 60% to 92% with change in glycerol to DMC molar ratio from 1:3 to 1:5. With further increase in the molar ratio there was no appreciable change in overall activity.

It was also reported that the transesterification reaction was preferably carried out at a molar ratio of glycerol to DMC of 1:2 to 1:5 (Li and Wang, 2010). There was not much variation in activity with further increase in the glycerol to DMC molar ratio. The maximum activity was achieved at a molar ratio of 1:5 and similar observations were also reported in the literature (Malyaadri et al., 2011; Ochoa-Gómez et al., 2012).

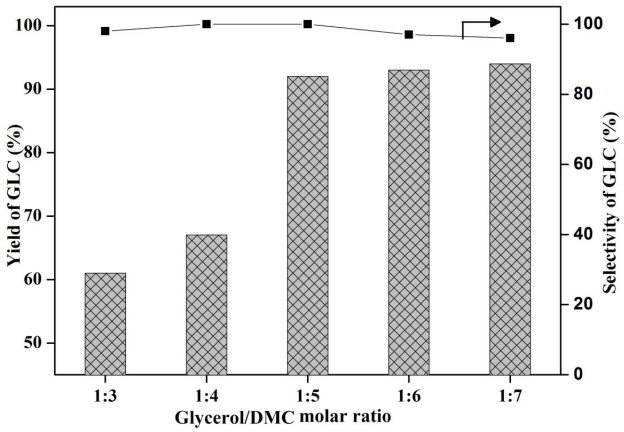

FIG. 6: The role of glycerol to DMC ratio on the transesterification of glycerol with DMC. Reaction conditions: glycerol: 21.73 mmol; DMC: 108.5 mmol; catalyst weight: 0.3 g; temperature: 90°C; time: 90 min

3.4.4 Influence of Catalyst Amount

The effect of catalyst amount on the synthesis of GLC was examined using SZ-31 at 90°C for 90 min; the results are depicted in Fig. 7. The yield of GLC was found to be increased with increase in catalyst concentration from 5 to 15 wt%. About 92% yield of GLC was achieved with use of 15 wt% of catalyst, and with further increase in the catalyst loading up to 20 wt%, there was not much variation in the yield. This indicates the stability of the catalyst against possible emulsification of a solid-liquid mixture. The substantial increase in activity with increase in catalyst amount is mainly related to the availability of a greater number of active basic sites that participate in the transesterification reaction.

3.5 Reusability of Catalyst

Heterogeneous catalysts' main features are recycling of the catalyst and good separation from the reaction mixture. The reusability of the catalyst was employed by separating the catalyst by simple filtration after reaction. The thus obtained solid was washed with water followed by methanol to remove any adsorbed organic products and dried in an oven at 110°C for 2 h. The used catalyst was subjected to the next run of transesterification reaction. The same procedure was employed in up to four cycles. The recycling results are presented in Fig. 8. It was found that the conversion of glycerol decreased marginally after the fourth recycle. The results suggest that SrO-ZrO_2 mixed oxide is a promising heterogeneous base catalyst for selective synthesis of glycerol carbonate from glycerol and DMC. The XRD patterns of the used SZ-31 catalyst are shown in Fig. 9. The present results are in accordance with the reported literature (Khayoon and Hameed, 2013).

3.6 Kinetic Studies

The present glycerol transesterification reaction falls into the category of typical liquid-liquid-solid reaction with glycerol, DMC being in liquid phase and the catalyst in solid suspended form within the reaction system. A kinetic model was proposed for the above reaction and it is verified. Prior to development of the models representing true kinetics of reaction through experimentation, it is necessary to ensure mass and heat transfer resistances within the system. The SZ-31 catalyst considered in the present study was taken in powdered form; the reaction occurs on the surface and therefore pore diffusion resistances were treated as negligible. Further, liquid phase mass transfer resistance was considered to be insignificant; as DMC in liquid phase was taken in excess, thorough and uniform

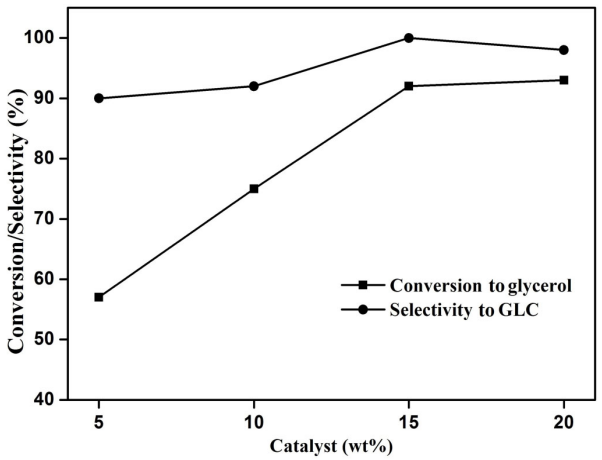

FIG. 7: Effect of catalyst amount on glycerol tranesterification with DMC. Reaction conditions: glycerol: 21.73 mmol; DMC: 108.5 mmol; temperature: 90°C; time: 90 min

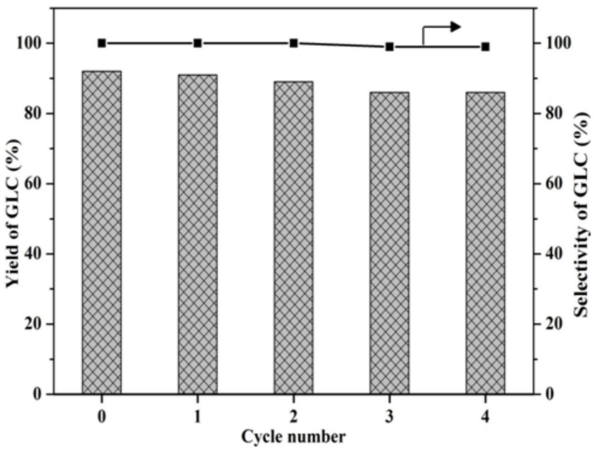

FIG. 8: The activity data during the reusability of SZ-31 catalyst. Reaction conditions: glycerol: 21.73 mmol; DMC: 108.5 mmol; catalyst weight: 0.3 g; temperature: 90°C; time: 90 min

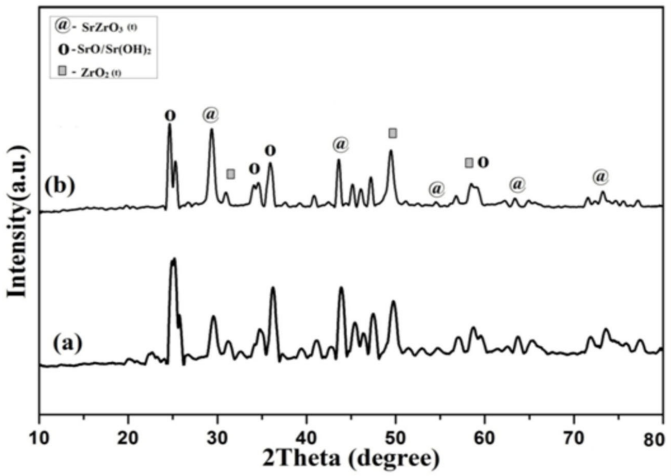

FIG. 9: XRD patterns of used SZ-31 catalyst (a) used, and (b) fresh

mixing was provided throughout. Uniform mixing of the reactants was ensured by studying the effect of stirring on the reaction rate within the range of 400–600 rpm. It was observed that there is no significant change in reaction rate with the change in stirrer speed beyond 500 rpm. In addition, the heat transfer resistances were also considered to be negligible as there was no temperature gradient observed within the reactor.

Batch experimentation was carried out for glycerol transesterification reaction using the optimal SZ-31 catalyst as suggested in Table 1. A power-law type of kinetic model was considered for the study and the model parameters were evaluated. Similar types of models were considered in recent works in the literature for expressing the kinetics of heterogeneous catalytic reactions including glycerol hydrogenolysis (Vasiliadou and Lemonidou, 2013; Rekha et al., 2015). The rate expression representing the glycerol transesterification reaction is given by

$$-\left(r_{\mathrm{gly}}\right)=-\frac{dC_{\mathrm{gly}}}{dt}=k\left(C_{\mathrm{gly}}\right)^{m}\left(C_{\mathrm{DMC}}\right)^{n}, \tag{1}$$

where the rate of glycerol consumption k is the overall reaction rate constant; C_{gly}, C_{DMC} are the respective molar concentrations of glycerol and DMC; and m, n are the apparent reaction orders with respect to glycerol and DMC, respectively. The experimental data were obtained by conducting the reactions with the glycerol mole ratio varying from 0.5 to 1.5 while maintaining all other parameters constant at their optimal values and these data were used for determining the apparent reaction order with respect to glycerol. Similarly, the experiments are conducted by varying the DMC mole ratio from 3 to 7 and the respective data were used to determine the reaction order with respect to DMC. The rate of consumption of glycerol was plotted with respect to the concentration of glycerol and DMC as shown in Figs. 10(a) and 10(b), respectively. From these figures it is observed that the rate of conversion of glycerol is improved by increasing the glycerol and DMC concentrations.

For transesterification of glycerol in the presence of DMC using the SZ-31 catalyst, the order of reaction with respect to glycerol was found to be 1.8 and that with respect to DMC was 4.5. These values interpret that the concentration of DMC has a very significant impact on the rate of glycerol consumption as compared to that of the concentration of glycerol. Further, the temperature dependency of the rate constant k can be evaluated by using the Arrhenius law, given as

$$k=k_{o}e^{-E/RT}, \tag{2}$$

where k_o and E are the Arrhenius constants, R is the universal gas constant, and T is the temperature. In this case, reactions were carried out at different temperatures ranging from 50 to 110°C and the rate constants at corresponding temperatures were determined by using Eq. (2). The Arrhenius law plot of ln (k) vs. 1/T resulted in a straight line as shown in Fig. 11. The values of activation energy and frequency factors obtained from slope and intercept were

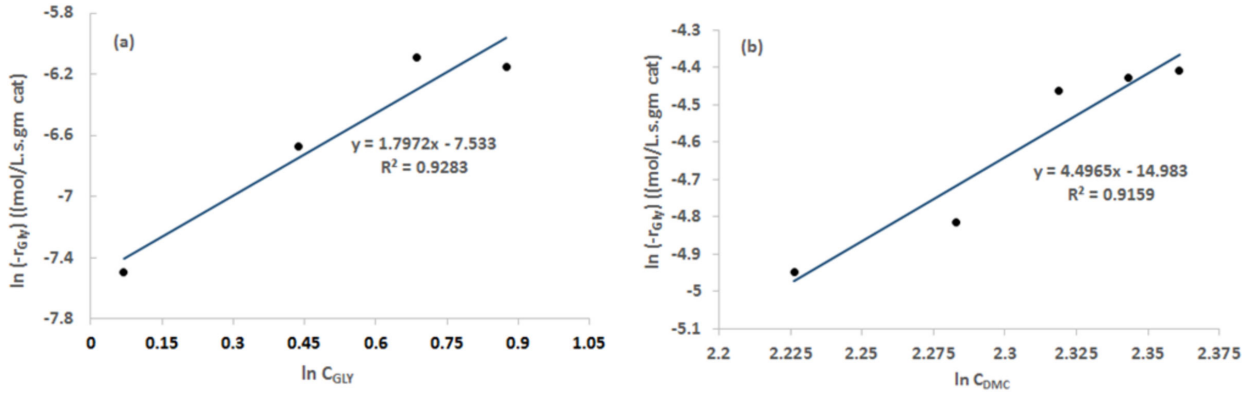

FIG. 10: Glycerol consumption rate: (a) apparent reaction order w.r.t glycerol and (b) apparent reaction order w.r.t DMC

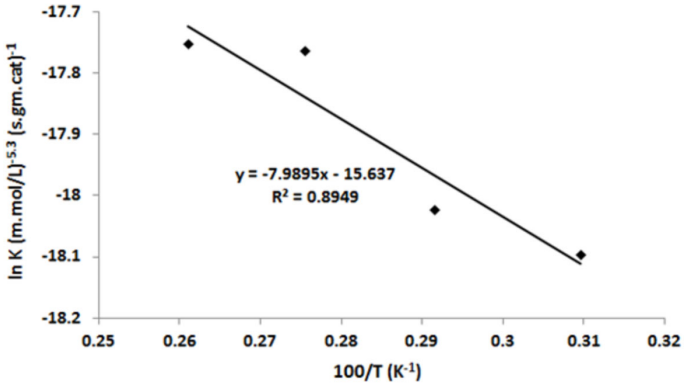

FIG. 11: Arrhenius plot for overall reaction of transesterification of glycerol

6.642 kJ/mol and 1.613×10^{-7} $(\text{mol/L})^{-5.3}$ $(\text{s.g.cat})^{-1}$, respectively. According to Arrhenius law, frequency factor k_o does not affect the temperature sensitivity of the reaction; however, in practice, there may be a slight dependency on temperature, which is negligible.

4. CONCLUSIONS

Selective synthesis of glycerol carbonate was successfully carried out through transesterification of glycerol with DMC using Sr-Zr binary mixed oxide catalysts. The catalysts' activity was dependent on the Sr to Zr molar ratio and calcination temperature. The catalyst with a Sr to Zr molar ratio of 3:1 and calcined at 650°C showed the highest activity. The formation of the $SrZrO_3$ phase along with SrO and t-ZrO_2 phases led to the generation of moderate to strong basic sites which guided the high transesterification activity. The transesterification activity also depended on the reaction temperature, time, catalysts' concentration, and glycerol to DMC molar ratios. The maximum GLC yield of 92% was obtained at a reaction temperature of 90°C, and a reaction time of 90 min with a glycerol to DMC molar ratio of 1:5. The catalyst can be readily recovered and reusable without any significant loss in activity. Further, kinetic studies were also performed and a kinetic expression was derived.

ACKNOWLEDGMENTS

The authors thank the Council of Scientific and Industrial Research (CSIR), New Delhi for the financial support in the form of Indus Magic (CSC-0123) project under the 12th Five Year Programme.

REFERENCES

Albuquerque, M.C.G., Santamaría-González, J., Mérida-Robles, J.M., Moreno-Tost, R., Rodríguez-Castellón, E., Jiménez-López, A., Azevedo, D.C.S., Cavalcante, Jr., C.L., and Maireles-Torres, P., MgM (M = Al and Ca) Oxides as Basic Catalysts in Transesterification Processes, *Appl. Catal. A*, vol. **347**, pp. 162–168, 2008.

Aresta, M., Dibenedetto, A., Nocito, F., and Ferragina, C., Valorization of Bio-Glycerol: New Catalytic Materials for the Synthesis of Glycerol Carbonate via Glycerolysis of Urea, *J. Catal.*, vol. **268**, pp. 106–114, 2009.

Bai, R., Wang, Y., Wang, S., Mei, F., Li, T., and Li, G., Synthesis of Glycerol Carbonate from Glycerol and Dimethyl Carbonate Catalyzed by NaOH/γ-Al_2O_3, *Fuel Process. Technol.*, vol. **106**, pp. 209–214, 2013.

Behr, A., Eilting, J., Irawadi, K., Leschinski, J., and Lindner, F., Improved Utilization of Renewable Resources: New Important Derivatives of Glycerol, *Green Chem.*, vol. **10**, pp. 13–30, 2008.

Climent, M.J., Corma, A., Frutos, P., Iborra, S., Noy, M., Velty, A., and Concepcion, P., Chemicals from Biomass: Synthesis of Glycerol Carbonate by Transesterification and Carbonylation with Urea with Hydrotalcite Catalysts. The Role of Acid–Base Pairs, *J. Catal.*, vol. **269**, pp. 140–149, 2010.

Du, M., Li, Q., Dong, W., Geng, T., and Jiang, Y., Synthesis of Glycerol Carbonate from Glycerol and Dimethyl Carbonate Catalyzed by K_2CO_3/MgO, *Res. Chem. Intermed.*, vol. **38**, pp. 1069–1077, 2012.

George, J., Patel, Y., Pillai, M., and Munshi, P., Methanol Assisted Selective Formation of 1,2-Glycerol Carbonate from Glycerol and Carbon Dioxide using $^{n}Bu_2SnO$ as a Catalyst, *J. Mol. Catal. A: Chem.*, vol. **304**, pp. 1–7, 2009.

Gerpen, J.V., Biodiesel Processing and Production, *Fuel Process. Technol.*, vol. **86**, pp. 1097–1107, 2005.

Guan, J., Song, Y., Lin, Y., Yin, X., Zuo, M., Zhao, Y., Tao, X., and Zheng, Q., Progress in Study of Non-Isocyanate Polyurethane, *Ind. Eng. Chem. Res.*, vol. **50**, pp. 6517–6527, 2011.

Hoydonckx, H.E., De Vos, D.E., Chavan, S.A., and Jacobs, P.A., Esterification and Transesterification of Renewable Chemicals, *Top. Catal.*, vol. **27**, pp. 83–96, 2004.

Hu, J., Li, J., Gu, Y., Guan, Z., Mo, W., Ni, Y., Li, T., and Li, G., Oxidative Carbonylation of Glycerol to Glycerol Carbonate Catalyzed by $PdCl_2$(Phen)/KI, *Appl. Catal. A*, vol. **386**, pp. 188–193, 2010.

Khayoon, M.S. and Hameed, B.H., $Mg_{1+x}Ca_{1-x}O_2$ as Reusable and Efficient Heterogeneous Catalyst for the Synthesis of Glycerol Carbonate via the Transesterification of Glycerol with Dimethyl Carbonate, *Appl. Catal. A*, vol. **466**, pp. 272–281, 2013.

Li, J. and Wang, T., Coupling Reaction and Azeotropic Distillation for the Synthesis of Glycerol Carbonate from Glycerol and Dimethyl Carbonate, *Chem. Eng. Process. Process. Intensif.*, vol. **49**, pp. 530–535, 2010.

Lima, J.R.O., Ghani, Y.A., Silva, R.B., Batista, F.M.C., Bini, R.A., Varanda, L.C., and Oliveira, J.E., Strontium Zirconate Heterogeneous Catalyst for Biodiesel Production: Synthesis, Characterization and Catalytic Activity Evaluation, *Appl. Catal. A*, vols. **445–446**, pp. 76–82, 2012.

Liu, P., Derchi, M., and Hensen, E.J.M., Synthesis of Glycerol Carbonate by Transesterification of Glycerol with Dimethyl Carbonate over MgAl Mixed Oxide Catalysts, *Appl. Catal. A*, vol. **467**, pp. 124–131, 2013.

Liu, Z., Wang, J., Kang, M., Yin, N., Wang, X., and Tan, Y., Structure-Activity Correlations of $LiNO_3/Mg_4AlO_{5.5}$ Catalysts for Glycerol Carbonate Synthesis from Glycerol and Dimethyl Carbonate, *J. Ind. Eng. Chem.*, vol. **21**, pp. 394–399, 2015.

Malkemus, J.D., Currier, V.A., and Bell, J.B., Method for Preparing Glycidol, US Patent 2,856,413, filed Jul 23, 1956, and issued Oct 14, 1958.

Malyaadri, M., Jagadeeswaraiah, K., Sai Prasad, P.S., and Lingaiah, N., Synthesis of Glycerol Carbonate by Transesterification of Glycerol with Dimethyl Carbonate over Mg/Al/Zr Catalysts, *Appl. Catal. A*, vol. **401**, pp. 153–157, 2011.

Ochoa-Gomez, J.R., Gomez-Jimenez-Aberasturi, O., Madurga, B.M., Rodriguez, A.P., Ramirez–Lopez, C., Ibarreta, L.L., Torrecilla-Soria, J., and Velasco, M.C.V., Synthesis of Glycerol Carbonate from Glycerol and Dimethyl Carbonate by Transesterification: Catalyst Screening and Reaction Optimization, *Appl. Catal. A*, vol. **366**, pp. 315–324, 2009.

Ochoa-Gómez, J.R., Gómez-Jiménez-Aberasturi, O., Ramírez-López, C., and Maestro-Madurga, B., Synthesis of Glycerol 1,2-Carbonate by Transesterification of Glycerol with Dimethyl Carbonate using Triethylamine as a Facile Separable Homogeneous Catalyst, *Green Chem.*, vol. **14**, pp. 3368–3376, 2012.

Olga, G.P.M., Rosas, J.M., Bedia, J., Jose, R.M., and Tomas, C., Recent Inventions in Glycerol Transformations and Processing, *Recent Pat. Chem. Eng.*, vol. **2**, pp. 11–21, 2009.

Pagliaro, M., Ciriminna, R., Kimura, H., Rossi, M., and Pina, C.D., From Glycerol to Value-Added Products, *Angew. Chem., Int.*

Ed., vol. **46**, pp. 4434–4440, 2007.

Parameswaram, G., Srinivas, M., Hari Babu, B., Sai Prasad, P.S., and Lingaiah, N., Transesterification of Glycerol with Dimethyl Carbonate for the Synthesis of Glycerol Carbonate over Mg/Zr/Sr Mixed Oxide Base Catalysts, *Catal. Sci. Technol.*, vol. **3**, pp. 3242–3249, 2013.

Rekha, V., Sumana, C., Douglas, S.P., and Lingaiah, N., Understanding the Role of Co in Co–ZnO Mixed Oxide Catalysts for the Selective Hydrogenolysis of Glycerol, *Appl. Catal. A*, vol. **491**, pp. 155–162, 2015.

Rokicki, G., Rakoczy, P., Parzuchowski, P., and Sobiecki, M., Hyperbranched Aliphatic Polyethers Obtained from Environmentally Benign Monomer: Glycerol Carbonate, *Green Chem.*, vol. **7**, pp. 529–539, 2005.

Shaikh, A.G. and Sivaram, S., Organic Carbonates, *Chem. Rev.*, vol. **96**, pp. 951–976, 1996.

Simanjuntak, F.S.H., Tanda, V.T., Kim, C.S., Ahn, B.S., Kim, Y.J., and Lee, H., Synthesis of Glycerol Carbonate from Glycerol and Dimethyl Carbonate using Magnesium–Lanthanum Mixed Oxide Catalyst, *Chem. Eng. Sci.*, vol. **94**, pp. 265–270, 2013.

Sonnati, M.O., Amigoni, S., Taffin, de Givenchy, E.P., Darmanin, T., Choulet, O., and Guittard, F., Glycerol Carbonate as a Versatile Building Block for Tomorrow: Synthesis, Reactivity, Properties, and Applications, *Green Chem.*, vol. **15**, pp. 283–306, 2013.

Takagaki, A., Iwatani, K., Nishimura, S., and Ebitani, K., Synthesis of Glycerol Carbonate from Glycerol and Dialkyl Carbonates using Hydrotalcite as a Reusable Heterogeneous Base Catalyst, *Green Chem.*, vol. **12**, pp. 578–581, 2010.

Take, J., Kikuchi, N., and Yoneda, Y., Base-Strength Distribution Studies of Solid-Base Surfaces, *J. Catal.*, vol. **21**, pp. 164–170, 1971.

Teles, J.H., Rieber, N., and Harder, W., Preparation of Glyceryl Carbonate, US Patent 5,359,094, 1994.

Teng, W.K., Ngoh, G.C., Yusoff, R., and Aroua, M.K., A Review on the Performance of Glycerol Carbonate Production via Catalytic Transesterification: Effects of Influencing Parameters, *Energy Convers. Manage.*, vol. **88**, pp. 484–497, 2015.

Vasiliadou, E.S. and Lemonidou, A.A., Kinetic Study of Liquid-Phase Glycerol Hydrogenolysis over Cu/SiO_2 Catalyst, *Chem. Eng. J.*, vol. **231**, pp. 103–112, 2013.

Yang, Z. and Xie, W., Soybean oil Transesterification over Zinc Oxide Modified with Alkali Earth Metals, *Fuel Proc. Technol.*, vol. **88**, pp. 631–638, 2007.

Yoo, J.W., Mouloungui, Z., and Gaset, A., Method for Producing an Epoxide, in Particular of Glycidol, and Installation for Implementation, US Patent 6,316,641, filed Mar 6, 1998, and issued Nov 13, 2001.

Zhang, J. and Dehua, H., Synthesis of Glycerol Carbonate and Monoacetin from Glycerol and Carbon Dioxide over Cu Catalysts: The Role of Supports, *J. Chem. Technol. Biotechnol.*, vol. **90**, pp. 1077–1085, 2015.

Zhou, C.H., Beltramini, J.N., Fan, Y.X., and Lu, G.Q., Chemoselective Catalytic Conversion of Glycerol as a Biorenewable Source to Valuable Commodity Chemicals, *Chem. Soc. Rev.*, vol. **37**, pp. 527–549, 2008.

SYNTHESIS OF 3-METHOXYCATECHOL FROM PYROGALLOL AND DIMETHYL CARBONATE IN LIQUID PHASE SLURRY REACTOR

Pooja R. Tambe,[1] Riitta Keiski,[2] & Ganapati D. Yadav[1,*]

[1]*Department of Chemical Engineering, Institute of Chemical Technology, Nathalal Parekh, Marg, Matunga, Mumbai 400019, India*

[2]*Department of Mass and Heat Transfer, University of Oulu, Finland*

*Address all correspondence to: Ganapati D. Yadav, Department of Chemical Engineering, Institute of Chemical Technology, Nathalal Parekh, Marg, Matunga, Mumbai 400019, India; Tel.: +91 223 361 1001/1111/2222; Fax: +91 223 3611 1020, E-mail: gd.yadav@ictmumbai.edu.in

Original Manuscript Submitted: 6/19/2017; Final Draft Received: 2/23/2018

Selective mono O-methylation of pyrogallol (trihydroxy benzene) is traditionally carried out with a polluting homogenous base catalyst and various alkali salts. A heterogeneous catalytic system was developed to achieve the same in a liquid phase slurry reactor. Calcined hydrotalcite was synthesized by different synthesis routes, and its activity was studied for selective mono O-methylation of pyrogallol using dimethyl carbonate as a methylating agent. The reaction was optimized by studying different reaction parameters to illustrate the reaction kinetics. The reaction at optimum conditions, i.e., catalyst concentration of 0.035 g/cm^3, 180°C, 1400 rpm, and mole ratio of pyrogallol to dimethyl carbonate (DMC) as 1:5 gave 52% conversion of pyrogallol with 89% selectivity toward 3-methoxy catechol. The catalyst is reusable over three cycles. The activation energy for the reaction was calculated as 8.81 kcal/mol. Use of DMC as the methylating agent adds the green content to the current work.

KEY WORDS: *solid base, calcined hydrotalcite, dimethyl carbonate, 1,2,3-trimethoxy benzene (pyrogallol), 3-methoxy catechol*

1. INTRODUCTION

One of the major principles of green chemistry is the use of heterogeneous catalysts. Most of the base catalyzed processes for production of bulk chemicals make use of liquid alkali as a catalyst. Neutralization of the alkaline medium contributes a significant amount of product cost due to extraction of product, its purification, and treatment of the large amount of waste water generated and impurities in the final products (Cavani et al., 1991; Arpe and Weissermel, 2010). Methylation of 1, 2, 3-trihydroxy benzene (pyrogallol) was carried out using various alkylating agents, such as dimethyl sulfonate, methyl halides, etc., which are detrimental, and corrosive chemicals, which require stoichiometric amount of base to neutralize the acid produced. Different homogenous catalysts, such as NaOH, K_2CO_3, ionic liquids, etc., are employed for methylation of trihydroxy benzene. Solid base catalysts give excellent yields of oxy-alkylated products in the alkylation of phenol derivatives (Fu and Ono, 1993; Vishwanathan et al., 2001; Bal et al., 2002; Bal and Sivasanker, 2003; Fu et al., 2005). Dimethyl carbonate (DMC) can be used as a methylating or carboxymethylating agent, depending on the conditions of reaction (Kirumakki et al., 2002, 2004; Yadav and Salunke, 2013). DMC favors the carboxymethylation with methanol as a co-product at lower temperature; whereas, at higher temperature,

NOMENCLATURE

C_P	concentration of P (mol/cm^3)	DMC	dimethyl carbonate
C_Q	concentration of Q (mol/cm^3)	M	initial molar ratio of dimethyl carbonate to pyrogallol
C_{Po}	initial concentration of P at solid (catalyst) surface (mol/cm^3)	P	reactant species, pyrogallol
C_{Qo}	concentration of Q at solid (catalyst) surface (mol/cm^3)	Q	reactant species, DMC
k_i	reaction rate constant (mol/g$_{cat}$ S)	R,S,T	3-methoxy catechol, methanol, carbon dioxide
CHT	calcined hydrotalcite	w	catalyst loading (g/cm^3)
		X_P	fractional conversion of P

it favors the methylation reaction with methanol and carbon dioxide as a co-product. Thus, it can be a better substitute to the corrosive and toxic methylating agents, such as diazomethane, dimethyl sulfate, etc. (Davis, 1900; Yadav and Krishnan, 1998). Use of DMC as a solvent as well as reactant makes a green approach for the reaction under study.

Hydrotalcite is an anionic clay of layered double hydroxides in which a divalent cation is replaced by a trivalent cation (Cavani et al., 1991). The hydrotalcite derived from different compounds holds wide applications, depending on its physical properties, such a surface area, basicity, phase stability, etc. These compounds are used as catalysts, catalyst supports, antacids, and ion exchangers, depending on the tailor-made physical properties. Synthesis of hydrotalcite is reported with different synthetic routes, such as co-precipitation (Yadav and Aduri, 2012), hydrothermal, sol-gel, etc. (Lopez et al., 1996). The combustion method used for the synthesis of the catalyst holds many advantages when compared in terms of two factors, i.e., reproducibility and time requirement. Generation of a nanoscale tailor-made catalyst with high surface area and mesoporosity is the major advantage of the combustion method over other synthetic routes. Also, it is a greener route compared to co-precipitation and sol-gel method. As in the case of the sol-gel method, acid treatment is employed, which in turn, affects the surface acidity of resultant catalyst; whereas, in the case of co-precipitation, a large amount of water treatment is required to ensure that the catalyst is free from other interfering anions, such as OH^- and NO_3^{2-}. Depending on the application of the catalyst, combustion synthesis is quite advantageous for preparation with tailored pore sizes, pore shapes and surface areas in less time (Roth, 2007; Yadav and Fernandes, 2013).

3-Methoxy catechol finds wide applications in agrochemicals, and pharmaceutical industries as starting material, stabilizers for plastics, precursor in perfume industries, starting material in dye industries, etc. Reports are available for O-methylation of phenol and catechol with dimethyl carbonate under vapor phase conditions (Jyothi et al., 2001). The temperature conditions for these processes were in the range of 240–300°C. Using CHT as a catalyst for O-methylation of phenol 97% conversion of phenol (at 200°C) with 100% selectivity toward anisole was reported. While in case of catechol, 96% conversion of catechol (at 300°C) with 84% selectivity for guaiacol was observed with hydrotalcite as a catalyst. This indicates that with an increase in the hydroxyl group on the benzene ring, there is a decrease in the selectivity of the mono-alkylated product. Thus, selective synthesis of 3-methoxycatechol is a challenging task and there are no reports available for O-methylation of pyrogallol using a heterogeneous catalyst. Herein, we report a process for selective synthesis of 3-methoxycathechol in liquid phase slurry reactor at moderate temperature of 180°C, which adds an advantage over the processes studied thus far.

Aim of the current work was to prepare a calcined hydrotalcite catalyst by different synthetic routes (i.e., co-precipitation, sol-gel, and combustion methods) followed by application of these catalysts for synthesis of 3-methoxy catechol. The reaction parameters were optimized to achieve higher selectivity toward the desired product. An insight of reaction mechanism and kinetic model is also provided.

2. MATERIAL AND METHODS

2.1 Chemicals

Pyrogallol, methanol, dimethyl carbonate, glycerol, magnesium nitrate hexahydrate, and aluminum nitrate nonahydrate were procured from M/s S.D. Fine Chemicals Pvt. Ltd., Mumbai, India.

2.2 Catalyst Preparation

Known amounts of magnesium nitrate (0.048 mol), aluminum nitrate (0.016 mol), and glycerol (0.065 mol as a fuel) were dissolved in 15 mL water. The precursor proportions were adjusted to get Mg:Al ratio as 3:1. This solution was then heated at 80°C in a crucible until excess water was removed to form a thick gel. The gel was fed into a preheated muffle furnace at 500°C, leading to spontaneous combustion. The white voluminous solid obtained was calcined for 3 h at 650°C. The catalyst was termed as calcined hydrotalcite (CHT-C). CHT-P (Calcined hydrotalcite by co-precipitation), and CHT-SG (Calcined hydrotalcite by sol-gel) were prepared as per reported by Bhanawase and Yadav (2016) and Valente et al. (2007), respectively.

2.3 Reaction Procedure

The O-methylation of pyrogallol was carried out in 50 cm^3 capacity stainless steel (SS-316) autoclave (Autoclave Engineers mini reactor magnetic drive III) fitted with temperature and speed controllers, and pressure indicator. A typical reaction was carried out with 0.02 mol pyrogallol, 0.2 mol DMC, and methanol (solvent) to make the total volume 40 cm^3. The reaction temperature was raised to 180°C using an agitation speed of 1000 rpm and 0.025 g/cm^3 of catalyst. The agitation was started once the reaction temperature was attained. A zero time sample was collected, and thereafter, sampling was done periodically.

2.4 Analytical Method

Analysis was carried out by using a GC [Agilent Technologies 6890N] (equipped with 0.25 mm I.D., 30 m length) BPX-50 capillary column with FID detector and an auto sampler (7683B series) equipped with 10 µl syringe. The product is identified by GC-MS.

3. RESULTS AND DISCUSSION

3.1 Catalyst Characterization

X-ray diffraction (XRD) patterns for calcined hydrotalcite was determined on a Bruker AXS, D8 Discover instrument (The Bruker Corporation, Karlsruhe, Germany) using Cu-Ka radiation at l = 1.5406 Å from $2y = 10$–901 with a scan step of 1 s and a step size of 0.1. Temperature-programmed desorption (TPD) analysis with 10% CO_2 and 10% NH_3 was performed to determine catalyst basic and acidic sites with an Autochem II (Micromeritics, Norcross, Georgia, USA) instrument equipped with a thermal conductivity detector (TCD) detector. Scanning electron microscope (SEM) images for CHT-C and CHT-C reused were recorded using a JEOL JSM 7400 microscope operated at 20 kV. The pore size distribution, pore volume, and surface area were measured by Barrett, Joyner, and Halenda (BJH) and multipoint Brunauer, Emmett, and Teller (BET) methods using a Micromeritics ASAP-2010 instrument.

3.1.1 SEM and Energy-Dispersive X-Ray (EDX) Spectroscopy

SEM images of CHT-C and reused CHT-C were recorded to study the change in surface morphology of catalyst after reuse. SEM images for CHT-C confirmed that the synthesized catalyst has irregular morphology, which is a significant characteristic of combustion synthesis, with uniform particle size ranging from 50 to 100 µm [Fig. 1(a)]. The reused catalyst also showed the same irregular morphology [Fig. 1(b)] and particle size, which signifies that the

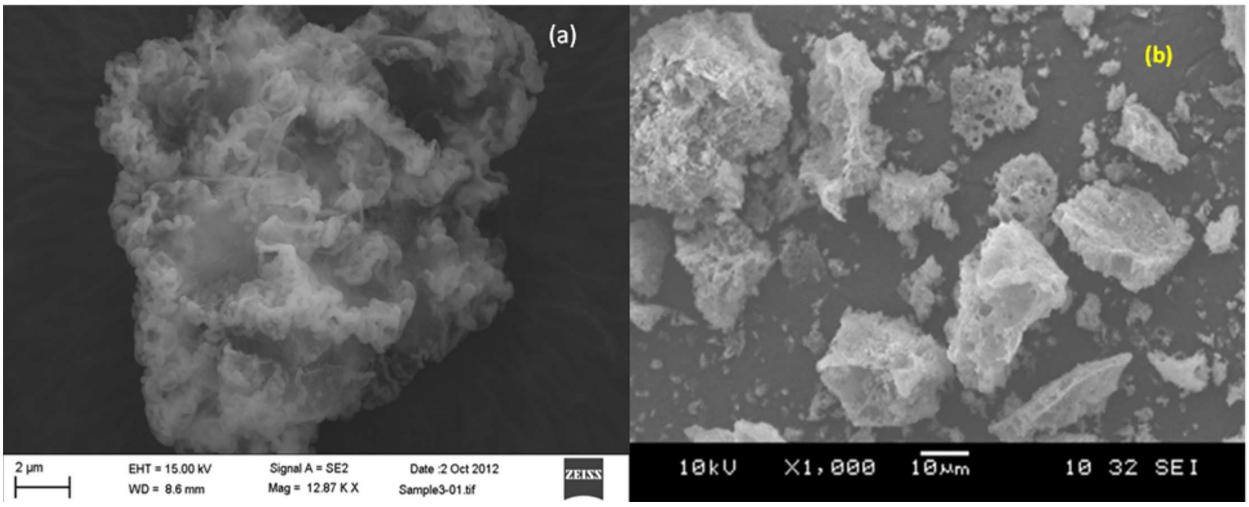

FIG. 1: SEM images of (a) fresh CHT-C and (b) reused CHT-C

catalyst retains its activity even after reuse. EDX results confirm the composition of synthesized CHT has the Mg:Al ratio of 3:1 (Table 1).

3.1.2 XRD

The XRD pattern for CHT (3:1) showed characteristic reflections (Fig. 2) at $2\theta \approx 43$ and 62 deg corresponding to mixed Mg–Al oxide and, especially, MgO (JCPDS card number 02-1207). The reflection (0 0 3), (0 0 6), and (0 1 2) for 2θ values of 11.441, 23.168, and 34.138, respectively (JCPD card number 35-0965), were observed for CHT. This confirms the layered crystalline structure of the prepared catalyst. The nanocrystalline nature of CHT was confirmed by broadening of the peaks.

3.1.3 BET Surface Area and Pore Size Analysis

Nitrogen adsorption-desorption was used for BET surface area measurement. An isotherm of type IV or V was observed for the prepared catalyst. The details of surface area and pore diameter for catalyst synthesized by different routes are presented in Table 2. The average BET surface area of fresh CHT was 140 m^2/g [Fig. 3(a)]. The average BET surface area of the reused catalyst was 132 m^2/g [Fig. 3(b)]. This confirms the mesoporosity of the catalyst was retained even after the reuse.

3.1.4 Temperature-Programmed Desorption

Total acidic and basic sites of the CHT were measured by TPD using 10% NH_3 in helium (v/v) and 10% CO_2 in helium (v/v). Prior to the analysis, the catalyst was degassed in the degassing port maintained at 150°C. The NH_3 desorption analysis for CHT-C showed peak at 152°C with peak concentration of 0.67 mmol/g, which indicates weak acidic sites (Fig. 4). Physisorbed basic oxygen, which contributes to the weak basic site, is observed in the region of 100–250°C with peak concentration of 0.92 mmol/g (Fig. 5). Presence of peak in the region of 250–350°C with peak concentration of 0.33 mmol/g confirms that a few moderate basic sites are also present in the prepared catalyst.

TABLE 1: EDX analysis of CHC-C

Catalyst	Mg (wt%)	Al (wt%)	O (wt%)
CHT-C	31.35	10.50	58.15

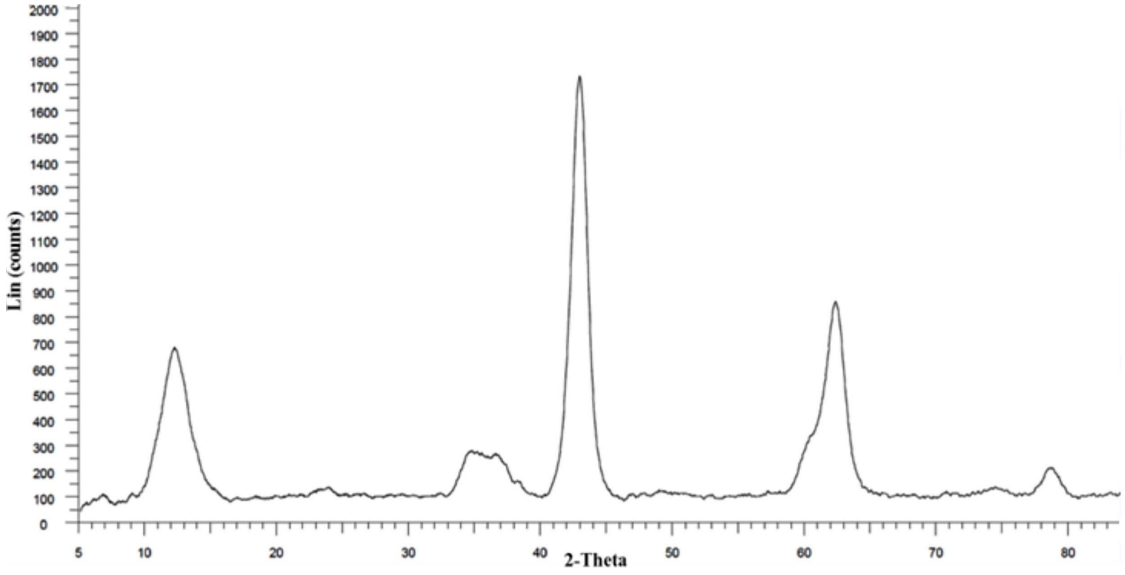

FIG. 2: XRD of CHT-C

TABLE 2: Textural properties of CHT prepared by different routes

Catalyst	Surface area (m^2/g)	Pore size (nm)	Pore volume (mmol/g)	Total basicity (mmol/g)	Total acidity (mmol/g)
CHT-CP	240.5	15.9	0.97	1.53	0.68
CHT-SG	289	41.5	0.812	1.58	0.59
CHT-C	140	14.0	0.2817	1.25	0.67
CHT-C reused	132	13.5	0.2547	1.15	0.62

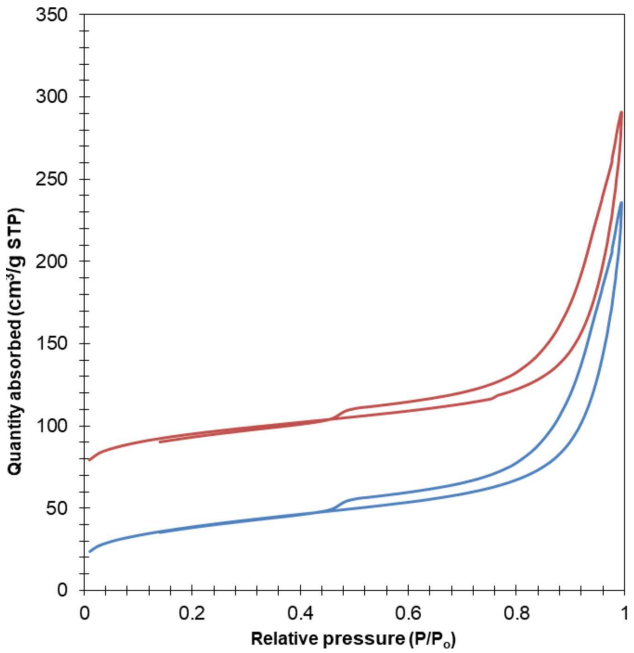

FIG. 3: BET surface area analysis of fresh and reused catalyst

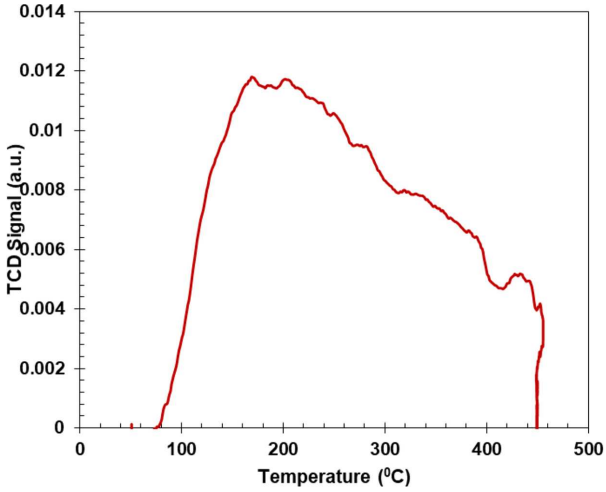

FIG. 4: TPD of CHT-C with 10% NH_3

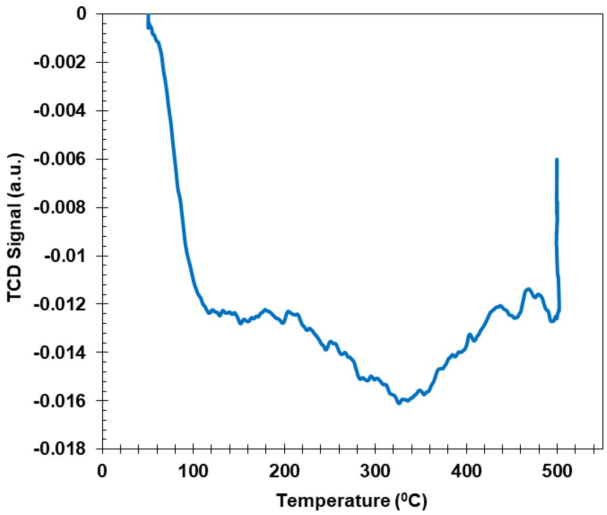

FIG. 5: TPD of CHT-C with 10% CO_2

3.2 Reaction Parameter Optimization

3.2.1 Catalyst Screening

O–Methylation using DMC as a methylating agent is favored by a base catalyst (Scheme 1). Thus, various base catalysts were screened (Fig. 6) to compare the conversion of pyrogallol and selectivity of 3-methoxy catechol.

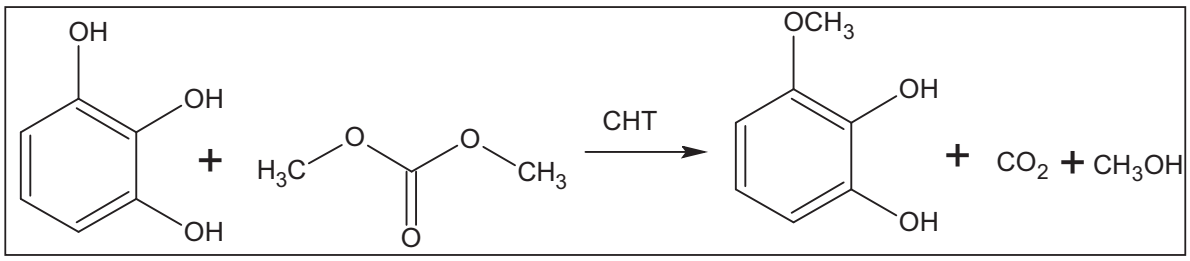

SCHEME 1: Synthesis of 3-methoxy catechol from trihydroxy benzene and dimethyl carbonate

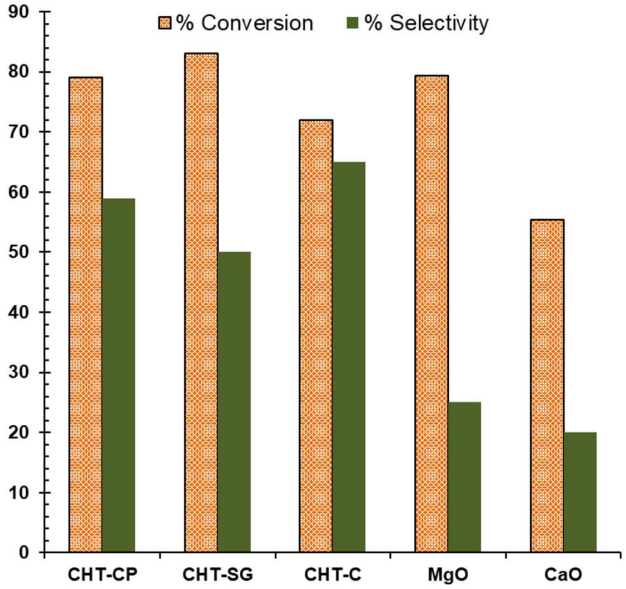

FIG. 6: Effect of various catalysts on conversion of pyrogallol: catalyst concentration 0.025 g/cm^3, 190°C, mole ratio 1:10 (pyrogallol: DMC), speed of agitation 1200 rpm, and solvent MeOH

Several catalysts, such as MgO, CaO, CHT-CP, CHT-SG, and CHT-C, were tested for the reaction. Activities of these catalysts were compared with respect to two factors, (i) conversion of pyrogallol and (ii) selectivity of 3-methoxy catechol (mono-methylated product). With MgO and CaO as a catalyst, higher conversion of pyrogallol was observed, but selectivity for 3-methoxy catechol was less because it promotes further conversion of mono- to di- and tri-methylated products. With CHT-CP and CHT-SG 76% and 83%, conversion of pyrogallol was observed, with 59 and 50% selectivity of 3-methoxy catechol, respectively; whereas, CHT-C gave 72% conversion of pyrogallol with 65% selectivity. Though, in comparison to CHT-CP and CHT-SG, CHT-C gave less conversion but selectivity of the desired product was higher compared to the other two catalysts. This may be due to the fact that the pore size and surface basicity of CHT-C are less compared to other catalysts, which in turn inhabit the formation of undesired co-products. Therefore, CHT-C was optimized as the best catalyst for further experiments.

3.2.2 Effect of Speed of Agitation

The speed range of 800–1400 rpm was studied to observe its effect on conversion of pyrogallol (Fig. 7). Beyond 1200 rpm, there was no effect on conversion and reaction rate. Thus, further reactions were done at 1400 rpm to eliminate the effect of mass transfer resistance. The details for the absence of external mass transfer resistance is provided in earlier work (Tambe and Yadav, 2017), and calculation for absence of mass transfer resistance is explained in electronic supplementary information (ESI).

3.2.3 Effect of Catalyst Loading

When external mass transfer resistance is absent, the rate of reaction increases proportionally with catalyst concentration. Thus, the catalyst concentration was studied over a range of 0.015–0.045 g/cm^3 (Fig. 8). A proportional increase in the number of catalytic sites with catalyst loading increases the conversion of pyrogallol. Beyond 0.035 g/cm^3 of catalyst concentration, the conversion of pyrogallol increases but the selectivity of 3-methoxy catechol decreases. The increased catalyst concentration favors the series reactions (i.e., di- and tri-methylation of pyrogallol), which in turn decreases the selectivity of 3-methoxy catechol. Thus, further reactions were done with a catalyst concentration of 0.035 g/cm^3 to achieve better selectivity of 3-methoxy catechol.

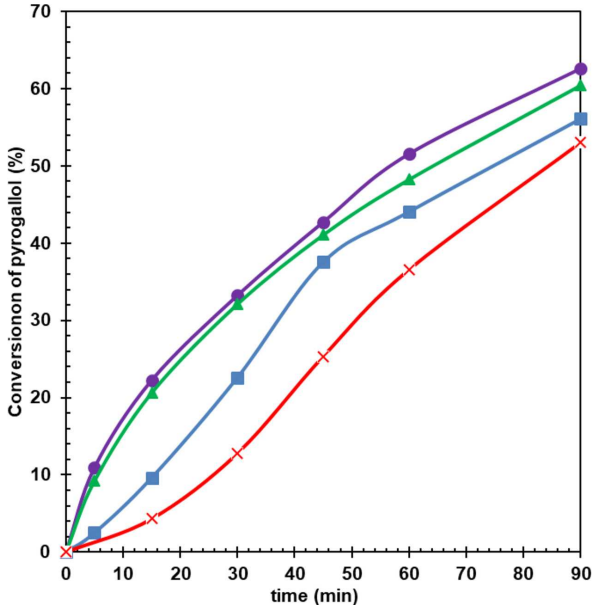

FIG. 7: Effect of speed of agitation on conversion of pyrogallol catalyst: CHT-C (3:1), catalyst concentration: 0.025 g/cm^3, 180°C, mole ratio 1:10 (pyrogallol: DMC), solvent: MeOH (●) 1400 rpm, (▲) 1200 rpm, (■) 1000 rpm, and (×) 800 rpm

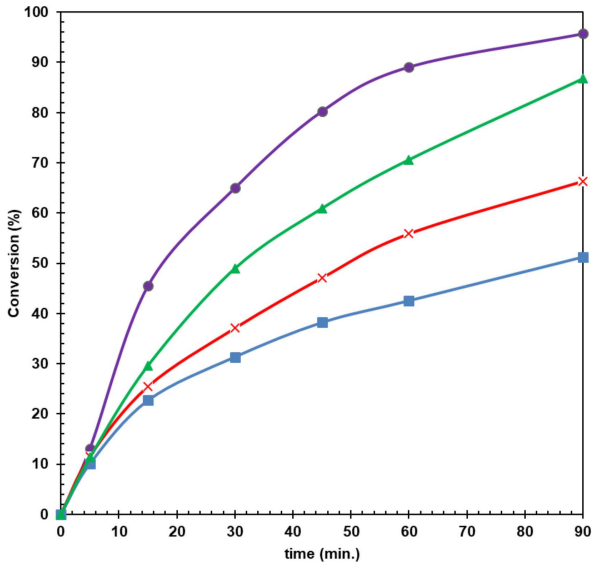

FIG. 8: Effect of catalyst loading on conversion of pyrogallol catalyst: CHT-C (3:1), 180°C, mole ratio 1:10 (pyrogallol: DMC), speed of agitation: 1400 rpm, solvent: MeOH (●) 0.045, (▲) 0.035, (×) 0.025, and (■) 0.015 g/cm^3

3.2.4 Effect of Mole Ratio

The mole ratio of pyrogallol to DMC was varied by keeping the reaction volume constant. The total reaction liquid volume was maintained to 40 cm^3 for all experiments using methanol as a solvent. The mole ratio of pyrogallol to DMC was varied from 1:2 to 1:10 to study its effect on the reaction rate and selectivity (Fig. 9). The initial rate of reaction is directly proportional to the concentration of DMC, but the availability of more methyl groups produces di- and tri-methylated products, making it less selective for 3-methoxy catechol. Significant conversion

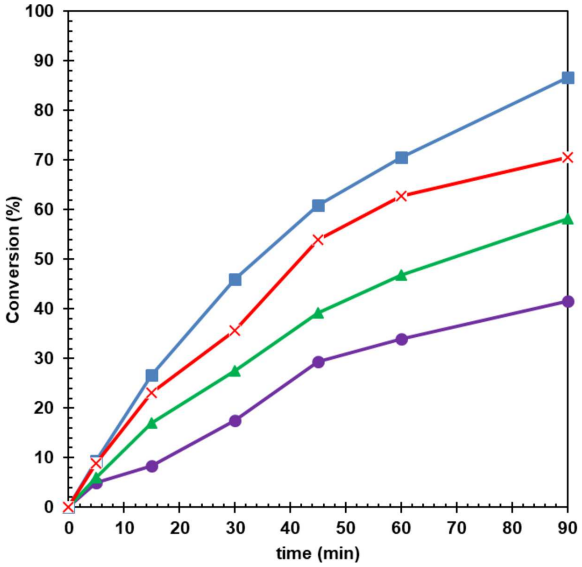

FIG. 9: Effect of mole ratio on conversion of pyrogallol catalyst: CHT-C (3:1), catalyst concentration: 0.035 g/cm^3, speed of agitation: 1400 rpm, 180°C, solvent: MeOH (●) 1:2, (▲) 1:5, (×) 1:8, and (■) 1:10

with good selectivity was obtained at a mole ratio of 1:5; therefore, further reactions were studied with a mole ratio of 1:5.

3.2.5 Effect of Temperature

The effect of temperature was studied from 140 to 190°C (Fig. 10). It was observed that, with an increase in temperature, the reaction rate also increases. This signifies that the reaction is intrinsically kinetically controlled, which will be discussed in Section 4.

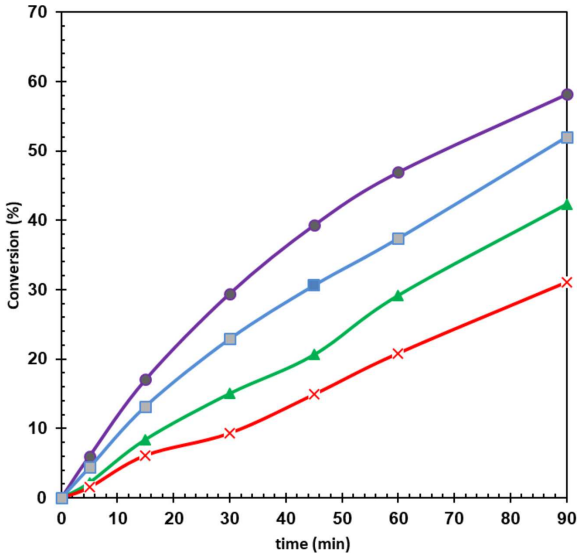

FIG. 10: Effect of Temperature on conversion of pyrogallol catalyst: CHT-C (3:1), catalyst concentration: 0.035 g/cm^3 mole ratio 1:5 (pyrogallol: DMC), solvent: MeOH (●) 190°C, (■) 180°C, (▲) 160°C, and (×) 140°C

3.2.6 Reusability of Catalyst

For the reusability study, the catalyst was filtered off after completion of the reaction. The filtered catalyst was refluxed with 10 cm^3 methanol to remove undesired absorbed materials from the surface and pores of the catalyst. After reflux, the catalyst was dried at 120°C followed by calcination at 650°C for 3 h. The catalyst was cooled and weighed. The loss of catalyst due to filtration and handling was made up with fresh catalyst, and reusability of catalyst was investigated (Fig. 11). The catalyst was reusable for three cycles.

4. KINETIC MODELING AND MECHANISM

A possible reaction mechanism was proposed (Scheme 2). The kinetics of the reaction can be explained by the Langmuir-Hinshelwood-Hougen-Watson (LHHW) model (Tiwari et al., 2014). According to the LHHW model, there was chemisorption of pyrogallol (P) on the basic site (B) and DMC (Q) on acidic site (A) followed by attack of electron-rich oxygen on the electrophilic methyl group to give the 3-methoxy catechol (R). The intermediate formed underwent rearrangement to give 3-methoxy catechol, followed by evolution of methanol (S) and carbon dioxide (T).

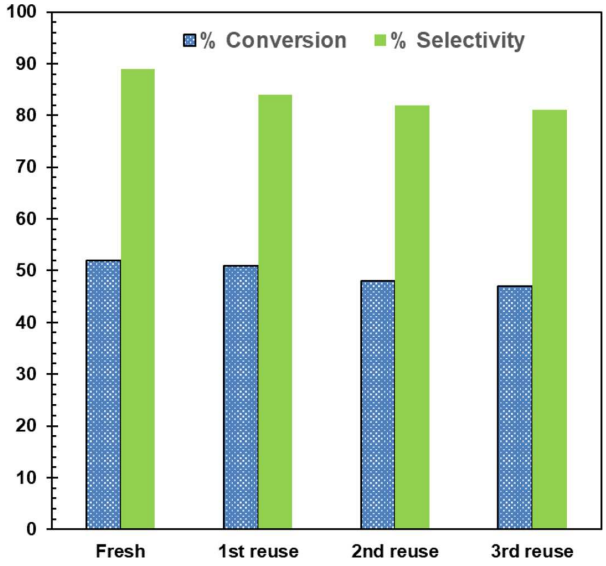

FIG. 11: Reusability study catalyst: CHT-C (3:1), speed of agitation: 1400 rpm, catalyst concentration: 0.035 g/cm^3, mole ratio 1:5 (pyrogallol: DMC), 180°C, and solvent: MeOH

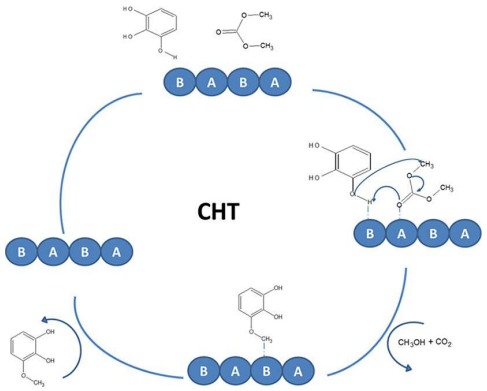

SCHEME 2: Proposed mechanism for reaction

When the analysis was completed, it was found that all the reactants were weakly adsorbed; thus, the power law model was applied to give rate of reaction as follows:

$$-\frac{dC_Q}{dt} = k_{\mathrm{R}_1} w C_P C_Q \tag{1}$$

Let $C_{Q_0}/C_{P_0} = M$ be the initial molar ratio of dimethyl carbonate to pyrogallol at time $t = 0$. Then, Eq. (1) reduces after consideration of fractional conversion

$$\frac{dX_P}{dt} = k_{\mathrm{R}_1} w C_{P_0}(1 - X_P)(M - X_P) = k_1(1 - X_P)(M - X_P) \tag{2}$$

On integration, we have

$$\ln \frac{(M - X_P)}{[M(1 - X_P)]} = k_1(M - 1)t \tag{3}$$

Thus, plots of $\ln\{(M - X_P)/[M(1 - X_P)]\}$ versus time (Fig. 12) were drawn to prove the linear relation, where X_P is the fractional conversion of pyrogallol. The reaction follows the second-order kinetics. The model was validated by plotting it for different temperatures, and the slopes of these lines are used to plot the Arrhenius plot (Fig. 13). The apparent activation energy is calculated as 8.6 kcal/mol, which signifies that the reaction is kinetically controlled.

5. CONCLUSION

Calcined hydrotalcite catalysts prepared by different methods (i.e., combustion, hydrothermal and co-precipitation) were screened for the above reaction. The combustion route was found to be the greener route compared to the co-precipitation and sol-gel methods. As in the case of the sol gel method, acid treatment is employed which, in turn, affects the surface acidity of the resultant catalyst; whereas, in the case of co-precipitation, a large amount of water treatment is required to ensure the catalyst is free from other interfering anions, such as OH^-, NO_3^{2-}. CHT-C showed good conversion and better selectivity compared to others, CHT-P and CHT-SG. A systematic study was done to optimize the reaction conditions to achieve better selectivity of 3-methoxy catechol and kinetic modeling of reaction.

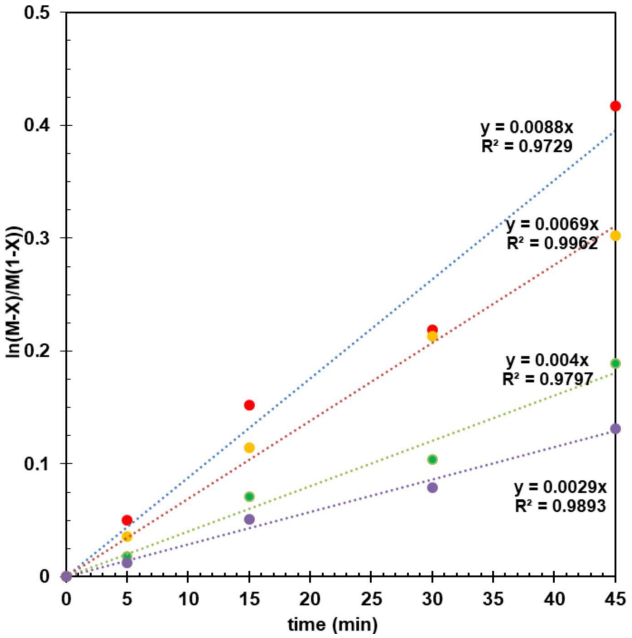

FIG. 12: Plot of $\ln\{(M - X_P)/[M(1 - X_P)]\}$ versus time

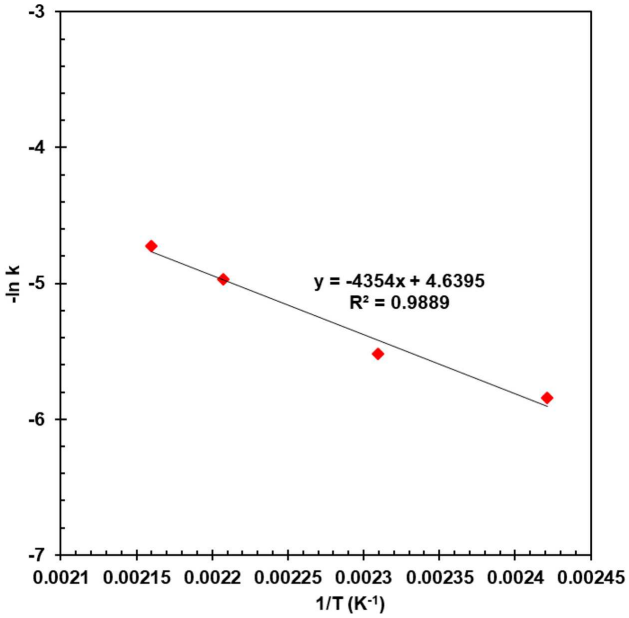

FIG. 13: Arrhenius plot

At optimum conditions of 180°C, 1.5 h, and 0.035 g/cm^3 catalyst concentration, the 1:5 pyrogallol to DMC mole ratio gave 52% conversion of pyrogallol with 89% selectivity of 3-methoxy catechol. The reaction rate is intrinsically kinetically controlled. The overall order of the reaction follows second-order kinetics. The activation energy for the reaction was calculated as 8.81 kcal/mol.

ACKNOWLEDGMENTS

This work was done under the collaborative project "Sustainable Catalytic Syntheses of Chemicals using Carbon Dioxide as Feedstock (GreenCatCO2)" supported by the Department of Science and Technology, Government of India (DST-GOI), and the Academy of Finland. GDY acknowledges support from R.T. Mody Distinguished Professor Endowment and J.C. Bose National Fellowship from DST-GOI. PRT acknowledges the Department of Science and Technology for awarding the Junior Research Fellowship under the Indo-Finnish Project.

REFERENCES

Arpe, H. and Weissermel, K., *Industrial Organic Chemistry*, Weinheim, Germany: Wiley-VCH, 2010.

Bal, R. and Sivasanker, S., Vapor Phase Selective O-Alkylation of Phenol over Alkali Loaded Silica, A*ppl. Catal. A*, vol. **246**, pp. 373–382, 2003.

Bal, R., Tope, B., and Sivasanker, S., Vapor Phase O-Methylation of Dihydroxy Benzenes with Methanol over Cesium-Loaded Silica, a Solid Base, *J. Mol. Catal. A*, vol. **18**, pp. 161–171, 2002.

Bhanawase, S.L. and Yadav, G.D., Activity and Selectivity of Different Base Catalysts in Synthesis of Guaifenesin from Guaiacol and Glycidol of Biomass Origin, *Catal. Today*, vol. **291**, pp. 213–222, 2017.

Cavani, F., Trifir, F., and Vaccari, A., Hydrotalcite-Type Anionic Clays: Preparation, Properties and Applications, *Catal. Today*, vol. **11**, pp. 173–301, 1991.

Davis, W.A., IV—Etherification of Derivatives of β-naphthol, *J. Chem. Soc. Trans.*, vol. **77**, pp. 33–45, 1900.

Fu, Z. and Ono, Y., Selective O-Methylation of Phenol with Dimethyl Carbonate over X-Zeolites, *Catal. Lett.*, vol. **21**, pp. 43–47, 1993.

Fu, Z., Yu, Y., Yin, D., Xu, Y., Liu, H., Liao, H., Xu, Q., Tan, F., and Wang, J., Vapor-Phase Highly Selective O-Methylation of Catechol with Methanol over $ZnCl_2$ Modified γ-Al_2O_3 Catalysts, *J. Mol. Catal. A*, vol. **232**, pp. 69–75, 2005.

Jyothi, T.M., Raja, T., Talawar, M., and Rao, B., Selective O-Methylation of Catechol using Dimethyl Carbonate over Calcined Mg/Al Hydrotalcites, *Appl. Catal. A*, vol. **211**, pp. 41–46, 2001.

Kirumakki, S., Nagaraju, N., Chary, K., and Narayanan, S., A Facile O-Alkylation of 2-Naphthol over Zeolites Hβ, HY, and HZSM5 using Dimethyl Carbonate and Methanol, *J. Catal.*, vol. **221**, pp. 549–559, 2004.

Kirumakki, S., Nagaraju, N., Murthy, K., and Narayanan, S., Esterification of Salicylic Acid over Zeolites using Dimethyl Carbonate, *Appl. Catal. A Gen.*, vol. **226**, pp. 175–182, 2002.

Lopez, T., Bosch, P., Ramos, E., Gomez, R., Novaro, O., Acosta, D., and Figueras, F., Synthesis and Characterization of Sol-Gel Hydrotalcites, Structure and Texture, *Langmuir*, vol. **12**, pp. 189–192, 1996.

Roth, P., Particle Synthesis in Flames, *Proc. Combust. Inst.*, vol. **31**, pp. 1773–1788, 2007.

Tambe, P.R. and Yadav, G.D., Green Synthetic Route for a Perfumery Compound (2-Methoxyethyl) Benzene using Li/MgO Catalyst, *J. Chem. Sci.*, vol. **129**, pp. 1771–1779, 2017. DOI: 10.1007/s12039-017-1395-y

Tiwari, M.S., Yadav, G.D., and Ng, F.F.T., Selective Hydrogenation of 3,4-Dimethoxybenzophenone in Liquid Phase over Pd/C Catalyst in a Slurry Reactor, *Can. J. Chem. Eng.*, vol. **92**, pp. 2157–2165, 2014.

Valente, J.S., Cantú, M.S., Cortez, J.G.H., Montiel, R., Bokhimi, X., and López-Salinas, E., Preparation and Characterization of Sol-Gel Mg Al Hydrotalcites with Nanocapsular Morphology, *J. Phys. Chem. C*, vol. **111**, pp. 642–651, 2007.

Vishwanathan, V., Ndou, S., Sikhwivhilu, L., Plint, N., Raghavan, K.V., and Coville, N.J., Evidence for Weak Base Site Participation in the Vapor Phase Methylation of Catechol over Solid Base Catalysts, *Chem. Commun.*, no. 10, pp. 893–894, 2001.

Yadav, G.D. and Aduri, P., Aldol Condensation of Benzaldehyde with Heptanal to Jasminaldehyde over Novel Mg–Al Mixed Oxide on Hexagonal Mesoporous Silica, *J. Mol. Catal. A*, vol. **355**, pp. 142–154, 2012.

Yadav, G.D. and Fernandes, G.P., Selective Synthesis of Natural Benzaldehyde by Hydrolysis of Cinnamaldehyde using Novel Hydrotalcite Catalyst, *Catal. Today*, vol. **207**, pp.162–169, 2013.

Yadav, G.D. and Krishnan, M.S., Etherification of β-Naphthol with Alkanols using Modified Clays and Sulfated Zirconia, *Ind. Eng. Chem. Res.*, vol. **37**, pp. 3358–3365, 1998.

Yadav, G.D. and Salunke, J.Y., Selectivity Engineering of Solid Base Catalyzed O-Methylation of 2-Naphthol with Dimethyl Carbonate to 2-Methoxynaphthalene, *Catal. Today*, vol. **207**, pp. 180–190, 2013.